

# **Quantitative Evaluation of Human Skin Surface Characteristics Based on Image Processing**

by

**WU, Yue**

**Dissertation**

Submitted by WU, Yue

In Partial Fulfillment of the Requirements for the Degree of  
**Doctor of Engineering (Ph.D.)**

Supervisor: Prof. TANAKA, Toshiyuki, Ph.D.

**Graduate School of Science and Technology  
Keio University**

August, 2021

# Contents

<b>List of Tables</b> . . . . .	<b>vi</b>
<b>List of Figures</b> . . . . .	<b>viii</b>
<b>Abstract</b> . . . . .	<b>xi</b>
<b>Acknowledgments</b> . . . . .	<b>xiv</b>
<b>1 Introduction</b> . . . . .	<b>1</b>
1.1 Skin structure . . . . .	2
1.1.1 Epidermis . . . . .	2
1.1.2 Dermis . . . . .	3
1.1.3 Accessory organs . . . . .	3
1.2 Skin optical properties . . . . .	4
1.2.1 Scattering and absorption components . . . . .	5
1.2.2 Detour and sieve components . . . . .	6
1.2.3 Fluorescence components . . . . .	6
1.3 Overview of skin surface characteristics and measurement . . . . .	7
1.3.1 Introduction of skin micro-relief and measurement . . . . .	7
1.3.2 Introduction of skin color and measurement . . . . .	8
1.3.3 Introduction of skin barrier function and measurement . . . . .	11
1.3.4 Introduction of skin microbiological flora and measurement . . . . .	14
1.4 Effect of light source on images . . . . .	14
1.5 Classic image processing algorithms . . . . .	16

1.5.1	Color models . . . . .	16
1.5.2	Fundamental morphological operations . . . . .	20
1.5.3	Binarization . . . . .	21
1.5.4	Labeling . . . . .	24
1.5.5	Texture processing . . . . .	26
<b>2</b>	<b>Quantitative Evaluation of Skin Micro-relief . . . . .</b>	<b>27</b>
2.1	Introduction of skin Micro-relief . . . . .	28
2.2	Methods and materials . . . . .	30
2.2.1	Image capture device . . . . .	30
2.2.2	Skin micro-relief image analysis methods . . . . .	31
2.2.3	Skin parameters extraction and calculation . . . . .	32
2.2.4	Study population and design . . . . .	32
2.2.5	Statistical Analysis . . . . .	33
2.3	Quantitative evaluation results of skin micro-relief . . . . .	34
2.3.1	Skin micro-relief features extraction . . . . .	34
2.3.2	Age-dependent changes with skin micro-relief . . . . .	39
2.3.3	Correlation among skin micro-relief related parameters . . . . .	41
2.4	Discussion . . . . .	42
2.5	Conclusion . . . . .	44
<b>3</b>	<b>Quantitative Evaluation of Skin Color . . . . .</b>	<b>46</b>
3.1	Introduction of skin color . . . . .	47
3.2	Methods and materials . . . . .	49
3.2.1	Study population . . . . .	49
3.2.2	Design of study population . . . . .	50
3.2.3	Skin color measurement . . . . .	50
3.2.4	skin color measurement from digital images . . . . .	51
3.2.5	Individual typology angle . . . . .	53

3.2.6	Hue angle . . . . .	54
3.2.7	Statistical analysis . . . . .	54
3.3	Results of quantitative skin color measurement . . . . .	55
3.3.1	Subject population . . . . .	55
3.3.2	Spectral characteristics of the white LED lamp . . . . .	55
3.3.3	Evaluation of skin color in different skin anatomical sites . . . . .	56
3.3.4	Comparison of skin color by different instruments . . . . .	57
3.3.5	Comparison of skin color indexes . . . . .	58
3.3.6	Comparison of age-related skin color variations . . . . .	60
3.4	Discussion . . . . .	60
<b>4</b>	<b>Quantitative Evaluation of Skin Porphyrins . . . . .</b>	<b>68</b>
4.1	Skin porphyrin introduction . . . . .	69
4.2	Methods and materials . . . . .	71
4.2.1	Skin fluorescence image captured device . . . . .	71
4.2.2	Image processing . . . . .	72
4.2.3	Age-dependent changes in cheek porphyrins . . . . .	75
4.3	Skin red fluorescence of porphyrins evaluation results . . . . .	75
4.4	Age-dependent changes in facial porphyrins . . . . .	78
4.5	Discussion . . . . .	79
4.6	Conclusions . . . . .	82
<b>5</b>	<b>Quantitative Evaluation of Skin Barrier Function: a Preliminary Study . . . . .</b>	<b>83</b>
5.1	Introduciton of Skin barrier function . . . . .	84
5.2	Methods and materials . . . . .	86
5.2.1	Skin hydration evaluation instruments . . . . .	86
5.2.2	Database of skin hydration . . . . .	87
5.3	Image processing . . . . .	88
5.3.1	Statistical analysis . . . . .	90

5.4	Results of skin hydration evaluation . . . . .	91
5.4.1	Image processing results . . . . .	91
5.4.2	Before-after variation trends of skin hydration . . . . .	93
5.4.3	Correlation with skicon and corneometer . . . . .	94
5.5	Discussion . . . . .	95
5.6	Conclusion . . . . .	96
<b>6</b>	<b>Comprehensive Evaluation System of Skin Conditions . . . . .</b>	<b>97</b>
6.1	Introduction . . . . .	98
6.2	Comprehensive skin evaluation system structure . . . . .	98
6.2.1	Radar chart introduction . . . . .	98
6.2.2	Five-level evaluation rating scales design . . . . .	99
6.2.3	Evaluation index chosen standards . . . . .	99
6.3	System algorithm design . . . . .	100
6.3.1	Skin health algorithm design . . . . .	100
6.3.2	Skin aging algorithm design . . . . .	101
6.3.3	Skin color algorithm design . . . . .	103
6.3.4	Skin roughness algorithm design . . . . .	104
6.3.5	Skin pores algorithm design . . . . .	104
6.4	Application for skin conditions evaluation . . . . .	105
6.5	Discussion . . . . .	107
<b>7</b>	<b>Conclusions and Future Work . . . . .</b>	<b>109</b>
7.1	Conclusions . . . . .	110
7.2	Future research prospects . . . . .	111
	<b>Lists of Author's Publications . . . . .</b>	<b>113</b>
	<b>References . . . . .</b>	<b>115</b>

# List of Tables

1.1	Comparison of skin micro-relief measurement [1] . . . . .	9
1.2	Comparison of skin hydration measurement [2] . . . . .	11
1.3	Comparison of skin TEWL measurement [2] . . . . .	12
1.4	Comparison of skin sebum measurement [2] . . . . .	13
1.5	Calculation result of color rendering index of white LED lamp . . . . .	15
1.6	Selection of color models . . . . .	20
2.1	Related work of skin micro-relief evaluation . . . . .	30
2.2	Subject information for skin micro-relief evaluation . . . . .	33
3.1	Age distribution of study subjects for skin color measurement . . . . .	55
3.2	Classification of female cheek skin color in East Asia . . . . .	58
3.3	Descriptive analysis of the skin color parameters of the cheek . . . . .	59
4.1	Related work of skin porphyrin evaluation . . . . .	70
4.2	Age distribution of study subjects for skin porphyrin measurement . . . . .	75
4.3	Verification of porphyrin image processing . . . . .	77
4.4	Comparison with other methods . . . . .	78
5.1	Related work of skin hydration evaluation . . . . .	86
5.2	Pearson correlation coefficient . . . . .	94
6.1	Level standard of porphyrin number among age groups . . . . .	101
6.2	Level standard of mean intensity of porphyrins among age groups . . . . .	101
6.3	Level standard of contrast among age groups . . . . .	102

6.4	Level standard of furrow length among age groups . . . . .	102
6.5	Level standard of furrow width among age groups . . . . .	103
6.6	Level standard of average area of closed polygon among age groups . . .	103
6.7	Level standards of skin color . . . . .	104
6.8	Level standards of skin roughness among age groups . . . . .	104
6.9	Level standards of average skin pores area among age groups . . . . .	105
6.10	Skin health level calculation . . . . .	106
6.11	Skin aging, pores, and roughness calculation . . . . .	106
6.12	Skin color calculation . . . . .	106

# List of Figures

1.1	Illustration of the skin layers and their optical properties . . . . .	4
1.2	Absorption spectra of chromophores . . . . .	5
1.3	Replica example . . . . .	8
1.4	Classification of ultraviolet, visible, and infrared light . . . . .	16
1.5	Dilation Principal Illustration . . . . .	21
1.6	Erosion principal illustration . . . . .	21
1.7	Illustration of usual connected component . . . . .	24
1.8	Example of usual connected component in labeling . . . . .	25
2.1	Skin micro-relief illustration . . . . .	28
2.2	Skin image capture operation [3] . . . . .	31
2.3	Pre-processing illustration . . . . .	32
2.4	Skin micro-relief evaluation flowchart . . . . .	33
2.5	Flowchart of skin surface extraction . . . . .	34
2.6	Flowchart of skin pore classification . . . . .	37
2.7	Flowchart of skin furrow extraction . . . . .	38
2.8	Skin furrow extraction illustration, (a)watershed transform result; (b)skin furrow extraction; (c)skin furrow area extraction without pores . . . . .	38
2.9	Flowchart of skin closed polygon extraction . . . . .	39
2.10	Skin micro-relief parameters changes with age . . . . .	41



2.11	Relationships among parameters with significant differences: black lines represent the weak correlation; blue lines represent the mediate correlation; green lines represent the high correlation . . . . .	42
3.1	Flowchart of skin color measurement . . . . .	49
3.2	Overview of image processing for skin color measurement . . . . .	52
3.3	Skin color categories: Individual typology angle . . . . .	53
3.4	Skin color categories: hue angle . . . . .	54
3.5	spectroscopic characteristics of the built-in white LED lamp of the image capturing device . . . . .	56
3.6	The ITA values of 91 subjects . . . . .	57
3.7	Skin color comparison of anatomical sites . . . . .	57
3.8	Comparison of hue angles by different devices . . . . .	58
3.9	Effect of geographic location and age on skin color . . . . .	61
3.10	UVA dose received in main Asian cities . . . . .	65
4.1	Smart Skin Care <sup>®</sup> device illustration [3] . . . . .	71
4.2	UV-LED lamps' spectrum characteristics . . . . .	72
4.3	Fluorescence images . . . . .	72
4.4	Flowchart of skin fluorescence image processing . . . . .	73
4.5	HSV color model illustration . . . . .	73
4.6	Processed porphyrin images with contours . . . . .	76
4.7	Comparison results of extracted skin porphyrins . . . . .	77
4.8	Porphyrin trends with age examples . . . . .	78
4.9	Porphyrin variation with age . . . . .	79
4.10	Information illustration of the skin fluorescence image . . . . .	81
5.1	The whole facial skin image capture instrument: EPISCAN [4] . . . . .	87
5.2	Skin hydration database . . . . .	88
5.3	The flowchart of skin hydration extraction . . . . .	88

5.4	The illustration of HSI color model . . . . .	89
5.5	Color model conversion example . . . . .	91
5.6	The example of mono image, CLAHE image, and skin reflectance image .	92
5.7	ROI comparison in original image and skin reflectance image . . . . .	92
5.8	Before-after skin hydration content variation trends . . . . .	93
5.9	Linear regression among GVR, Corneometer, and Skicon . . . . .	94
6.1	Skin evaluation score of average level . . . . .	100
6.2	Skin samples captured by microscope . . . . .	106
6.3	Radar chart of skin conditions . . . . .	107
7.1	Future research perspectives . . . . .	111

# Quantitative Evaluation of Human Skin Surface Characteristics Based on Image Processing

WU, Yue  
buestu95@keio.jp  
Keio University, 2021

Supervisor: Prof. TANAKA, Toshiyuki, Ph.D.  
tanaka@appi.keio.ac.jp

## Abstract

With the spread of image technology such as computer graphics, research applying image analysis technology to cosmetics and medical diagnosis is thriving. Traditionally, visual evaluation and spectrophotometer have been used as useful methods. Although it is limited to surface observation visually, quantitative evaluation is possible by image analysis. However, since the skin changes depending on disease, aging or season, conventional skin measurement is not sufficient. In addition, various measurement methods are utilized, but mainly single-use instruments. In dermatology treatment, it is necessary to simultaneously evaluate a plurality of items such as moisture, sebum amount and texture, while the conventional single-purpose device does not perform high effectively. Therefore, establishment of an objective evaluation method of skin condition using multi-measured skin scope and the image analysis technique aimed at this research is an extremely important task.

In order to assess skin condition objectively and comprehensively, several properties are involved in evaluation system, including skin hydration, skin sebum, skin micro-relief, skin color, and skin microbiological flora. Chapter 1 introduces the fundamental knowledge of skin structure and skin surface properties. Besides, an overview of existing measurement of these characteristics is provided. With rapid development of image processing technology, typical and classic image processing algorithms are given a presentation, as the basis for subsequent algorithms in Chapter 2 to 6.

Skin micro-relief has been researched by a variety of devices and methods, which usually are expensive or complicated. On the other hand, skin micro-relief relates to quite a few parameters, and it is hard to evaluate all of them at the same time. In chapter 2, we propose a quantitative evaluation algorithm of skin micro-relief and extract four aspects, including skin surface properties, skin pores, skin furrows, and the skin closed polygons. The age-dependent changes of these parameters are also explored, which reveals that most parameters increased as age went on with significant differences. In addition, skin coarseness is proved to be strongly related to the skin pore area.

Skin color is one of the most obvious features of the skin. Various information can be extracted from the analysis of skin color, including age and health, which means that an objective and reproducible measurement of skin color would be of significant value. According to the CIE-L\*a\*b\* color model, we perform a skin color measurement in Chapter 3, utilizing the individual typology angle (ITA) and hue angle, indexes that are calculated from digital images with specific algorithms. The changes of skin color parameters by age, anatomical sites, and geographic locations are figured out.

*Propionibacterium acnes* (P. acnes) is a member of the anaerobic organisms, which is involved in the induction of skin, acne and produce porphyrins that absorb ultraviolet light and emit red fluorescence in response. Chapter 4 develops a novel approach to segment skin porphyrins induced by P. acnes from ultraviolet images, which has the potential to predict skin conditions as an assisted tool. We also investigate the age-dependent changes, that all parameters of porphyrins arrive at the peak at 30 years old.

Abundant hydration in the skin is quite important for skin barrier function. However, skin hydration assessment applying image processing is rare, focusing on skin capacitive images and near-infrared images at large, which are costly. A prior study for quantitative evaluation algorithm of skin surface hydration by visible optical image processing is proposed in Chapter 5. Skin hydration content is successfully extracted and has a heavy correlation with the results measured by commercial instruments.

The skin condition is full of changes and complexity, which results in a simplified measurement unsatisfied with the diagnosis of the condition of the skin in practice. Chapter 6 establishes a comprehensive skin condition measurement system from 5 sides by combining the parameters extracted from Chapter 2 to 5. The measurement system is displayed as a radar chart with 5 levels. The integrated quantitative evaluation of skin surface characteristics has become reality so far.

Finally, Chapter 7 summarizes the conclusions and imagines the continued research perspectives of this work in the future.

# Acknowledgments

It has been my best three years learning in Keio University so far. I am deeply impressed by the spirit of Keio University. I would like to express my sincere gratitude to my supervisor, Professor Toshiyuki Tanaka, who gives me the opportunity to carry out my doctoral research and allow me to grow as a researcher. His guidance provides the continued support of my Ph.D. study and related research, for his kindness, patience and knowledge. His guidance helped me in all the time of research and writing of this thesis.

I am particularly grateful for the assistance given by Dr. Makio Akimoto. Thanks to his recommendation, I have the chance to learn in Keio University. He always considers the next step for me in advance and offers me a lot of technical help from color science and measurement science. I would also like to extend my gratitude to the rest of my thesis committee member, Professor Yoshimitsu Aoki, Professor Masaaki Ikehara, and Professor Yutaka Hori, for their insightful comments, which help me improve the thesis to a better scientific level.

Assistance provided by Keio Leading Edge Laboratory (KLL), for offering the research grant to support my trip to ICBME 2019 and other conferences. The research grant helps me to share the work we have done and discuss with some researchers in the related field. I would like to thank the IT Access Co.,Ltd and CBON Co., Ltd for their assistance with the collection of my data.

Finally, I am grateful to my family for their encouragement and all supporting not only financially but also spiritually. Words cannot express how grateful I am. My special thanks to my friends, both in China and Japan, especially the members from Tanaka lab. I got huge relax from our trip together. I hope we still other opportunities to meet again.

# **Chapter 1**

## **Introduction**

## **1.1 Skin structure**

The skin is an organ that covers the entire human body and protects vital activities, which covers 1.6 m<sup>2</sup> of the adult body and accounts for 16% of the body weight. The skin is also the largest organ of the human body and plays a crucial role in retaining moisture and preventing foreign substances from entering the body. It also takes a great impact on protecting the body from danger by feeling pain and itch, and by releasing water through sweat when it is hot, maintaining the body temperature at an appropriate level as well. The skin can be roughly divided into three main layers: epidermis, dermis, and subcutaneous tissue. Within each layer is further layers and cells. Accessory organs include sweat glands, sebaceous glands, hair, and nails. The color of the skin is determined by the blood vessels, fat, and chromophores within these layers.

### **1.1.1 Epidermis**

The epidermis, which is the most superficial part of the skin, plays the most important role in maintaining the body. The thickness of the epidermis and dermis is about 0.6–3.0 mm (average about 1.4 mm). The average thickness of the epidermis is about 0.2 mm, and 95% of it is composed of keratinocytes. There are 4 layers in epidermis [5], including the stratum basale, stratum spinosum, stratum granulosum, and stratum corneum from inside out respectively. The stratum basale, also known as the basal layer, is the innermost layer of the epidermis, where the main cell type is the keratinocyte that may or may not divide. Melanocytes are present in the basal layer and consist of 5–10% of the cell population. The stratum spinosum is formed during the process of keratinocytes moving on the stratum corneum, where the Langerhans cell could be ascertained. The stratum granulosum is constitutive of flattened cells holding abundant keratohyaline granules in their cytoplasm, which are responsible for further synthesis and modification of proteins involved in keratinization [6]. The outermost layer is the stratum corneum, which is commonly researched in dermatology and aesthetic dermatology. Keratinocytes divide continuously



in the innermost part of the epidermis and move to the stratum corneum when they mature. Arranged in a concentric manner around the nucleus, the keratin filaments in the cytoplasm are bound to desmosomal plates at one end and remain free at the end closer to the nucleus [7]. When they mature, they move to the surface, and finally become keratinocytes and peel off. In this way, the epidermis is kept from growing old by being replaced by new cells one after another. This replacement of cells is called metabolism, and it usually takes about 28 days in body skin and 14 days in facial skin.

### **1.1.2 Dermis**

The thickness of dermis changes in different anatomical sites, which is over 5 mm on the back while less than 1 mm on the eyelids. The dermis is delimited in the exterior by its junction with the epidermis and in the interior by the subcutaneous fat. As conjunctive tissue, the dermis contains cells, a ground substance and fibers. The soil substance is composed of polysaccharide and proteins that interact to produce hygroscopic proteoglycan macromolecules. The cells are fibroblasts that synthesize collagen and elastin fibers. Collagen accounts for 75% of the dry weight and up to 30% of the volume of the dermis, 75% of which is made of type I collagen and another 15% is type III collagen. Elastin fibers influence the elasticity to the skin.

### **1.1.3 Accessory organs**

Accessory organs include sweat glands, sebaceous glands, hair, and nails. sweat glands mainly influence the thermal regulation. Sebaceous glands secrete sebum and provide lubrication action, which mainly locates on the face and scalp. Hair is formed from keratin in hair follicles. The hair growth cell cycle consists of three stages: anagen, catagen, and telogen. Fingernails are composed of the underlying nail bed and the nail plate. The underlying nail bed contains blood vessels, nerves, and melanocytes and has parallel rete ridges, while the nail plate is formed from matrix keratinocytes. They combine together to provide protection to the fingertips, enhance sensation, and allow small objects to be grasped [8].

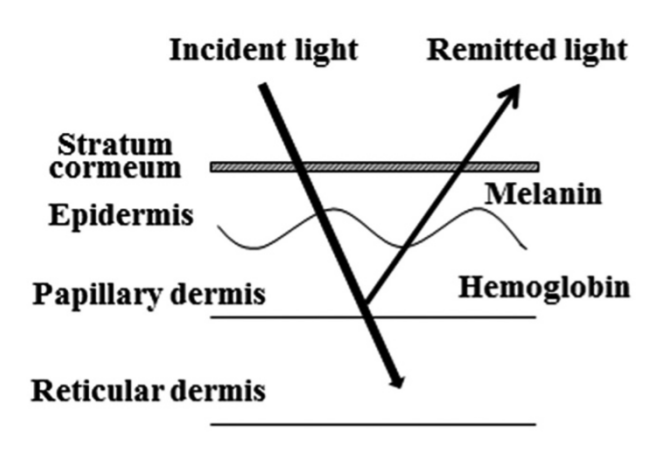


Figure 1.1: Illustration of the skin layers and their optical properties

## 1.2 Skin optical properties

Due to the multilayered skin structure and its non-flat surface, skin optical properties are researched and overviewed. It is difficult to find a material more complex than human skin from a tissue optics perspective, which explains the wide range of variations in skin appearance observed in the world population. As shown in the illustration in Fig. 1.1, the skin consists of layers with distinct functions and optical properties. When white light shone onto the skin penetrates the superficial skin layers, some of it is reflected back to the environment and others are absorbed or scattered to internal layers by the specific molecules or structures, such as melanin. The stratum corneum is a protective layer consisting of keratin-impregnated cells that varies considerably in thickness. Apart from scattering the light, it is optically neutral. The epidermis is largely composed of connective tissue. It also contains melanin-producing cells. Melanin is a pigment that strongly absorbs light in the blue part of the visible spectrum. The dermis is made of collagen fibers. Hemoglobin, present in blood vessels across the whole dermis, acts as a selective absorber of light.

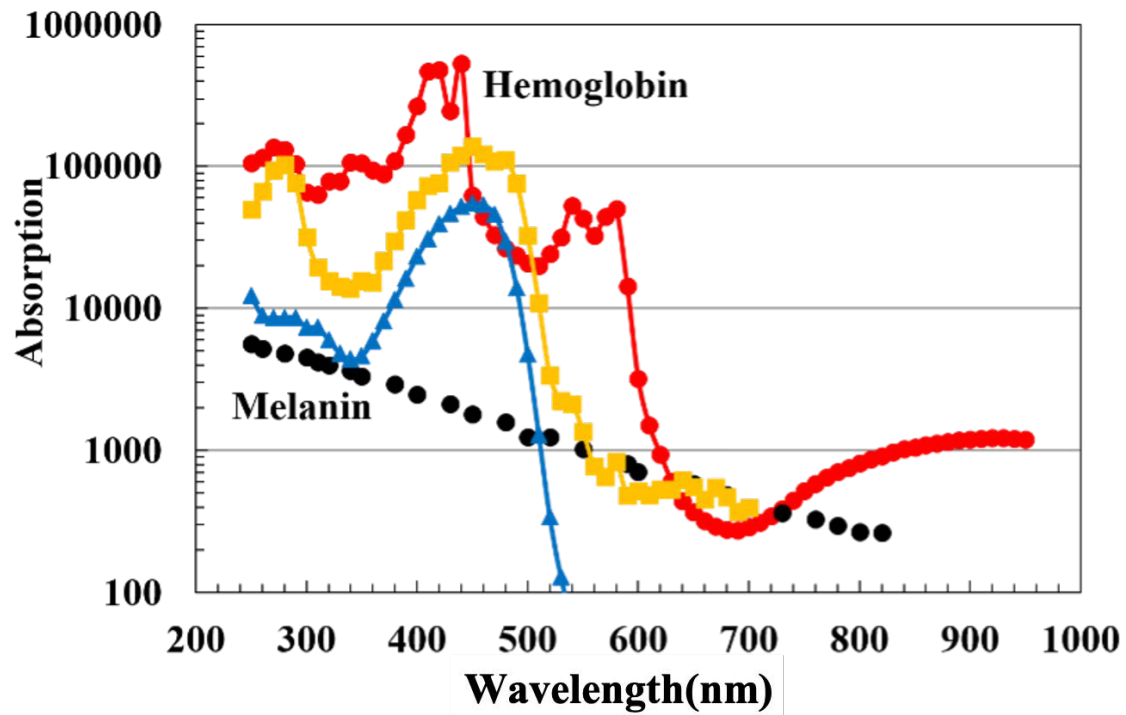


Figure 1.2: Absorption spectra of chromophores

### 1.2.1 Scattering and absorption components

The average scattering properties of the skin are defined by the scattering properties of the dermis with its big thickness (up to 4 mm) and comparable scattering coefficients of the epidermis and the reticular dermis [9].

The distribution of blood and chromophores and pigments in skin are random and inhomogeneous, which results in variations of average optical properties of skin layers. Skin absorption properties are determined by summary absorption of hemoglobin and water of skin dermis, as well as melanin and lipids of skin epidermis. Figure 1.2 illustrates the absorption spectra of these chromophores and pigments with different wavelength. Melanin decreases linearly with wavelength rises. Dermis is the main absorbers in visible spectra, where the hemoglobin, carotene, and bilirubin play vital roles. The absorption of carotene and bilirubin arrives at the peak around 460 nm. The highest absorption of hemoglobin is around 420 nm.

## **1.2.2 Detour and sieve components**

Detour effect refers to the phenomenon that when light traverses a turbid medium like human skin, refractive index differences between the structures and the surrounding materials may cause multiple external and internal reflections which increase the light optical path length. In contrast, Sieve effect refers to the phenomenon when light traverses the human skin and may not encounter a pigment-containing structure [1]. Detour effect has the potential of increasing light absorption by the pigment of interest, while sieve effect would reduce the light absorption on the contrary. The results of these two effects rely on several factors in general, and one of the most obvious influence is the size, shape, and distribution of skin melanosomes.

## **1.2.3 Fluorescence components**

When electromagnetic radiation propagating at a certain wavelength is absorbed by a material, it may excite the orbital electrons of the atoms or molecules of this material to a higher quantum state. Upon return of these electrons to their ground state, they emit photons of light at another wavelength, which is called fluorescence. The process has a timescale of approximately 8-10 seconds or shorter. The excitation and emission spectra are the pivotal properties [1].

Ultraviolet-induced fluorescence components are mainly found out within the human skin, including porphyrins, nicotinamide adenine dinucleotide (NADH), keratin, collagen, elastin, and so on. Porphyrins are produced by *P. acnes* generally, which could be seen red visibly under ultraviolet light or wood's lamp [10]. Collagen is located in the dermis layer, which is also considered as the main fluorophore of human skin.

## **1.3 Overview of skin surface characteristics and measurement**

Measuring skin is quite crucial in experimental dermatology with its quantitative evaluation of the real conditions and the effect. It is bearing the brunt of the definition and classification of skin surface characteristics.

### **1.3.1 Introduction of skin micro-relief and measurement**

Skin is a surface consisted of pores, furrows, and closed polygons, which is the area rounded by furrows. Therefore, skin surface is not flat even though it looks smooth. Close observation of the micro-relief reveals that the furrow has a directional depth. There are mainly two types of furrows, deep and wide primary furrows (20-200  $\mu\text{m}$ ) and superficial secondary furrows (30-70  $\mu\text{m}$ ). Across the intersections of the furrows, there are pore openings. This network of skin micro-relief has two roles: it provides the skin a protective mechanical stretching ability in the direction of the constraints the skin sustains and it is also useful for the evacuation and retention of sebum and sweat and to capture substances applied to the skin.

It is known that the shape of the skin micro-relief varies from one person to another, and that the micro-relief changes depending on the skin condition and environment, and also changes greatly with age. In addition, the correlation between skin texture and facial attractiveness has been studied, and they found out even and homogeneous skin was more attractive [11].

Skin pores are easily visible on the cheeks and head of the nose. Pores on the cheeks and head of the nose are easily visible, and the size of a pore that is noticeable to the naked eye is said to be 0.2 mm square or larger. Skin furrows are initially short and shallow and then become deep and longer to form the wrinkles gradually with the increase of age. Skin closed polygons varies towards the irregular shape with age.

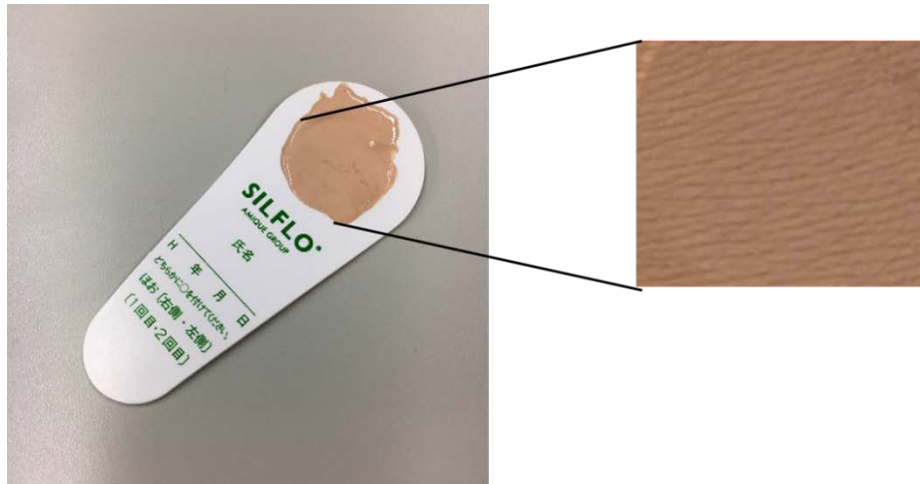


Figure 1.3: Replica example

Skin micro-relief measurement has large application perspectives both in clinical and aesthetic research. In contrast to other skin characteristics, the measurement of skin surface micro-relief is more complicated since the structure is three dimensional. Some popular measurement is concluded in Table 1.1 [1]. Mechanical profilometry is the earliest method developed to measure skin surface, which needs replica to get the skin surface information, as shown in Fig. 1.3. With progress of technology, different profilometry methods are developed with higher accuracy, since the contact between the instrument and the human skin is avoided. Recently, researchers utilize image processing methods to extract the features of skin wrinkles, and other parameters.

### 1.3.2 Introduction of skin color and measurement

Pigments such as hemoglobin in blood, melanin in skin tissue, and carotenoids exist in the translucent skin tissue are determined by the absorption and reflection of light in these complex tissues. Skin color is not always uniform, and there are brown spots and freckles where melanin is unevenly distributed. In addition to the concept of pigmentation, skin color is a complex phenomenon that differs depending on the sebum and sweat secreted from the skin surface, as well as the surface morphology such as hair growth, scaling, pores and wrinkles. In general, skin color is measured by a spectrum-Reflectometer. The

Table 1.1: Comparison of skin micro-relief measurement [1]

measurement	principles	instrument example
(In vivo) Mechanical profilometry	Based on a touch sensor to measure the 2D profile or 3D surface, and use the inductive sensor to transform relief variations into signal.	Silicon replica (Silflo, Japan)
(In vivo) 2D optical images	Use image processing to extract related features, such as GLCM.	
(In vivo) Laser profilometry	Based on dynamic focalisation or (simple or double) triangulation, uses the movement of a mobile lens or a spotlight reflected on a sensor to measure the height at each point of a sample surface.	
(In vivo) 3D reconstruction by optical profilometry	Detect the contrast formed by the wrinkle and the adjacent skin	Primos (GFM in Germany)
(In vitro) Pofilometry by transmission	Measure the variation of intensity of light shining through a replica. Applying the Beer-Lambert law, the absorption of light is linked to the transparency and therefore the thickness of the replica.	Silicon replica (Silflo, Japan)
(In vivo) Fringe projection	Project structured light onto the investigated surface. Fringes are deformed (modulated) by the relief. Several acquisitions with different phases of the projected network are recorded by a camera; after processing by a dedicated software, the tridimensional profile of the studied area is reconstructed within a few seconds.	DermaTop Blue (Eotech in France) Primos (GFM in Germany)

components in the skin that determine skin color include melanin, hemoglobin, bilirubin, and carotene. Among these, melanin and hemoglobin are most strongly involved.

The skin color of humans and other mammals is produced by a complex interplay of various factors, including hemoglobin in the blood, surface conditions of the skin, moisturizers, and pigment. The melanin pigment is the largest of these, and its role is to mitigate the skin damage caused by ultraviolet rays. The melanin pigment in the skin is produced by melanocytes (pigment cells) in the basal layer of the epidermis. When the skin is exposed to ultraviolet rays, the melanin synthesis switch is turned on and the skin darkens, but the switch is turned off with the passage of time and the skin returns to its normal color. However, even if the skin is not exposed to ultraviolet rays, the switch remains on and does not return to its original state, resulting in excessive production of melanin pigment and deposition of brown pigment in the skin (hyperpigmentation). This condition is called “spotting” or “freckling”. Spots are large to some extent, while freckles are generally small dots.

The distribution of melanocytes varies considerably depending on the part of the body, which may be due to the effect of ultraviolet rays. The number of melanocytes in the exposed area (face) is more than twice as large as that in the clothed area (upper limbs). There is no significant difference in the number of melanin depending on race or sex, but the number decreases with age, and by the age of 50 to 60, it is said to be about half of what it was in childhood. The synthesis of melanin is carried out by intracellular organelles called melanosomes in melanocytes. The size, morphology, and distribution of melanosomes vary by race. Comparing Caucasians and blacks, the amount of melanin synthesized by Caucasians is obviously lower than that by blacks, and that by Japanese is in between.

Pigmentation appearing on the face and other parts of the body is often referred to as “blemishes” in general. These include chloasma, freckles, and post-inflammatory pigmentation, but senile pigmentation increases with age in both men and women. Senile pigmented macules are round, brown to black pigmented spots with clear borders, and



are especially common in sun-exposed areas. Pigmentation, such as spots and freckles, is caused by abnormal melanin production by keratinocytes, which is most strongly influenced by ultraviolet rays, but female hormones and stress are also said to be involved. The mechanism of late-onset pigmentation, such as senile pigmentation, is also due to abnormal melanin production by keratinocytes, but it is unclear why pigmentation occurs only in localized areas. The increase of melanin pigmentation with aging has also been suggested as one of the factors of dullness in aging skin.

### 1.3.3 Introduction of skin barrier function and measurement

#### Skin hydration

Water is regarded as the ultimate moisturizer that improves subjective perception of the mechanical properties of human skin. The keratin proteins and filaggrin proteins in the stratum corneum act as a barrier to prevent the evaporation of water and external stimulus. Since the skin has a multilayered structure, the amount of moisture contained in each area varies. The average SC hydration content is expected to be about 30% in the cheek site. Skin hydration measurement is summarized in Table 1.2 and Skicon® and Corneometer® are the most commonly used for measurement as commercial instruments [2].

Table 1.2: Comparison of skin hydration measurement [2]

measurement	principles	instrument example
Electrical measurement	Electrical capacitance	Corneometer CM825
	electrical conductance	Skicon-200
	Electrical capacitance image analysis	Moisuture Map MM100 (Courage+ Khazaka)
bioimpedance	bioimpedance	
Thermal measurement	Differential scanning calorimetry	
Photothermal and photoacoustic	Pulse raddiometry	
	Photoacoustic spectrometry	
Optical measurement	Near infrared spectroscopy	
	Confocal Raman Microspectroscopy	
	D-Squames and image analysis	

## Skin transepidermal water loss (TEWL)

Skin transepidermal water loss is one of the important indexes representing skin barrier function. TEWL decrease during the aging process. Therefore, the objective measurement of skin TEWL is quite important. The summary of TEWL measurement is shown in Table 1.3. three main methods are introduced, and the biggest difference among them is if the instrument could avoid the influence of humidity in the environment.

Table 1.3: Comparison of skin TEWL measurement [2]

measurement	principles	instrument example
Open-chamber system	The 11 mm probe chamber has 2 sensors mounted 3 and 6 mm above the skin surface. The probe is held against the skin and thus operates in the approximately 10 mm high water vapor gradient surrounding the skin as an invisible water vapor mantel. This water vapor layer over the visible skin surface is an important part of the physiological water barrier of the skin. From recording of humidity change between the 2 sensors, the flux of water over the stratum corneum water barrier into the chamber and to the open air is estimated.	Evaporimeter EP1 (Servomed AB, Stockholm, Sweden)
Semiopen system	A grid serving as a semiopen windshield has been incorporated directly in the top of the open probe of this instrument, which could protect the sensor against ambient air convections.	Dermalab (Cortex Technology, Hadsund, Denmark)
Closed-chamber system	a humidity sensor in the closed chamber measures the gradual build-up of humidity.	VapoMeter (Delfin Technologies Ltd, Kuopio, Finland)

## Skin sebum

Skin surface lipid is composed of lipids derived from the skin and the sebaceous glands. Keratinocytes synthesise the lipids present in the cell in the form of odd terrestrial bodies

and between the cells in the form of intercellular bilayers important for the function of barrier. As a holocrine excrete, sebum produced by the sebaceous gland is an oily mixture of lipids, keratin, and cellular membrane. The dominating lipids of sebum include triacylglycerol (triacylglyceride), fatty acid, cholesterol, ceramides, phosphoric acid, and other mixtures of lipids. Several measurement has been researched since the absorbent paper was invented in 1886. The introduction of widespread skin sebum measurement is shown in Table 1.4. Sebutapes can be evaluated by image processing methods to obtain the sebum content quantitatively, which also has the merit of mapping sebum distribution visually. In addition, opalescent film imprint method applies fat changing the light transmission to measure sebum content, with the merit that it can get the certain value immediately.

Table 1.4: Comparison of skin sebum measurement [2]

measurement	principles	instrument example
Sebum-absorbent tapes	a reliable morphologic method with which not only the sebum excretion rate in general, but also the output of individual follicles can be monitored	Sebutapes
Opalescent film imprint	the correlation of the change in light scattered by a frosted plastic film after it has been pressed against the skin surface.	sebumeter
Gravimetric analysis	weighing the amount of sebum accumulated in various absorbent papers.	
Fluorescence photography	According to the porphyrin fluorescence related to sebum, and use image processing method.	

### Skin pH value

Skin surface pH is a key index and the regulator of the SC barrier function. The optimum SC pH value is a precondition for activating lipid hydrolases in the cornea layer. It is responsible for the post-secretory treatment of lamellar bodies, which is an important step in the development of the cutaneous barrier. Maintaining SC pH value acidulously is helpful for skin health. Normal skin pH value is at the range of 4.0-7.0. pH is measured by flat glass electrode at the skin surface with a hydrated skin–electrode interface [12].

Recently, more complex high-resolution methods have also been invented, like the fluorescence lifetime imaging microscopy (FLIM).
















### **1.3.4 Introduction of skin microbiological flora and measurement**

Human skin is colonized by microbiological flora, including bacteria, fungi, and bacteriophages. Most of them are unharmed, and some may turn into pathogenic due to the change of skin condition. Therefore, the measurement of skin flora is necessary. In clinical research, it is already realized to measure skin flora status directly using comedone extractor and cyanoacrylate glue.

## **1.4 Effect of light source on images**

Even for the same object, with the variation of illumination type, the spectral distribution of the reflected light changes and the color appears different. This phenomenon, in which the color of an object differs depending on the type of illumination, is called color rendering property. Methods for evaluating the color rendering properties of light sources are specified by the International Commission on Illumination (Commission Internationale de l'Eclairage, CIE) and the Japanese Industrial Standards (JIS). Table 1.5 shows the test colors used in the calculation.

Table 1.5: Calculation result of color rendering index of white LED lamp

No.	Munsell notation	Color image	Color rendering index
1	7.5R6/4		64.5
2	5Y6/4		81.8
3	5GY6/8		92
4	2.5G6/6		62.1
5	10BG6/4		65.5
6	5PB6/8		75.8
7	2.5P6/8		81.6
8	10P6/8		48.3
9	4.5R4/13		-58.4
10	5Y8/10		57.9
11	4.5G5/8		57.8
12	3PB3/11		39.8
13	5YR8/4		69.3
	European skin color		
14	5GY4/4		94.9
15	1YR6/4		53.7
	Japanese skin color		

White LED lamps are used not only for indoor lighting, but also for measurement technology and efficiency improvement. There are two main methods to obtain white light: (a) Red LED + Green LED + Blue LED; (b) Blue LED + yellow phosphor. The

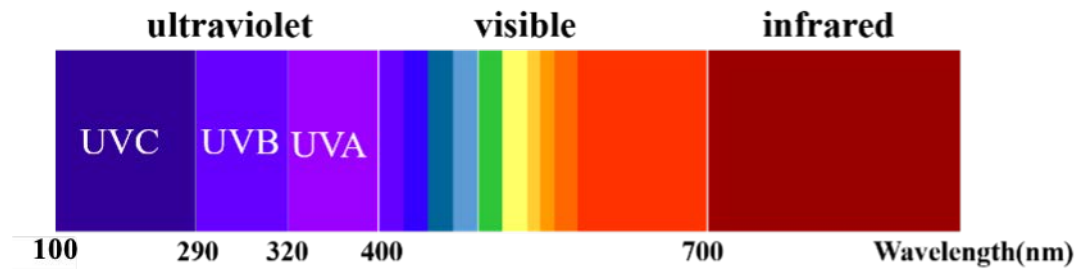


Figure 1.4: Classification of ultraviolet, visible, and infrared light

method (a) has the advantage of good color rendering, but is not commonly used due to its low efficiency. The method (b), which has high efficiency, is generally used. However, method (b) has the disadvantage of inferior color rendering compared to method (a) due to the lack of red component.

Ultraviolet (UV) radiation is an electromagnetic wave with a wavelength between 100 and 400 nm, which is shorter than that of visible light (violet) and longer than that of X-rays. The classification of ultraviolet, visible and infrared lights is shown in Fig. 1.3. There are three main types of UV lights, UVC, UVB, and UVA, which have different effect on human skin. The wavelength of UVC is the shortest, most of which would be absorbed by ozone sphere and cannot reach the earth surface. The wavelength of UVB is 290 to 320 nm, which could reach the epidermis of skin and cause sunburn with erythema. UVA has the longest wavelength of UV radiation and it has the ability to reach the dermis that would increase skin melanin content and cause other damage like skin aging.

## 1.5 Classic image processing algorithms

### 1.5.1 Color models

#### RGB color model

Red (R), blue (G), and green (B) are called the three primary colors of light, and there is a principle that all colors can be created by mixing these three colors together. Actually, it is impossible that all colors can be created by projecting and mixing the three light colors R, G, and B. The method of defining colors from the three RGB colors is called the RGB color system, which was adopted by CIE in 1931. The monochromatic light of

700nm (red), 546.1nm (green), and 435.8nm (blue) corresponding to each cone is mainly used because the cone cells of the eye respond specifically to red, green, and blue.

### **XYZ color model**

When representing colors in the RGB color system, there are colors that can be represented only by making the RGB values negative. The XYZ color system is a three-dimensional space. Therefore, the CIE approved the XYZ color system as a standard color system in 1931, which uses fictitious protistimulus values based on the RGB color system with a number transformation that does not include negative values. The XYZ color model is more commonly used than the RGB color system in actual color representation.

In the RGB color system, negative values occur for colors between 440 nm and 545 nm (blue-violet to yellow-green), making it impossible to accurately reproduce monochromatic light in this color range. The XYZ color system was conceived to mathematically avoid this problem. We created the non-existent primary colors X, Y, and Z (imaginary colors) to enable the representation of colors that cannot be reproduced by mixing real color light, red (R), blue (G), and green (B). These X, Y, and Z are called the primary stimuli, and the numerical value indicated by XYZ, which is the amount of color mixing of the three primary stimuli X, Y, and Z, is called the tristimulus value. Y is the only stimulus value that represents brightness (visual reflectance and visual transmittance) among the primary stimuli along with the green component.

$$X = 100(0.3933(R/255)^{2.2} - 0.3651(G/255)^{2.2} + 0.1903(B/255)^{2.2}) \quad (1.1)$$

$$Y = 100(0.2133(R/255)^{2.2} - 0.7010(G/255)^{2.2} + 0.0858(B/255)^{2.2}) \quad (1.2)$$

$$Z = 100(0.0182(R/255)^{2.2} - 0.1117(G/255)^{2.2} + 0.9570(B/255)^{2.2}) \quad (1.3)$$

### **CIE-L\*a\*b\* color model**

The CIE-L\*a\*b\* color model is a color model that can quantify human visual differences and is used in a wide range of fields. it was standardized by the CIE in 1976 and has been

adopted by JIS in Japan. The CIE L\*a\*b\* color system can be thought of as a sphere, where the vertical axis is the L\* value representing lightness from 0 to 100. The larger the L\* value and the closer it is to 100, the brighter and whiter the color, and the smaller the value and the closer it is to 0, the darker and more achromatic the color.

Hue and saturation are expressed in terms of a\* and b\* on the horizontal axis. a\* becomes more reddish as its absolute value increases in the positive direction, and more greenish as its absolute value increases in the negative direction. When both a\* and b\* are 0, the color is achromatic. When both a\* and b\* are zero, the color is achromatic. a\* and b\* are called “chromaticity index”. All color information consists of a\* and b\*, which indicate the location along the red-to-green axis and the blue-to-yellow axis, respectively. All color information is in the a\* and b\* layers, and the Euclidean distance metric is used to measure the distance between the two colors.

The values of CIE-L\*a\*b\* are calculated by XYZ color model and the formula is shown as follows.

$$L^* = 116(Y/Y_n)^{1/3} - 16 \quad (1.4)$$

$$a^* = 500[(X/X_n)^{1/3} - (Y/Y_n)^{1/3}] \quad (1.5)$$

$$b^* = 200[(Y/Y_n)^{1/3} - (Z/Z_n)^{1/3}] \quad (1.6)$$

$$f(x) = \begin{cases} x^{\frac{1}{3}} & \left(x > \left(\frac{6}{29}\right)^3\right) \\ 7.787x + \frac{16}{116} & \text{(otherwise)} \end{cases} \quad (1.7)$$

The reason why the expression of  $f(x)$  is divided into two parts by the domain of definition is to prevent the gradient from going to infinity when  $x = 0$ . In addition,  $x_0$ ,  $y_0$ , and  $z_0$  are the tristimulus values at the reference white point, as follows.

CIE standard luminance A simulates standard household tungsten filament lighting with a correlated color temperature of 2856 K.

$$x_0 = 109.86, y_0 = 100.00, z_0 = 35.58 \quad (1.8)$$



CIE standard luminance C simulates daylight in the average sky or northern sky at a correlated color temperature of 6774 K.

$$x_0 = 98.07 , y_0 = 100.00 , z_0 = 118.22 \quad (1.9)$$

CIE standard luminance D50 simulates warm daylight at sunrise or sunset with a correlated color temperature of 5003 K.

$$x_0 = 96.42 , y_0 = 100.00 , z_0 = 82.51 \quad (1.10)$$

CIE standard luminance D55 simulated daylight in the morning or mid-afternoon at a correlated color temperature of 5500 K.

$$x_0 = 95.68 , y_0 = 100.00 , z_0 = 92.14 \quad (1.11)$$

CIE standard luminance D65 simulates daylight at noon with a correlated color temperature of 6504 K.

$$x_0 = 95.04 , y_0 = 100.00 , z_0 = 108.88 \quad (1.12)$$

### **Grayscale color model**

When color information is not required and in order to facilitate feature detection in images, the conversion of a color image into an image that include only shading information is called grayscaling, and the resulting image is called a grayscale image. There are various methods for grayscaling, but the most common are the NTSC weighted average method, where each of R, G, and B is weighted and the average is taken, and the method of simply taking the average of the three RGB values. In this study, the NTSC weighted average method shown in equation (1.12) was used for the conversion. Grayscale model conversion of the NTSC is based on the fact that the structure of the human eye is better at recognizing shades of green than red or blue, the following equation with weighted coefficients for R, G, and B colors is used. These coefficients are specified by the CCIR (Consultative Committee on International Radio) Recommendation BT.601 (Rec. 601),

which was enacted in 1982.

$$gray(x, y) = 0.2989 \times R + 0.5870 \times G + 0.1140 \times B \quad (1.13)$$

Table 1.6: Selection of color models

Color model	Introduction	Component	Merit	Limitation
RGB	A method of defining colors from the three primary colors of light: red, blue, and green.	R(red); G(green); B(blue)	For digital or computer vision. The values are reproducible.	Cannot separate the lightness and color.  Not fit the human vision.
L*a*b*	It is thought of as a sphere, consisting of lightness, red to green and yellow to blue.	L*(lightness); a*(redness); b*(yellowness)	Has been widely applied to evaluate human skin color.	Only express better in normal human color.
HSV	A nonlinear transformation of RGB color model, often called "hexcone model".	H(hue); S(saturation); V(value)	Can be easily interpretable by humans.	S from HSV and HSI is different.
HSI	A nonlinear transformation of RGB color model, often called "bi-hexcone model".	H(hue); S(saturation); I(intensity)		The formula of V and I is different.

In conclusion, there are several color models could be chosen for image processing. The basic instruction, merits and limitations are summarized in Table 1.6. Compared to other color models, RGB color space is the original color space, which fits the computer vision, but it has the limitation that it cannot separate the lightness and color. L\*a\*b\* color model is commonly used for skin images, especially in skin color extraction. On the other hand, HSV and HSI have the advantage that can be easily interpretable by humans. These color models should be selected flexibly according to the demands.

## 1.5.2 Fundamental morphological operations

### Dilation

It is assumed that the background is set as white whose pixel value is 1, and the object is set as black whose pixel value is 0. The dilation process generally converts the pixel values of pixels in the 4 or 8 neighborhoods around the pixel of interest with a pixel value of 1 to 0 in a binarized image. An example of the dilation process is shown in Figure 1.5.

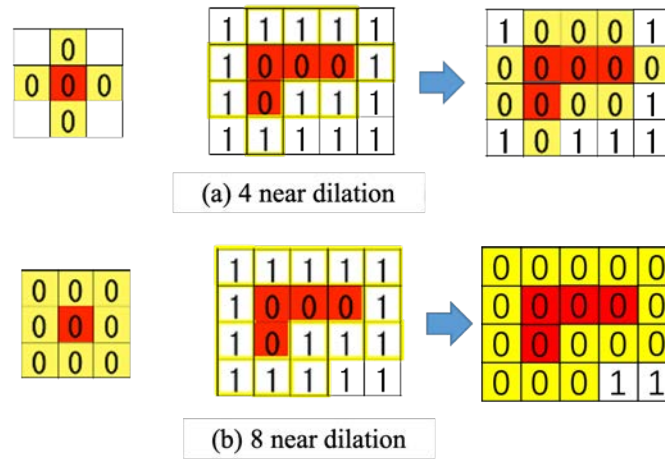


Figure 1.5: Dilation Principal Illustration

## Erosion

In contrast to the dilation operation, erosion is an operation that converts the pixel values of pixels in the 4 or 8 neighborhoods around the pixel of interest with a pixel value of 0 to 1 in a binarized image. An example of the erosion operation is shown in Fig. 1.6.

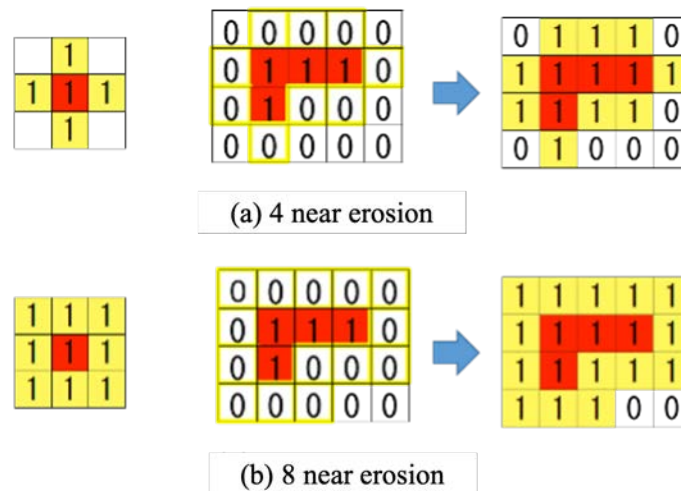


Figure 1.6: Erosion principal illustration

### 1.5.3 Binarization

In contrast to grayscale images, which are expressed in 256 shades from 0 to 255 with smooth shading, a binary image is one that is expressed in white (1) and black (0) by thresholding. This type of image is called a binary image. Binarization is one of the most crucial methods for image segmentation, which has a small amount of information and is

good at high-speed processing and low-cost processing. Compared to multi-level images, the theory of binarization is more systematic.

In this study, it was partially used to detect areas such as skin pores. In general, a certain threshold  $T$  (threshold) is set in the image, and if the pixel value of each pixel in the grayscale image is equal to or greater than  $T$ , the pixel is converted to 1, otherwise to 0.

In this study, it was partially used to detect areas such as skin pores. In general, a certain threshold  $T$  (threshold) is set in the image, and if the pixel value of each pixel in the grayscale image is equal to or greater than  $T$ , the pixel is converted to 1, otherwise to 0.

### **Fixed Threshold Method**

Based on the histogram of grayscale image and choosing the fixed threshold where the background and aim could be classified well, refers to as fixed threshold method. The formula is shown as follows (1.13). It is usually effective when there are not large scale of images and the capturing environment is certain.

$$B(x, y) = \begin{cases} 1 & \text{if } I(x, y) \geq T \\ 0 & \text{otherwise} \end{cases} \quad (1.14)$$

It is not sure the capturing environment in general research and adaptive threshold method is more popular.

### **Percentile Method**

When binarizing text materials such as books and newspapers, the area ratio of the foreground (the text part) to the white background part is roughly known. One of the static thresholding methods that can be used for such images is the percentile method. The Percentile Method is a method of binarizing an image by specifying the percentage (%) of the image area to be binarized in the total image area. The area of the whole image is  $S$ , and the area of the symmetrical figure is  $S_0$ , and the ratio of the group of pixels of interest

to the whole image is calculated as  $p$ .

$$p = \frac{S_0}{S} \quad (1.15)$$

If the pixel of interest is brighter than the background, the pixel is counted from the one with the larger luminance value, and if the background is brighter than the pixel of interest, the pixel is counted from the one with the smaller luminance value, and the number of pixels is set to  $N_0$ . If the number of pixels in the entire image is set to  $N$ , then  $p$  becomes the threshold, and each pixel can be binarized.

$$p = \frac{N_0}{N} \quad (1.16)$$

### **Mode method**

Mode method is always utilized when the histogram of grayscale image has apparent bimodal property. The minimum value between the two maximum values is usually chosen as the threshold.

### **Discriminant analysis method**

Discriminant analysis method is developed for normal images that need binarization. The Otsu's method is classified as a discriminant analysis method and is a method for setting a threshold value that maximizes the variance ratio. It is the most successful global thresholding method, which is effective when the difference in density between the object and the background has a certain magnitude. In the case of dividing an image into two classes, C1 and C2, we choose the threshold  $T$  such that the separation  $\eta(T)$  is maximized as shown below, where  $\sigma_B^2(T)$  is the interclass variance and  $\sigma_W^2(T)$  is the intraclass variance, which are given by

$$\eta(T) = \left[ \frac{\sigma_B^2(T)}{\sigma_W^2(T)} \right]_{max} \quad (1.17)$$

Intra-class variance:

$$\sigma_W^2 = \omega_1\sigma_1^2 + \omega_2\sigma_2^2 = \frac{1}{N} \left\{ \sum_{i \in S_1} (i - \mu_1)^2 n_i + \sum_{i \in S_2} (i - \mu_2)^2 n_i \right\} \quad (1.18)$$

Interclass variance:

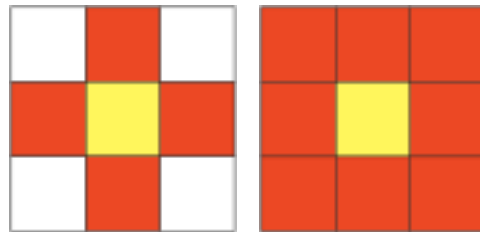
$$\sigma_B^2 = \omega_1(\mu_1 - \mu_T)^2 + \omega_2(\mu_2 - \mu_T)^2 = \frac{1}{N} \left\{ \sum_{i \in S_1} (\mu_1 - \mu_T)^2 n_i + \sum_{i \in S_2} (\mu_2 - \mu_T)^2 n_i \right\} \quad (1.19)$$

And the total variance  $\sigma_T^2$  is calculated by the formula:  $\sigma_W^2 + \sigma_B^2 = \sigma_T^2$ , where  $\omega_1$  and  $\omega_2$  are the occurrence probabilities of classes C1 and C2 (normalized number of pixels).  $\mu_1$  and  $\mu_2$  and  $\sigma_1^2$  and  $\sigma_2^2$  are the mean and variance of the concentration of pixels belonging to C1 and C2 respectively.

This method gives satisfactory results when the number of pixels in each class is close to each other [13, 14].

### 1.5.4 Labeling

Labeling is the process of assigning a unique name (label) to each graphic region (connected component). Normally, the labeling process assigns the same number to each pixel in the same region, starting from 1. The pixel value of the background is 0. This process makes it possible to treat each figure region separately and to examine the characteristics of each figure region. In general, four-connected and eight-connected neighborhoods are used for figure regions. Figure 1.7 shows each region. The yellow area indicates the pixel of interest and the red area indicates the neighboring pixels.



(a) 4 near neighborhood (b) 8 near neighborhood

Figure 1.7: Illustration of usual connected component

Labeling algorithms can be roughly classified into those using recursion and those using lookup tables, and in this study we used the lookup table method. The principle of the method is described below. In the method using the lookup table (LUT), the image is raster scanned twice. First, in the first scan (1-pass), a tentative label is assigned, and if different tentative labels are assigned in the same connected region, the connection between them is recorded in the LUT. Then, in the second scan (2-pass), we refer to the LUT and update it so that the labels in the same connected region become one. The specific procedure is described below.

### Step 1

Find an unlabeled pixel in the raster scan as an attention pixel, give a new label number to  $f_0$ , and move to the next attention pixel.

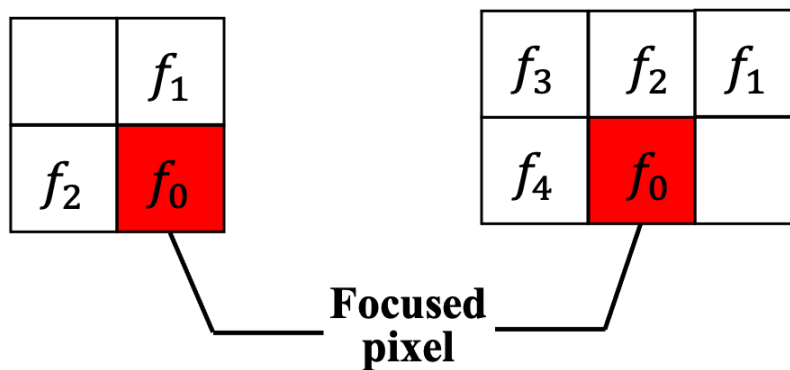


Figure 1.8: Example of usual connected component in labeling

### Step 2

If all of  $f_i$  ( $f_1, f_2$  for 4-connected pixels,  $f_1 \dots f_4$  for 8-connected pixels) in Fig. 1.8 are 0 (background pixels), give a new label to  $f_0$ . If there is one label number other than 0, the same label number is given to  $f_0$ . If there are two or more label numbers, give the smallest label number to  $f_0$ , and record the fact that they are the same connected components in the LUT. We move on to the next pixel of interest.

### **Step 3**

Repeat Step 2 (1-pass), and after the last scan, remove the unused label numbers that are integrated as the same connected region in the LUT, and update the label numbers so that there are no empty numbers.

### **Step 4**

The second scan is performed from the top-left corner, and the label numbers are reassigned so that each connected component has the same label in the LUT (2-pass).

## **1.5.5 Texture processing**

Texture refers to a pattern of regular fine shading. Based on textures, objects can be identified in an image and three-dimensional spatial perception (e.g., perspective) would be obtained. Therefore, attempts have been made to classify and divide regions based on textures in image processing. In such cases, some quantification that characterizes the texture is necessary, called texture features.

The obtained texture features can be treated as image features to be used in classification and region segmentation. For example, if the texture features of two regions in an image are the same, then the two regions are considered to have the same texture.



## **Chapter 2**

# **Quantitative Evaluation of Skin Micro-relief**

## 2.1 Introduction of skin Micro-relief

Human skin is the biggest organ in the body, which has a lot of characteristics and fundamental functions. On one hand, skin directly contacts the environment and can be influenced by chronological ages and environment changes, like humidity and temperature. On the other hand, skin can protect from Ultraviolet light. Skin is smooth, while the surface is not even due to the skin micro-relief, which is a pattern of the network consisting of furrows, polygonal forms, and pores. (Fig. 2.1). Skin micro-relief is one of the most important parameters of skin when mentioned to skin condition assessment and skin detection.

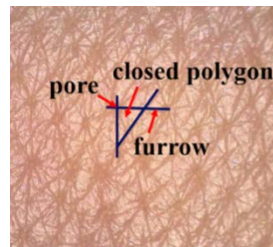


Figure 2.1: Skin micro-relief illustration

According to previous research, there are two main methods to evaluate skin micro-relief, which is using replica to get a copy of skin micro-relief, or using non-invasive devices to take the two-dimensional or three-dimensional images of skin micro-relief, like microscopy. These methods have their own merits. The replica can get the real and integrated topography of skin micro-relief, but it needs to cover the material over the assessment position, which is inconvenient and not easy to operate. M. Akimoto et al [15] used skin replica to get the copy of skin micro-relief, and then applied the image analysis method to measure the triangle area of the skin. Y. Masuda et al [16] also used skin replica, however, they measured skin micro-relief according to the result of Confocal laser scanning microscopy. Commonly, three-dimensional images gotten needs professional and expensive equipment, like the DermaTOP<sup>®</sup> [17]. Some two-dimensional images also need high resolution of the equipment, like skin microscopy. P. M. Maia Campos et al [18] explored the skin properties of oily skin, including skin micro-relief,

in which skin pores are counted with Visioface<sup>®</sup> equipment which could obtain high-resolution images. Y. Zou et al [19] proposed a method to evaluate skin micro-relief by segmenting skin closed polygons and calculating their average area from two-dimensional images. C. Bontozoglou et al [20] analyzed skin closed polygons and wrinkle length by skin capacitive images. C. I. Moon et al [21] developed a method to analyze skin micro-relief using the images taken by smartphone's camera, which has the weakness of low resolution and unstable environment influence. These methods are either complicated or need high resolution and expensive equipment. On the other hand, image processing algorithm development depends on the image type and resolution.

Skin micro-relief belongs to one series of texture. For the purpose of texture feature extraction from two-dimensional static images, analysis methods are categorized into seven classes: statistical way, structural way, transform-based way, model-based way, graph-based way, learning-based way, and entropy-based way [22]. Commonly used image analysis methods in skin micro-relief include grey level co-occurrence matrix (GLCM) [23–25], local binary pattern and variants(LBP) [26] which all belong to statistical way, and transform-based way comprising filter banks, Fourier transform, Gabor transform and so on. However, there's a common drawback among these methods, which has a shortage of relationship between processed results and visual results. Therefore, in this study, Tamura features algorithm is used as the skin surface analysis method, which is first proposed by H. Tamura et al [27] in 1978 and corresponded to visual perception. P. Howarth et al [28] compared the evaluation using GLCM, the Tamura features and Gabor filters, and it turned out Tamura features had a better visually meaningful result.

The related work is summarized in the Table 2.1. There are mainly two types for skin micro-relief evaluation by image processing, 2-dimensional image analysis (2DIA) and 3-dimensional image analysis (3DIA). By concluding the related works, it can be found out that for 2DIA, most researches only extract a few parameters related to micro-relief. While it has the advantage for 3DIA to extract the surface roughness, depth of pores and furrows. However, it is a big limitation for 3DIA to be used for normal people,

which usually needs huge and expensive devices and complicated operation. Therefore, a quantitative evaluation of skin micro-relief from 2D skin images is important.

Table 2.1: Related work of skin micro-relief evaluation

Approach	Image capture device	Image data	Algorithm	Extracted features
2DIA	VisioFace®	Full face photos with high resolution	Built-in algorithm with device	Pores [18], wrinkles, texture
	Handheld skin detector with LED and CCD	Partial skin image (6×8 mm)	Morphology transformation +Watershed transform [19, 21]	SPm [19] (average area of closed polygons)
	Smartphone's camera	Partial skin image		Wrinkle length, polygon number, and average area [21]
	Dermoscopy	Partial skin image	CNN+ Watershed transform [29]	Wrinkle length, width, polygon number, and area [29]
	Epsilon E100 capacitive imaging system	Capacitive partial skin image	Grey-Level Co-occurrence Matrix(GLCM) [23, 30] Vincent & Soille segmentation algorithm [30]	Skin furrow orientation; skin polygon number and surface area
3DIA	Replica+ confocal laser scanning microscopy	Partial skin image	ISO 25178; Gaussian filter [16]	Surface roughness and area, Furrow length, width, and depth Pore area, and polygon number [16]
	DermaTOP®	Partial skin image	Built-in algorithm with device	Roughness, wrinkle depth, pore depth

This study aims to evaluate skin condition using skin micro-relief images quantitatively and comprehensively. We establish an image analysis method to extract the skin micro-relief related parameters, assess the most essential parameter among them and calculate the relationship. Also, we apply the method in researching age-related change.

## 2.2 Methods and materials

### 2.2.1 Image capture device

The skin micro-relief image is captured at the cheek by the microscope called SmartSkin-Care® (IT Access Co., Ltd, Yokohama, Japan), with a camera, white LED lamps and UV-LED lamps (Fig. 2.2). The operation consists of four steps. First of all, the microscope should connect the application in the smartphone or tablet and connect the Wi-Fi to

use the cloud service. Secondly, make sure the light source and capture mode are appropriate since it has 4 modes to measure skin conditions, including skin micro-relief, color, porphyrins and sebum. After all the preparation been checked, the microscope should contact the skin vertically and softly so that the micro-relief image could be taken successfully. At last, captured image could be displayed and exported. The area evaluated is 12 mm × 9 mm and the resolution of the image taken is 1280 × 960 pixels, with 23.7× magnification.

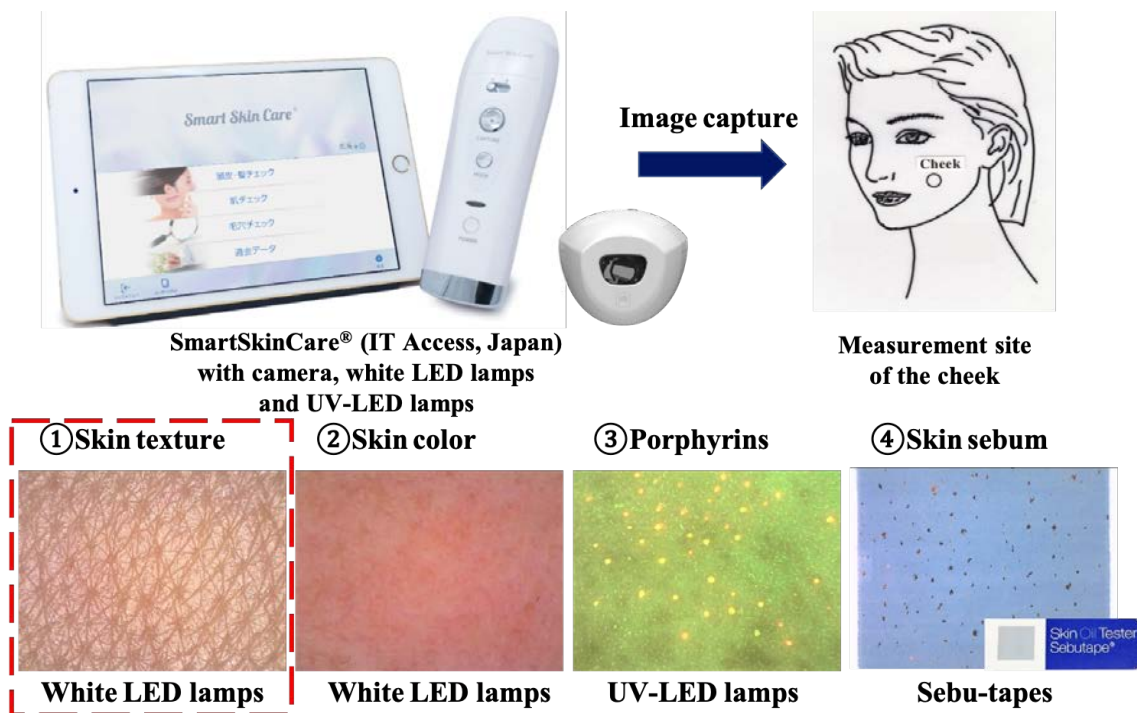


Figure 2.2: Skin image capture operation [3]

## 2.2.2 Skin micro-relief image analysis methods

### pre-processing

Before image analysis, it is essential to pre-process the image avoiding the influence of noise and light, since two-dimensional skin micro-relief images are taken by the microscope, which is easily affected by the surrounding environment.

In the pre-processing step, the region of interest (ROI) is chosen as the center part of the original image, whose size is 800 × 800 pixels. Then B component image from RGB matrix is extracted as the basic image due to its sharpness. Light uniform algorithm was

applied according to the method proposed by Q. Zhang et al [31], which has 4 steps, (a) calculate the global average luminance ( $Lum_g$ ) of the grayscale image; (b) separate the grayscale image into sub-blocks and calculate their average luminance ( $Lum_l$ ) and gain the luminance difference matrix D, which is calculated by the formula:

$$\Delta_{lum} = Lum_l - Lum_g \quad (2.1)$$

(c) Interpolation algorithm for matrix D until element numbers equal to  $800 \times 800$ ; (d) Merge matrix D and grayscale image into a new image, whose size is  $800 \times 800$  pixels. Finally, the uniformed grayscale ROI is gotten (Fig. 2.3).

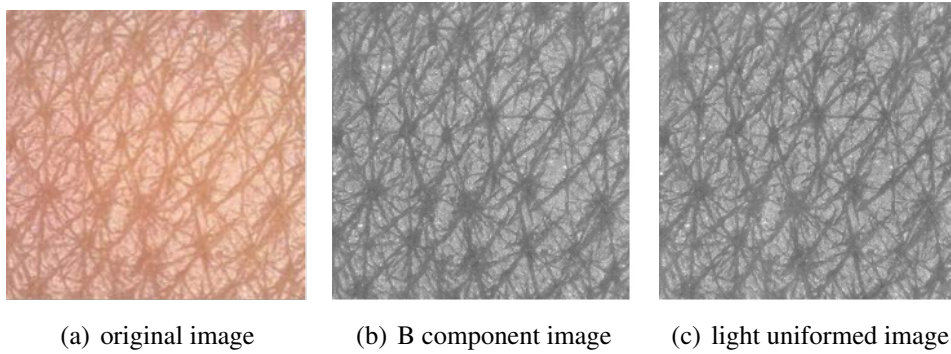


Figure 2.3: Pre-processing illustration

### 2.2.3 Skin parameters extraction and calculation

As shown in Fig. 2.4, 4 aspects and 11 skin parameters are separated from the original image with different image processing algorithms according to the properties of skin micro-relief, which are skin surface (coarseness, contrast and directionality), skin pores (number, area and average area), skin furrows (length and width) and skin closed polygons (number, area and average area). The details of processing algorithms are shown in the results part.

### 2.2.4 Study population and design

In this chapter, a total of 163 healthy Japanese female volunteers between 0 and 70 years old were enrolled. These females were divided into 6 groups: (a)0-10 years old, (b)20-30

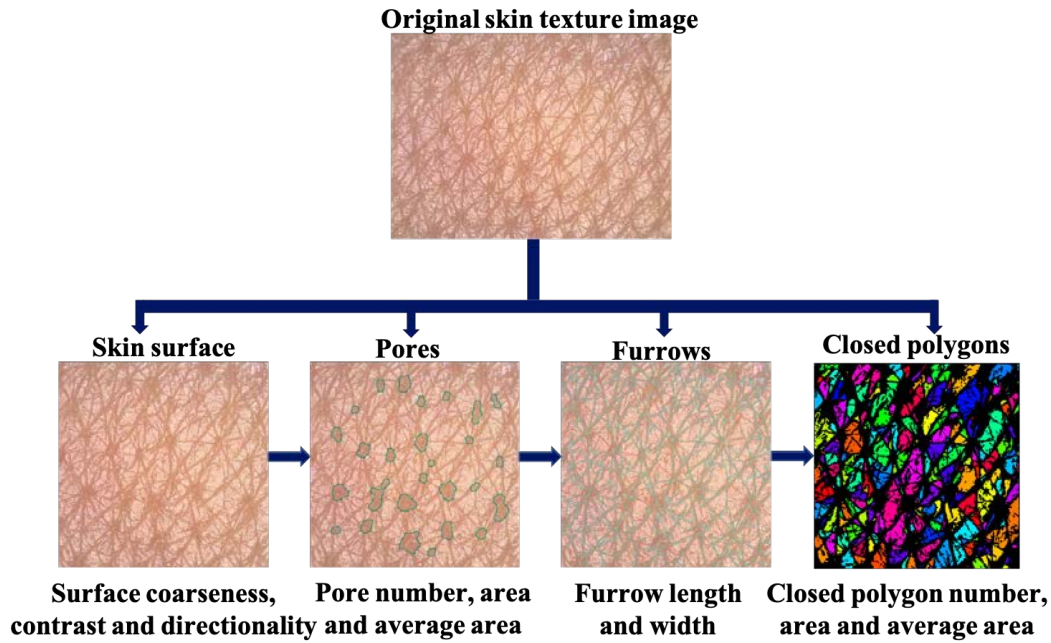


Figure 2.4: Skin micro-relief evaluation flowchart

years old, (c)30-40 years old, (d)40-50 years old, (e)50-60 years old, and (f)60-70 years old. The Subjects number and mean age of each group are shown in Table 2.2. The study was conducted according to the principles of the Declaration of Helsinki. Informed consent was obtained from all the subjects after the subjects were provided a complete explanation of the protocol. In the case of the child group, informed consent was obtained from their parents. Images were captured on the cheek of volunteers without any makeup.

Table 2.2: Subject information for skin micro-relief evaluation

Age group	0s	20s	30s	40s	50s	60s	Sum
Number	21	31	29	29	32	21	163
Mean age	5.10± 0.62	24.90± 1.19	34.86± 0.58	44.86± 0.74	53.69± 1.75	64.86± 1.15	

### 2.2.5 Statistical Analysis

SPSS 21.0 (SPSS Science, Chicago, IL) software was used for all statistical analyses. All data were expressed as the mean  $\pm$  SD (standard deviation). Pearson correlation coefficients were assessed between the age and all parameters. The linear fitting model was applied to analyze the trends of parameters with age. The correlation among all

parameters was calculated by Pearson correlation coefficients, in which lower than 0.3 representing weak correlation, 0.4-0.6 representing mediate correlation and higher than 0.6 representing high correlation. Pearson correlation coefficients was two-tailed with the following significance levels:  $p < 0.05$  and  $p < 0.01$ .

## 2.3 Quantitative evaluation results of skin micro-relief

### 2.3.1 Skin micro-relief features extraction

Two-dimensional skin micro-relief image was preprocessed first in order to analyze skin surface features and extract pores, furrows and closed polygons of the skin surface.

#### Skin surface

The flowchart of skin surface extraction is shown in Fig. 2.5. It's worth noting that for the purpose of evaluating the skin surface, Tamura features algorithm was applied to extract skin surface features, including coarseness, contrast and directionality, which are the most commonly used features calculated by Tamura features algorithm.

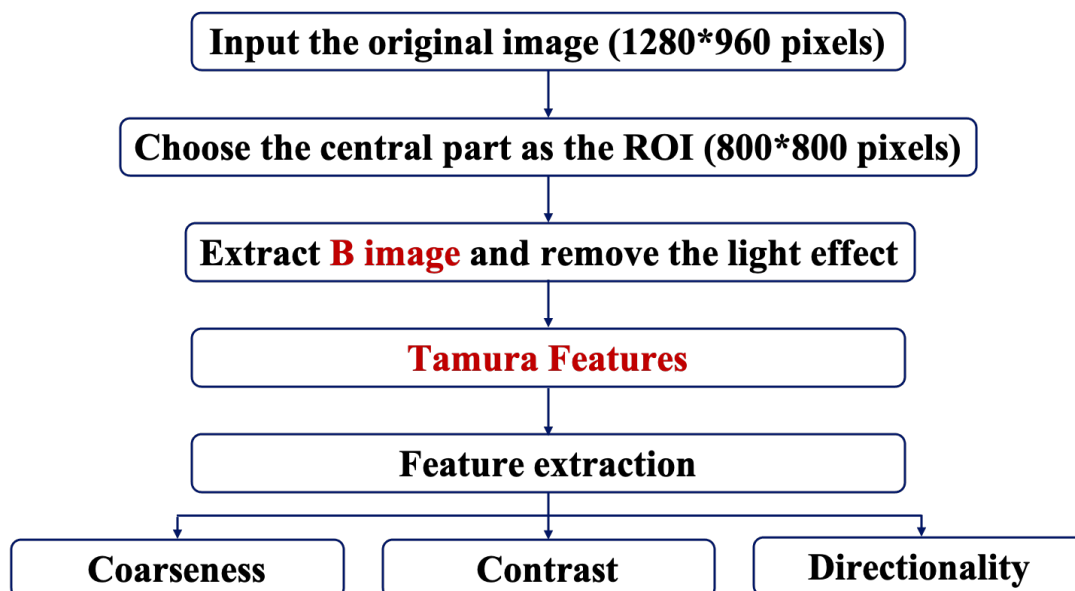


Figure 2.5: Flowchart of skin surface extraction

Tamura features algorithm is proposed by H. Tamura et al [27] to correspond to visual perception. For an image  $f$  with size  $m \times n$ , and the pixel at location  $x$  and  $y$  as  $f(x, y)$ .



(a)Coarseness: The bigger its element size and/or the less its elements are repeated, the coarser it is felt.

STEP 1. take averages of every point over neighborhoods, the size is  $2^k$ .

$$A_k(x, y) = \sum_{i=x-2^{k-1}}^{x+2^{k-1}-1} \sum_{j=y-2^{k-1}}^{y+2^{k-1}-1} f(i, j)/2^{2k} \quad (2.2)$$

STEP 2. take differences of horizontal and vertical sides for each point.

$$E_{k,h}(x, y) = |A_k(x + 2^{k-1}, y) - A_k(x - 2^{k-1}, y)| \quad (2.3)$$

$$E_{k,v}(x, y) = |A_k(x, y + 2^{k-1}) - A_k(x, y - 2^{k-1})| \quad (2.4)$$

STEP 3. At each point, pick the best size which gives the highest output value.

$$S_{best}(x, y) = 2^k; E_k = E_{max} = \max(E_1, E_2, \dots, E_h) \quad (2.5)$$

STEP 4. take the average of  $S_{best}$  over the image.

$$F_{crs} = \frac{1}{mn} \sum_i^m \sum_j^n S_{best}(i, j) \quad (2.6)$$

(b)Contrast: The larger the range of gray-scale values, the higher the contrast is. Gray-scale “histogram flattening” transformation is said to be used for the purpose of removing the effects of unequal overall brightness and contrast in the original images.

$$F_{con} = \sigma / (\alpha_4^{1/4}) \quad (2.7)$$

$$\alpha_4 = \mu_4 / \sigma^4 \quad (2.8)$$

$\sigma^2$ : standard variance of gray-levels;  $\mu_4$ : the fourth moment about the mean;  $\alpha_4$ : the kurtosis as the index of polarization.

(c)Directionality: Directionality in an original picture usually can be preserved in its Fourier power spectrum, but it is time-consuming. This method utilizes the fact that

gradient is a vector, so it has both magnitude  $\Delta G$  and local edge direction  $\theta$ .

$$|\Delta G| = (|\Delta_H| + |\Delta_V|)/2 \quad (2.9)$$

$$\theta = \tan^{-1}(\Delta_V/\Delta_H) + \pi/2 \quad (2.10)$$

$\Delta_H$ :horizontal differences measured by  $3 \times 3$  operator 1.

$\Delta_V$ :vertical differences measured by  $3 \times 3$  operator 2.

$$H_D(k) = N_\theta(k) / \sum_{i=0}^{n-1} N_\theta(i), \quad k = 0, 1, \dots, n-1 \quad (2.11)$$

operator 1:

-1	0	1
-1	0	1
-1	0	1

operator 2:

1	1	1
0	0	0
-1	-1	-1

$H_D$ : the desired histogram obtained by quantizing  $\theta$  and counting the points with  $\Delta G$ .

$$F_{dir} = \sum_p^{n_p} \sum_{\phi \in w_p} (\phi - \phi_p)^2 H_D(\phi) \quad (2.12)$$

$n_p$ : the number of peaks;  $\phi_p$ :  $p^{th}$  peak position of  $H_D$ ;  $w_p$ : the range of  $p^{th}$  peak between valleys.

## Skin pores

In an attempt to calculate skin pore number and area, Otsu's method [32] was applied primarily to choose a threshold from the grayscale image and convert it to a binary image. Then close and open morphology transforms were combined to identify skin pore candidates using a disk-shaped structuring element, whose radius is 12. From the inverse image of the skin pore candidates, areas smaller than 500 pixels and bigger than 8000

pixels were eliminated and those connected to image border were also removed. Finally, real pores were identified and features of pores were calculated, which are pore number, area, and average area (Fig. 2.6).

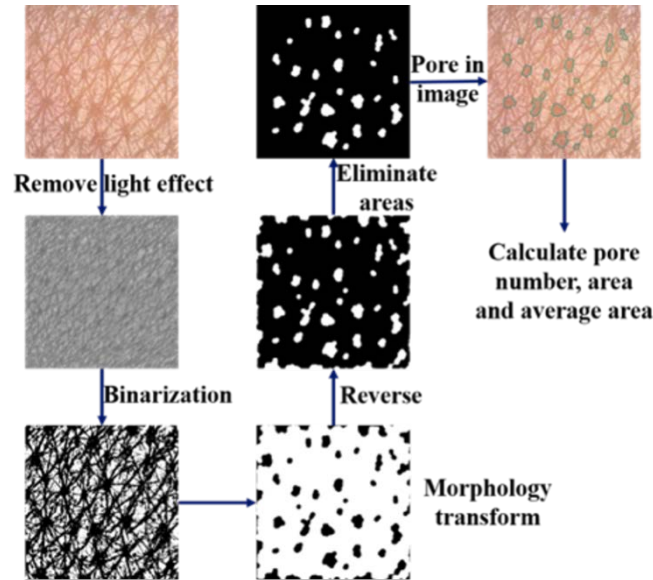


Figure 2.6: Flowchart of skin pore classification

### Skin furrow

The flowchart of skin furrow segmentation is shown in Fig. 2.7. Watershed transform was used as the main algorithm to extract skin furrow. Due to the properties of the Watershed transform, some pre-processing steps are necessary in case of over-segmentation.

Contrast limited adaptive histogram equalization (CLAHE) was used to enhance the details of the image, which caused some noise also remarkable. Therefore, Gaussian filter as the linear smoothing filter and median filter as the non-linear smoothing filter were applied to remove the noise. For the purpose of obtaining the huge contrast image between furrows and closed polygons, the top-hat and bottom-hat transforms were operated orderly and the top-hat image was added into the median filtered image and the bottom-hat image was subtracted from it. H-maxima transform, Extended maxima transform and morphology reconstruction were applied to acquire the binary image. Distance transform and watershed transform were used to get the furrow candidates. Identified pores were eliminated and skeleton pruning was used to suppress the extra lines other than furrows.

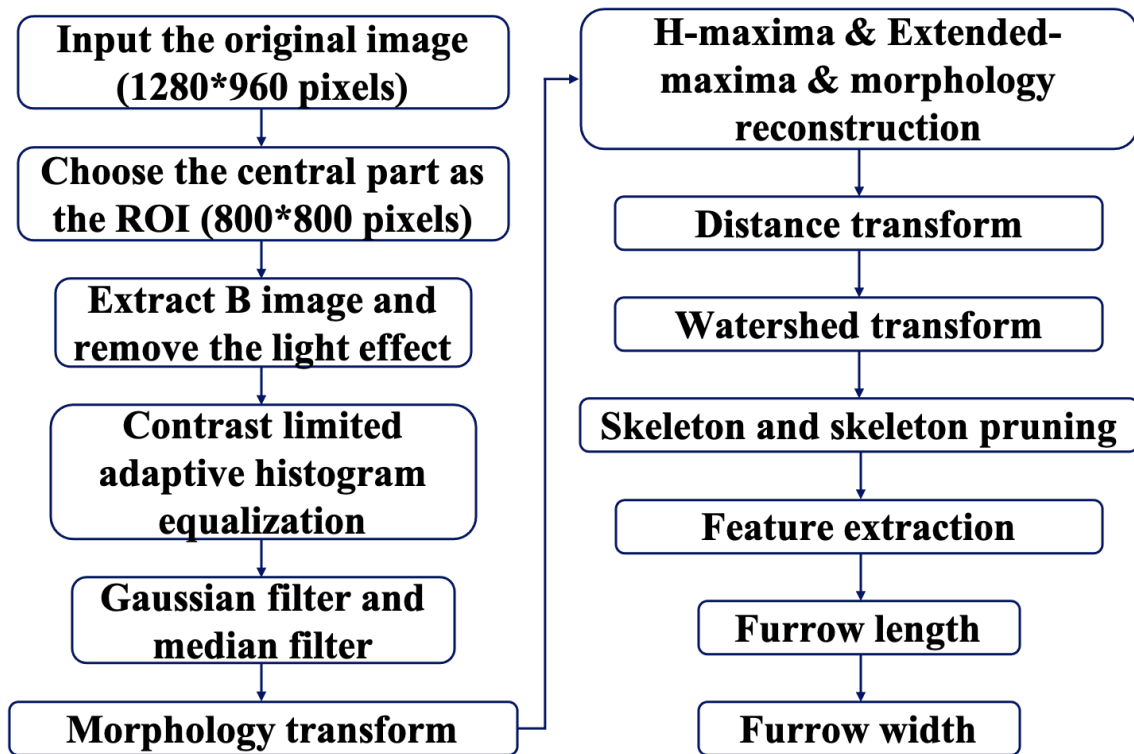


Figure 2.7: Flowchart of skin furrow extraction

Skeleton operation in morphological transform was used 5 times to get a suitable furrow area. In the end, furrow length was calculated and furrow width was got by furrow area dividing by furrow length (Fig. 2.8).

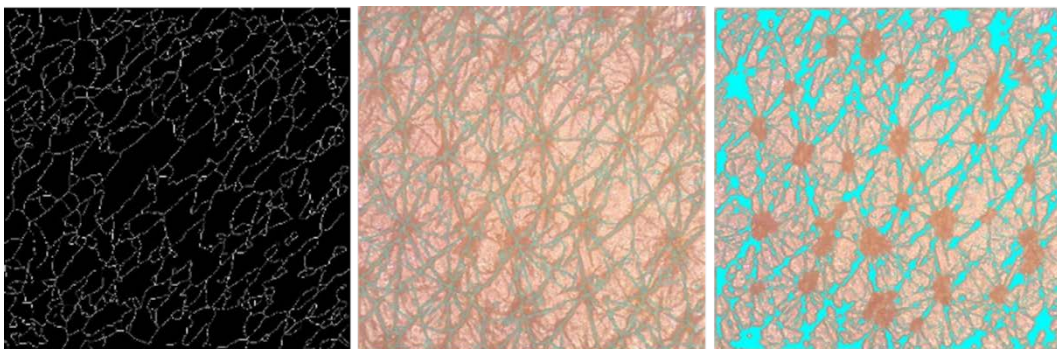


Figure 2.8: Skin furrow extraction illustration, (a) watershed transform result; (b) skin furrow extraction; (c) skin furrow area extraction without pores

### **Skin closed polygon**

Since skin furrow has been extracted, skin closed polygons were extracted by reversing furrow image with labeling (Fig. 2.9). Closed polygon number, area, and average area were calculated.

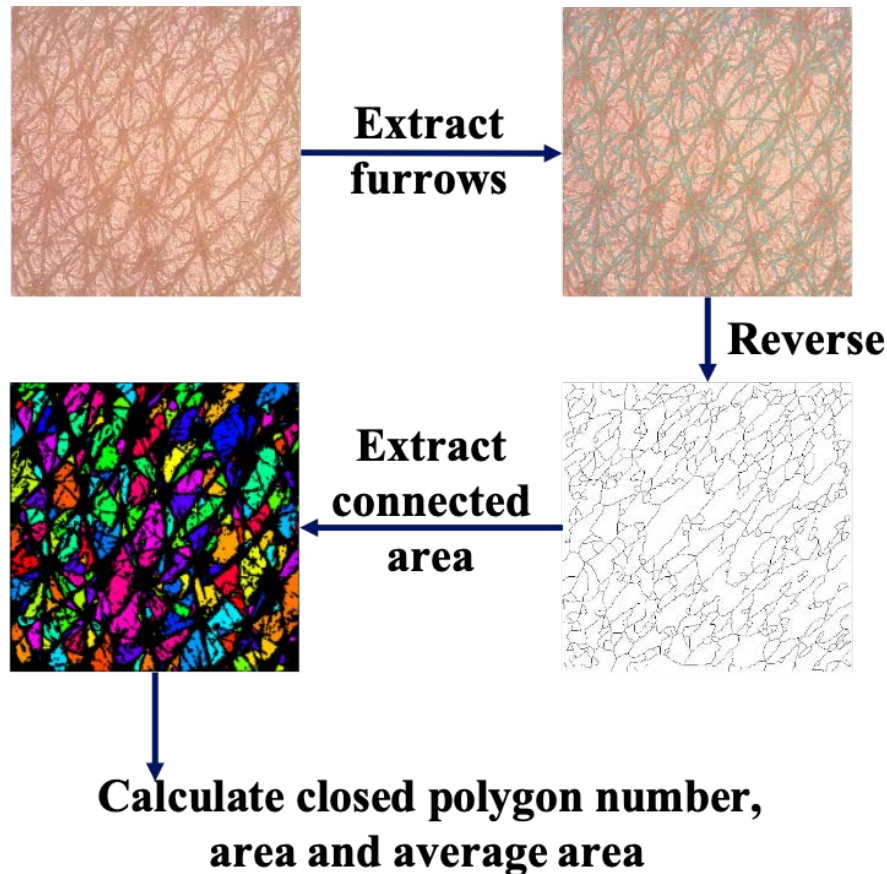
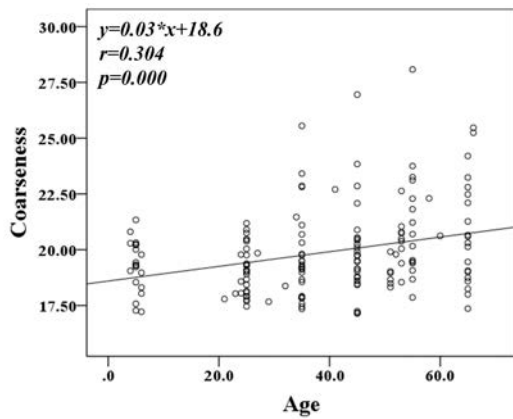


Figure 2.9: Flowchart of skin closed polygon extraction

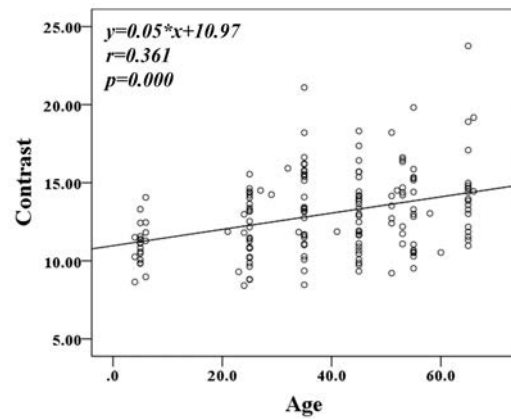
### **2.3.2 Age-dependent changes with skin micro-relief**

Age-dependent changes in the skin surface, pore, furrow, and closed polygon were examined and results are shown in Fig. 2.10. In the skin surface, all parameters increased with age, especially coarseness and contrast with significant differences. Skin pore number, area, and average area increased with age with significant differences, which indicates that skin pores become larger and more obvious with age went on. Skin furrow length decreased with age, while width increased with age. Skin closed polygon number decreases

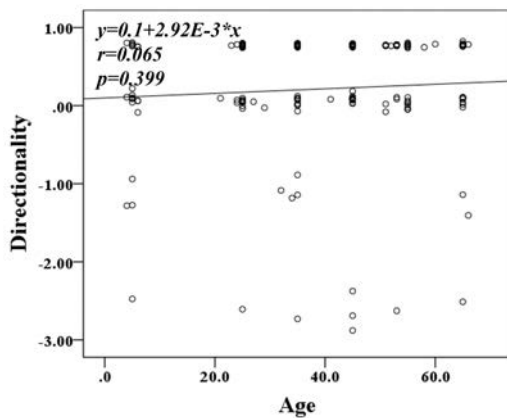
with age, however, their area and average area increase with age. According to the coefficient of correlation between age and all parameters, the relevance rank is contrast > closed polygon area > furrow length > coarseness > pore average area > furrow width > pore area > closed polygon number > closed polygon average area > pore number > directionality.



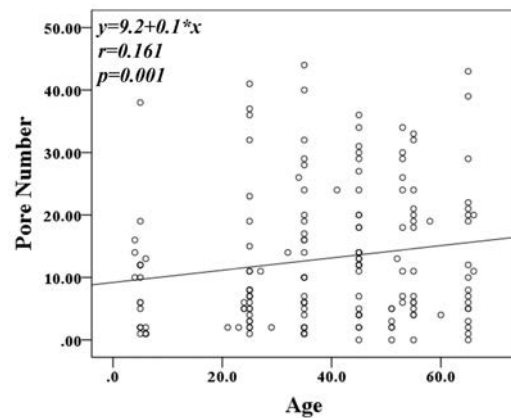
(a) skin surface coarseness



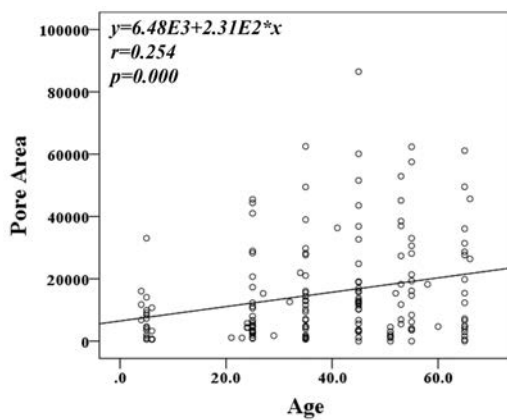
(b) skin surface contrast



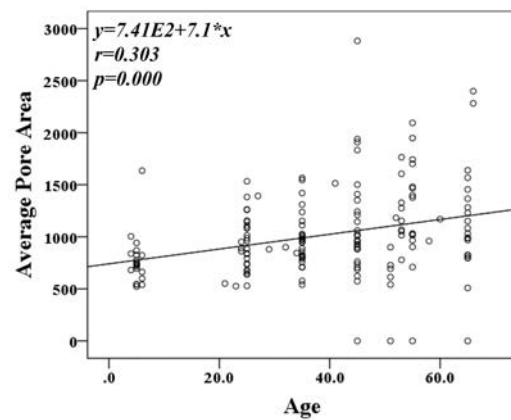
(c) skin surface directionality



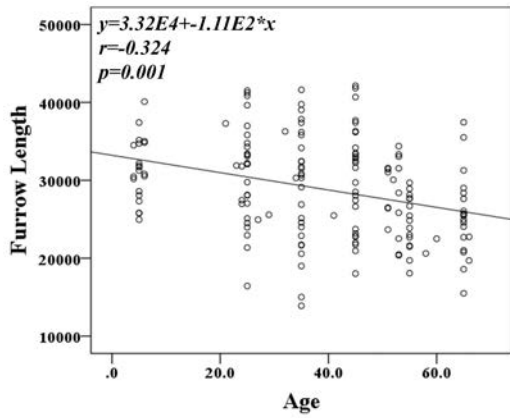
(d) skin pore number



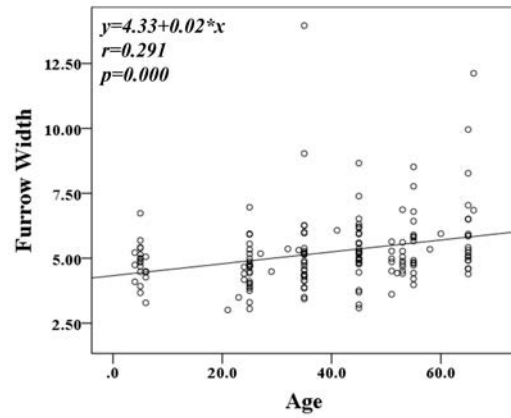
(e) skin pore area



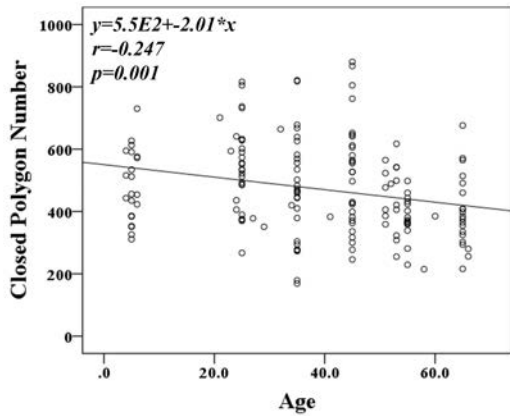
(f) skin pore average area



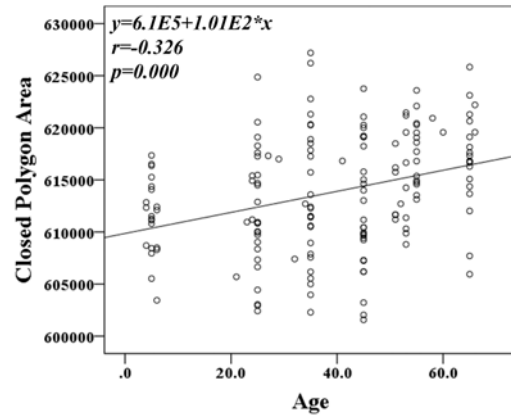
(g) skin furrow length



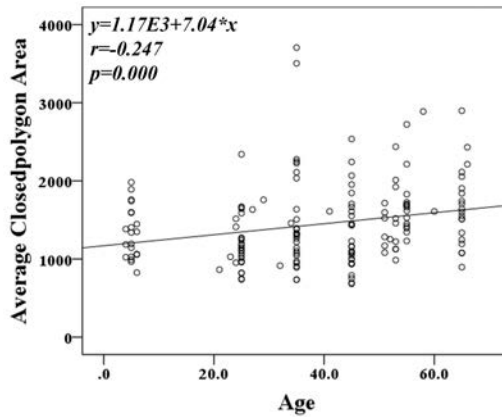
(h) skin furrow width



(i) skin closed polygon number



(j) skin closed polygon area



(k) skin closed polygon average area

Figure 2.10: Skin micro-relief parameters changes with age

### 2.3.3 Correlation among skin micro-relief related parameters

The correlation among all parameters is shown in Fig. 2.11, in which surface directionality did not have any correlation with other parameters. In contrast, pore average area and furrow width have the most correlation with others, which indicated that these two

parameters should be improved first if people want to refine their skin micro-relief conditions. In addition, the pore area and pore average area have a strong correlation with skin coarseness, which implies the larger pore area is, the worse skin coarseness is.

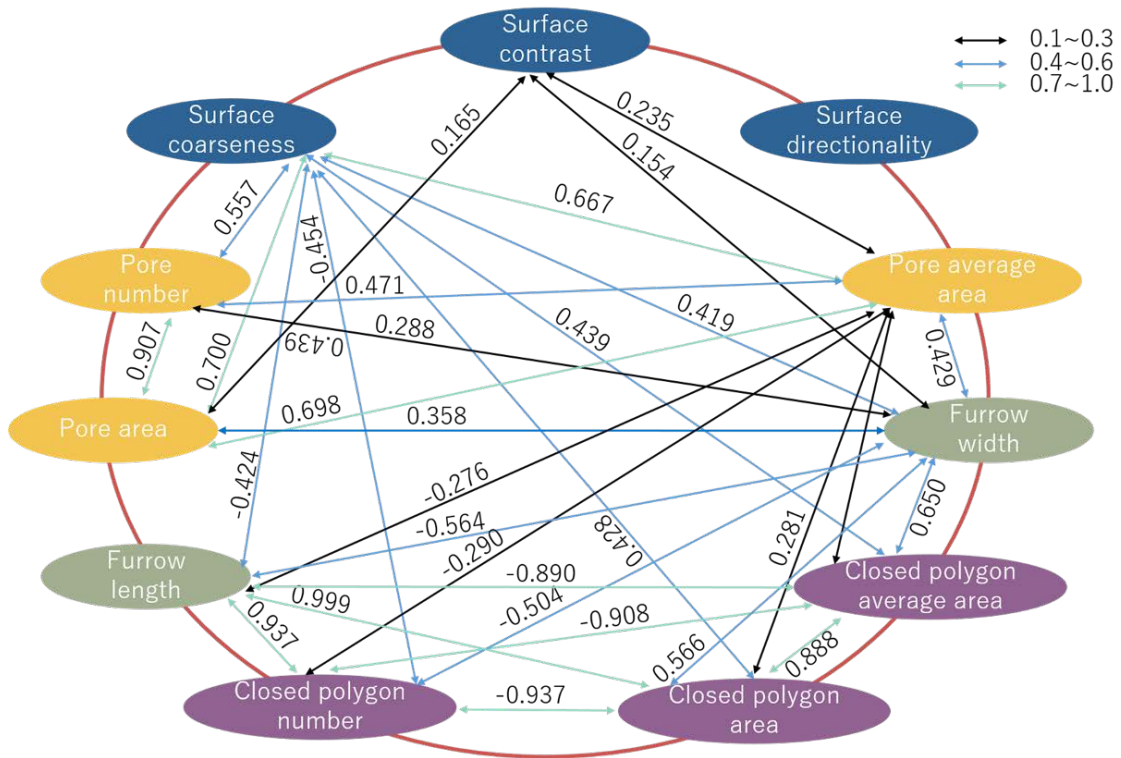


Figure 2.11: Relationships among parameters with significant differences: black lines represent the weak correlation; blue lines represent the mediate correlation; green lines represent the high correlation

## 2.4 Discussion

In this study, we proposed a skin micro-relief condition evaluation method by extracting skin pores, furrows, and closed polygons and analyzing the features of the two-dimensional image taken from the cheek position by the microscope. On top of that, we employed this method to evaluate age-related changes and explored the relationships among parameters. All-sided indexes of skin micro-relief, including skin surface, pores, furrows, and closed polygons, been extracted and analyzed into 11 precise quantitative parameters from one image is a key point of skin micro-relief assessment.

As mentioned in the literature review, there are many algorithms and parameters could be used to evaluate skin micro-relief condition. M. Uchida et al [33] used a short line



matching method to extract skin furrows and assessed the changes as piloerection becoming weak in order to estimate emotion. C. I. Moon et al [21] and Y. Zou et al [19] also used the watershed transform to extract skin closed polygons, but they did not extract skin pores, which could also affect skin micro-relief condition evaluation.

P. M. Arabi et al [25] compared GLCM and pixel intensity methods for skin texture analysis, and they believed pixel intensity is more useful and accurate. While in this research, considering about the image type and resolution, and for the purpose of fitting human visual perception, Tamura features algorithm was applied in the study.

As we have known, the older human is, the rougher skin is. However, the concrete mechanism is still under exploration. In the study, we found out that as pores getting more obvious, furrow length decreasing, furrow width becoming larger, and small closed polygons merging into large ones, the skin is seen rougher than before. H. J. Jung et al [34] also performed that pore counts increased with age and the increment was huge between 30s and 40s years, while there is no significant difference by gender. S. J. Lee et al [35] reviewed the major causes of pores enlargement, which includes high sebum excretion, decreased elasticity around pores and increased hair follicle volume. With age increasing, skin elasticity decreases significantly, which results in pore number and area increasing found in this study.

Skin furrow includes primary furrows (20-200 $\mu$ m) and finer secondary furrows (30-70 $\mu$ m). these furrows construct the triangle-shaped closed polygons originally. With age went on, especially the position exposed by sun, such as cheek, photo-aging also causes severe changes in the skin, like the lower expression of collagen production [36]. D. H. Kim et al [37] also found out that skin furrow width of forearm and hand increased with age with dermoscopy and SEM. It can be understood that primary furrows become deeper and this phenomenon reduces the number of skin closed polygons and enlarges the area of skin closed polygons.

For the correlation among skin micro-relief related parameters, the correlation is strong between skin coarseness and skin pore area. Therefore, it is considered that all

parameters deteriorating caused skin roughness, however, the major factor could be attributed to pores enlargement, which provides further support for the skin condition comparison according to age, gender or anatomic sites.

Compared to conventional methods, it has more potential to establish evaluation standards of skin surface micro-relief using the proposed method in the study. Using the same device makes sure all images have same magnification of skin and resolution. In addition, proposed algorithm divides skin surface micro-relief into four sections quantitatively, especially the objective and quantitative surface evaluation which was usually decided by human vision, such as roughness.

## **2.5 Conclusion**

This project was undertaken to design an objective and quantitative method from two-dimensional skin images using image analysis technology to evaluate skin micro-relief conditions comprehensively. The study confirmed skin micro-relief conditions get worse with age increases. For skin coarseness, skin pores enlargement is the most important factor. It has been proved the method proposed is an effective tool to evaluate skin aging. It is possible to assist dermatologist to diagnose and assess the therapeutic progress using the proposed method, such as eczema, which usually occurs adjoint sandpaper-like texture. In other words, this evaluation method of skin micro-relief from 2D images can be a powerful tool for cosmetic developers assessing skincare products, especially for skin anti-aging products. And it could also be used for customers to trace their skin changes.

The novelty of skin micro-relief includes most related features are extracted, including not only the surface status, but also the components of micro-relief. Furthermore, the cause of surface features is also revealed that coarseness is mostly influenced by pores. The method we proposed is the combination of Tamura features and morphology transform, which not only matches the relationship of human vision and image feature, but also explain the primary principle of it, such as coarseness influenced by pores, and contrast representing furrow depth.

In the future, the results of this method should be compared with visual perceptions. More skin parameters should be involved to evaluate skin conditions comprehensively.

## **Chapter 3**

# **Quantitative Evaluation of Skin Color**

### 3.1 Introduction of skin color

Skin is the largest and most easily observed organ of the human body and plays a significant role in the assessment of human age, beauty, attractiveness, and health. In particular, facial skin color distribution significantly influences the perception of age and attractiveness of female faces [38]. The major factor impacting skin color is genetic background, and to some degree, different ethnic groups are classified on account of skin color [39]. For East Asian people, whose skin tone phenotype is yellowish, skin color that is even, fair and glossy is perceived as beautiful and healthy. East Asian people, particularly Chinese and Japanese people, advocate for white and translucent skin because brightening products have been prominent from ancient times to modern times, as seen in the current cosmetic industry [40]. Skin color may also differ within the same ethnic group due to climate and geographic location, while related studies are few, and this phenomenon has not been thoroughly investigated. Most studies have discussed facial skin color variation according to age, gender, and anatomical site in a specific ethnic group. For this reason, our study chose Beijing and Tokyo as the assessment locations in East Asia, both of which are the capitals of their respective countries and are famous worldwide for their fashion industries.

Visual assessment by dermatologist is the main method of skin color evaluation, which depends not only on the subjective perception of color by the observer but also on the nature of the illumination and on the geometric position of the observer in relation to the skin position [41]. With the development of technology, several objective methods have recently been developed for skin color assessment. Tristimulus CIE colorimetry was built with the CIE 1976  $L^*a^*b^*$  color system and has been widely used for the collection of quantitative and objective data.  $L^*$ ,  $a^*$  and  $b^*$  as well as individual typology angle (ITA) and hue angle calculated using  $L^*$ ,  $a^*$  and  $b^*$  are efficient for detecting subtle differences in skin color within the same ethnic group.

Regarding the age-related variation in facial skin color, L. Machkova et al [42] observed that there is a significant negative correlation between age and ITA, while erythema

levels increase with age up to 50 years old in Caucasian women, and when menopause takes place, these levels decrease. J. de Rigar et al [43] compared age-based skin color changes in four ethnic groups and reported that a clear, significant darkening of the skin with age was found in four ethnic groups, while skin yellowing was shown in Chinese females. Chinese and Japanese people belong to the same Asian ethnicity, and they show similar skin color characteristics but differ in their living conditions. Plenty of reports focus on the skin color in these populations; however, a thorough investigation of these skin color differences has not been conducted. Moreover, skin whitening and anti-aging are the top issues for East Asians and related cosmetic products are best-sellers in this region.

The most studied field in conventional skin color measurement is color assessment, which is achieved either by reflectance spectrophotometry of the optical spectrum of visible light reflected by the skin or by a reflectance tristimulus colorimeter, which is in line with the CIE recommendations. These methods provide quantitative information on the skin color but their application is limited to a small surface area. The contact pressure, size of the measured field and measurement geometry can affect the results. The use of these devices involves contact between the aperture of the probe and the examination area, which eliminates the influence of background illumination on the measured color of the area. This contact is the source of several potential errors and limitations.

To avoid these constraints, we studied the development of several applications and performed an imaging analysis, as is commonly applied in aesthetic dermatology to assist in the diagnosis of erythema and pigmented skin treatment. This technique allowed us to study skin areas of various sizes and to take measurements without any contact with the skin. We would also like to contribute to the development of a skin color diagnostic support technology in cosmetic dermatology.

In this study, we investigated 5 skin color parameters of the cheek and compared the skin color in East Asian populations aged 18 to 50 (Fig. 3.1). The aim of the investigation was revealing baseline data for East Asians and to obtain skin color trends with age

to provide useful advice for both cosmetic companies and consumers. In addition, we proposed how the understanding of the process of image formation enables the derivation of diagnostically important facts about skin color from images. This information is used for the clinical diagnosis of erythema and pigmented skin. The algorithms were used to quantify the hue angle and individual typology angle (ITA).

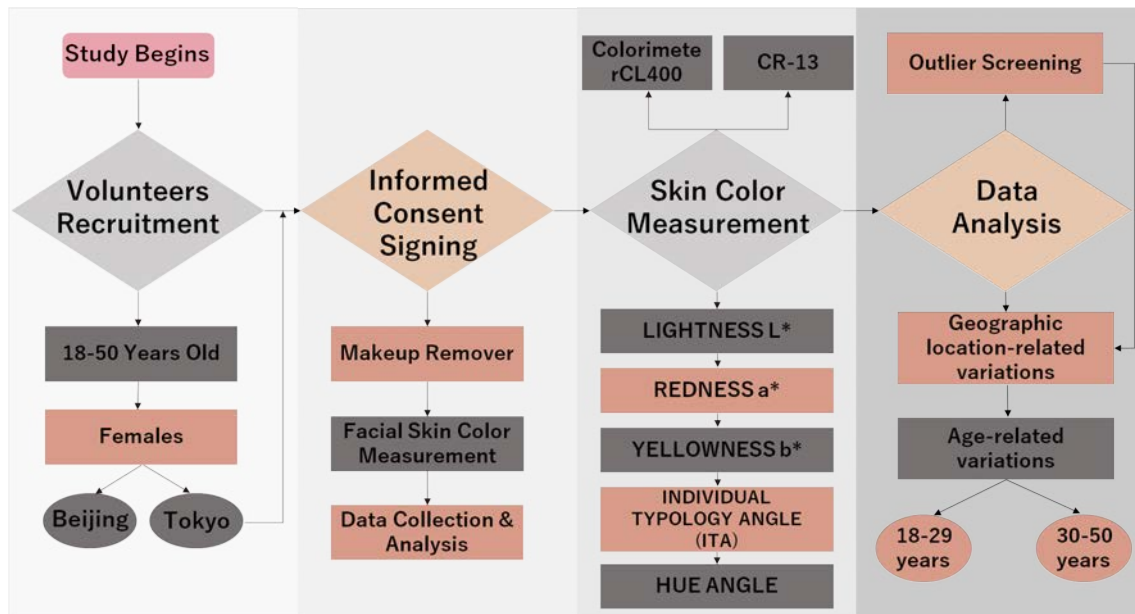


Figure 3.1: Flowchart of skin color measurement

## 3.2 Methods and materials

### 3.2.1 Study population

In this study, a total of 445 healthy female subjects between 18 and 50 years old were enrolled, including 362 Chinese women from Beijing, China and 83 Japanese women from Tokyo, Japan. These females were divided into two groups: 18-29 years old and 30-50 years old. Subjects who met the following criteria were excluded: (a) those with skin disease, (b) those who were pregnant, (c) those with sensitivity to sunlight, (d) those administered anti-immunologic medicines within the last 3 months, (e) those who received any forms of phototherapy within the last 6 months, (f) and those with skin lesions at the

measurement sites. The study was conducted according to the principles of the Declaration of Helsinki. Informed consent was obtained from all the subjects after the subjects were providing a complete explanation of the protocol.

For exploring skin color measurement, 91 healthy Japanese female volunteers of 18-60 years of age were included in the present study. The skin color of the forehead, cheek, and jaw was collected. Subjects undergoing either local or systemic treatment were not admitted. The subjects were informed of the details of the experimental process and their consent was obtained before the measurements were obtained. The study was performed at Tokyo University of Technology in Hachioji-city, Tokyo (Japan).

### **3.2.2 Design of study population**

Chinese subjects lived in Beijing (north latitude  $39^{\circ}56'$ , east longitude  $116^{\circ}20'$ ) for at least 1 year. Japanese subjects lived in Tokyo (north latitude  $35^{\circ}63'$ , east longitude  $139^{\circ}34'$ ) for at least 1 year. The measurements were performed in autumn to eliminate the influence of seasons and climates. Volunteers were required to remove their makeup and wait up for 20 minutes before the measurements. Skin color parameters were measured at the left cheek.

### **3.2.3 Skin color measurement**

Skin color parameters were measured according to the CIE-L\*a\*b\* color system, which includes brightness L\*, redness a\*, yellowness b\*, individual typology angle ITA, and hue angle. In Beijing, the parameters were measured by a Colorimeter CL400 (Courage Khazaka Electronic GmbH, Cologne, Germany), and in Tokyo, the parameters were measured by a CR-13 (Minolta, Osaka, Japan). During the measurements, the device was placed gently and fully on the measured area to avoid any pressure or outside light. The data for all parameters were repeated three times, and the mean values represented the facial skin color of each subject.

On the other hand, the re-Beau® (JMEC Co., LTD, Tokyo, Japan) imaging system consists of white LED lamps to illuminate the surface and a digital single-lens reflex



camera. The camera contains 4752 (horizontal)  $\times$  3168 (vertical) effective picture elements (pixels). Basic operations, such as capturing are performed on a tablet PC via a Wi-Fi connection. A fiber input multichannel spectrometer (USB2000+, Ocean Optics, U.S) is used to measure the spectral characteristics of the white LED lamp built into the re-Beau®. The spectral intensity is measured at intervals of 5 nm in the measurement wavelength range from 380 nm to 780 nm. A Color Reader CR-13 (Minolta, Osaka, Japan) was used for comparison. The optical system of the CR-13 consists of a tungsten halogen lamp, which is used to illuminate the surface, and six photodiodes.

### **3.2.4 skin color measurement from digital images**

The quantitative assessment of properties in an imaging analysis requires the subject to be in a steady position in relation to the camera and lighting during image acquisition. We used an ophthalmic table to fix the subject's face, in order to avoid any vertical or horizontal displacement. The camera was placed in the frontal position. On the image, we defined some guide marks composed of horizontal and vertical lines. These guide marks are linked to the initial image and are recalled for every new acquisition of the same subject.

The procedure of the experiment is as shown in the flowchart of Fig. 3.2. Images of faces were captured and saved in RGB format.

The conversion of RGB image pixel values to CIE XYZ tristimulus values of the color displayed on the monitor can be achieved using the next process. The images are displayed on a monitor that conforms to sRGB and which is controlled by the computer. The sRGB color space has been characterized by the International Electrotechnical Commission (IEC 61966-2.1). In the display, the relationship between the input value (digital value of RGB) and the output value (luminance of the image) is a nonlinear characteristic. Correction from nonlinear characteristics to linear characteristics is called gamma ( $\gamma$ ) correction. In general, the gamma correction of a Windows PC is set to  $= 2.2$ . The

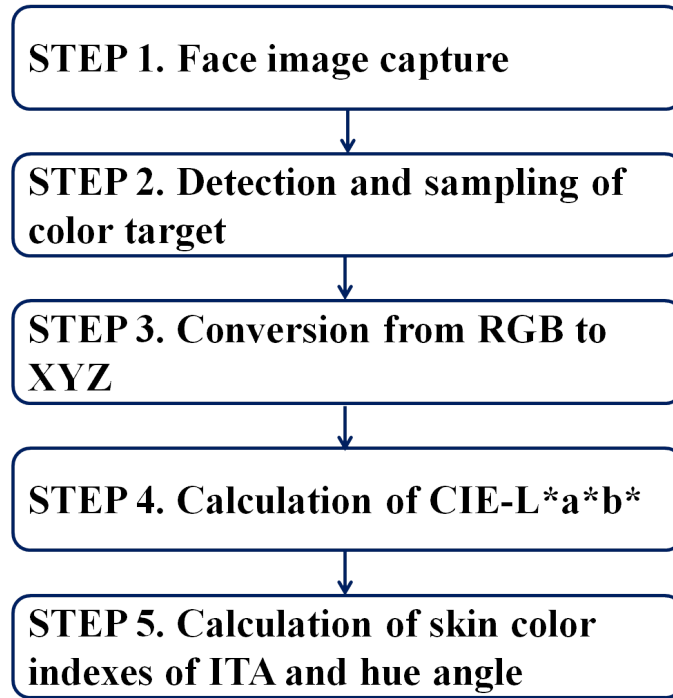


Figure 3.2: Overview of image processing for skin color measurement

formulae for converting between sRGB and XYZ tristimulus values for D65 white point are as follows:

$$\begin{pmatrix} X \\ Y \\ Z \end{pmatrix} = \begin{pmatrix} 0.4124 & 0.3576 & 0.1805 \\ 0.2126 & 0.7152 & 0.0722 \\ 0.0193 & 0.1192 & 0.9505 \end{pmatrix} \begin{pmatrix} R \\ G \\ B \end{pmatrix} \quad (3.1)$$

The next step transforms the values into the values of the CIE-L\*a\*b\* color system. It is organized in a cube form. L\* indicates lightness. The maximum value for L\* is 100, which indicates the white level; the minimum value is 0, which represents black. The a\* and b\* axes do not have specific numerical limits. The a\* axis represents red to green, with positive values indicating increased redness and negative values indicating increased greenness. The b\* axis represents yellow to blue, with positive values indicating increased yellowness and negative values indicating increased blueness. In the study of skin color, only the positive sides of the a\* and b\* parameters are considered. The expression method of skin color is important for evaluating pigmentation and detecting erythema. The CIE L\*a\*b\* system has been widely used in the study of skin color, due in part to its ease of use and the availability of instruments that can measure these parameters. For example,

increases in skin pigmentation can be graphed as a shift on the L\*-b\* plane, whereas skin reddening (erythema) is represented as a shift on the L\*-a\* plane.

### 3.2.5 Individual typology angle

The individual typology angle was proposed by Chardon in 1991 [44] as the degree of skin pigmentation as shown in the vector direction in the L\*-b\* plane, and the formula is as follows:

$$\text{Individual typology angle(ITA)} = \left[ \tan^{-1} \left( \frac{L^* - 50}{b^*} \right) \right] \times \frac{180}{\pi} \quad (3.2)$$

where ITA is given in degrees. It needs to be noted that ITA values are inversely related to skin pigmentation. The concept and angle range of ITA are shown in Fig. 3.3. The ITA values are inversely related to skin pigmentation. The ITA values allow skin color to be classified into six groups from very light to dark skin (Fig. 3.3). The ITA values are inversely related to skin pigmentation.

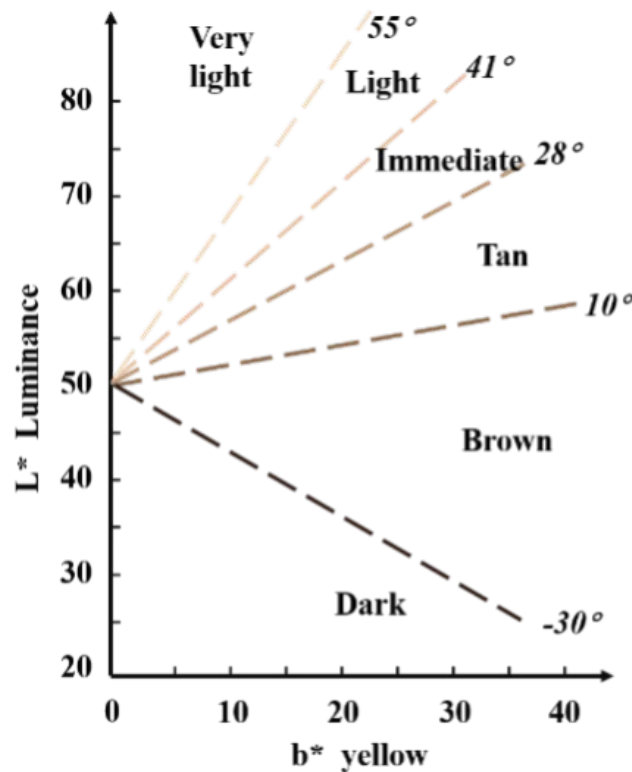


Figure 3.3: Skin color categories: Individual typology angle

### 3.2.6 Hue angle

The hue angle was defined according to the CIE-L\*a\*b\* color space as the degree of erythema calculated using redness (a\*) and yellowness (b\*) with the formula:

$$\text{hue angle}(h_{ab}^*) = \left[ \tan^{-1}\left(\frac{b^*}{a^*}\right) \right] \times \frac{180}{\pi} \quad (3.3)$$

where  $h_{ab}^*$  is given in degrees. The hue angle is measured in degrees starting with  $h_{ab}^* = 0$  in the  $+a^*$  axis direction and increasing counterclockwise. The concept and the angle range of hue angles are shown in Fig. 3.4. When expressing skin color, erythema can be detected by the hue angle, which is approximately correlated with a change in hue. It is thought that skin color mainly exists in the range of 0 to 90 degrees. The hue angle is shown in Fig. 3.4. It is thought that skin color mainly exists in the range of  $0^\circ$  to  $90^\circ$ . The hue angle values are inversely related to skin erythema.

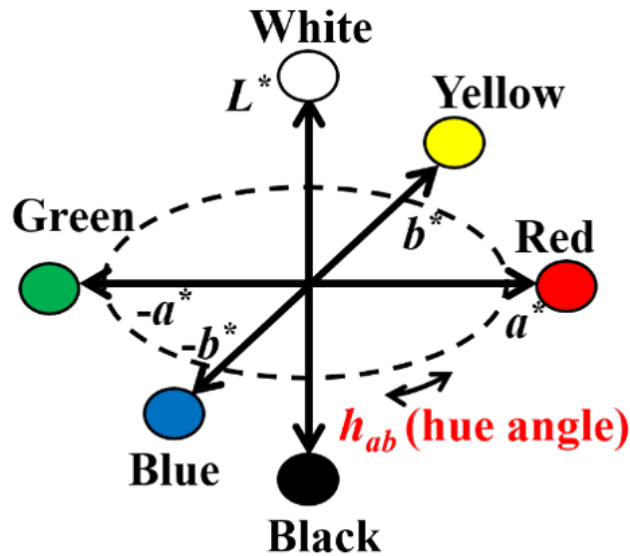


Figure 3.4: Skin color categories: hue angle

### 3.2.7 Statistical analysis

SPSS 21.0 (SPSS Science, Chicago, IL) software was used for all statistical analyses. All data were expressed as the mean  $\pm$  SD (standard deviation). Pearson correlation coefficients were assessed between the Beijing and Tokyo subjects. Multiple regression

analysis was applied to determine the relationships between age and skin color parameters in east Asia. The biophysical properties of the skin at anatomical sites were compared using an independent sample t-test. The statistical tests were two-tailed with the following significance levels:  $p < 0.05$  and  $p < 0.01$ .

### 3.3 Results of quantitative skin color measurement

#### 3.3.1 Subject population

Outlier screening was used before data analysis, and two outliers were deleted. All data from 443 people were analyzed, 360 of which were females from Beijing and 83 of which were females from Tokyo. Descriptive characteristics were calculated by descriptive analysis. The mean age of all subjects was  $32.8 \pm 10.48$  years. The mean age of all subjects in Beijing was  $34.03 \pm 9.93$  years, and that in Tokyo was  $27.43 \pm 11.14$  years old. Two age groups were created for the Beijing and Tokyo groups (Table 3.1). The mean age in the 18- to 29-year-old group was 20.74 in Beijing and 20.58 in Tokyo, while the mean age in the 30- to 50-year-old group was 39.73 in Beijing and 44.29 in Tokyo.

Table 3.1: Age distribution of study subjects for skin color measurement

Geographic location	18-29 years old		30-50 years old	
	Number	Mean (mean $\pm$ SD)	Number	Mean (mean $\pm$ SD)
Beijing	108	20.74 $\pm$ 3.6	252	39.73 $\pm$ 5.2
Tokyo	59	20.58 $\pm$ 1.07	24	44.29 $\pm$ 4.7
Total	167	20.68 $\pm$ 2.96	276	40.12 $\pm$ 5.31

#### 3.3.2 Spectral characteristics of the white LED lamp

The spectral characteristics of the built-in white LED lamp of the re-Beau® device are shown in Fig. 3.5. Generally, white LED light is obtained by mixing RGB LEDs or by using blue LEDs + yellow phosphor (Narendra et al., 2001). The white LED lamp incorporated in this device produces white light using blue LEDs + yellow phosphor. The calculation of the relative color temperature  $T_{cp}$  from the measured values of the spectral distribution yielded  $T_{cp} = 6136$  K.

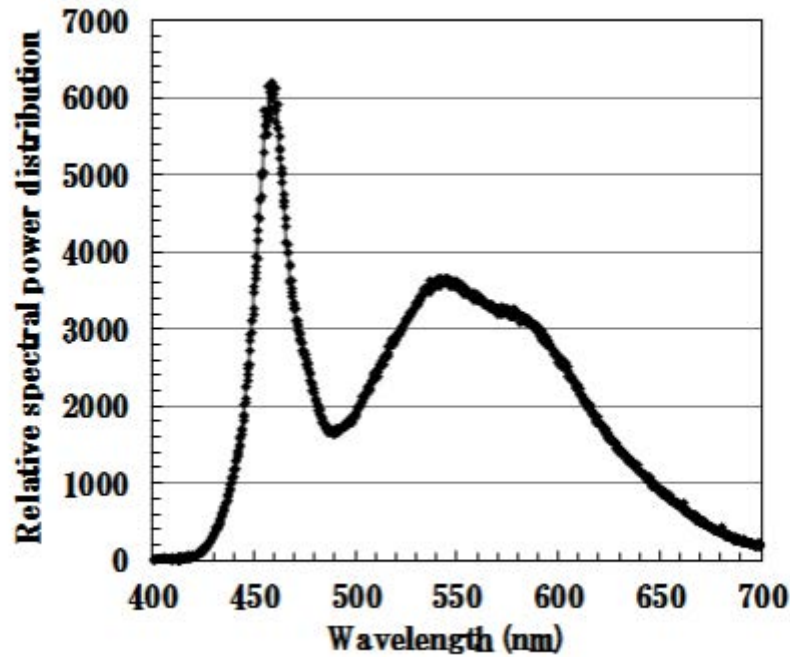


Figure 3.5: spectroscopic characteristics of the built-in white LED lamp of the image capturing device

### 3.3.3 Evaluation of skin color in different skin anatomical sites

The skin color of the subjects, in terms of the CIE  $L^*a^*b^*$  color parameters, ITA and hue angle are shown. Changes in the ITA values of the forehead, cheek, and jaw of 91 female subjects are shown in Fig. 3.6. The vertical  $L^*$  axis indicates the luminance of the skin and the  $b^*$  axis indicates the yellow component of the skin. The skin color areas are defined by dividing the skin color volume  $L^*-b^*$  projection into areas limited by the ITA.

A comparison of the ITA values of the forehead, cheek, and jaw is shown in Fig. 3.7(a). In each case, difference between two sites were compared using t-tests. Significant differences were observed between the forehead and cheek and between the cheek and chin. The skin color measurement result obtained from the image was found to well express the difference of each part of the forehead, cheek, and jaw. The difference in the hue angle is shown in Fig. 3.7(b). The hue angle was defined according to the recommendation of the CIE as the psychometric correlate of the visually perceived hue. A

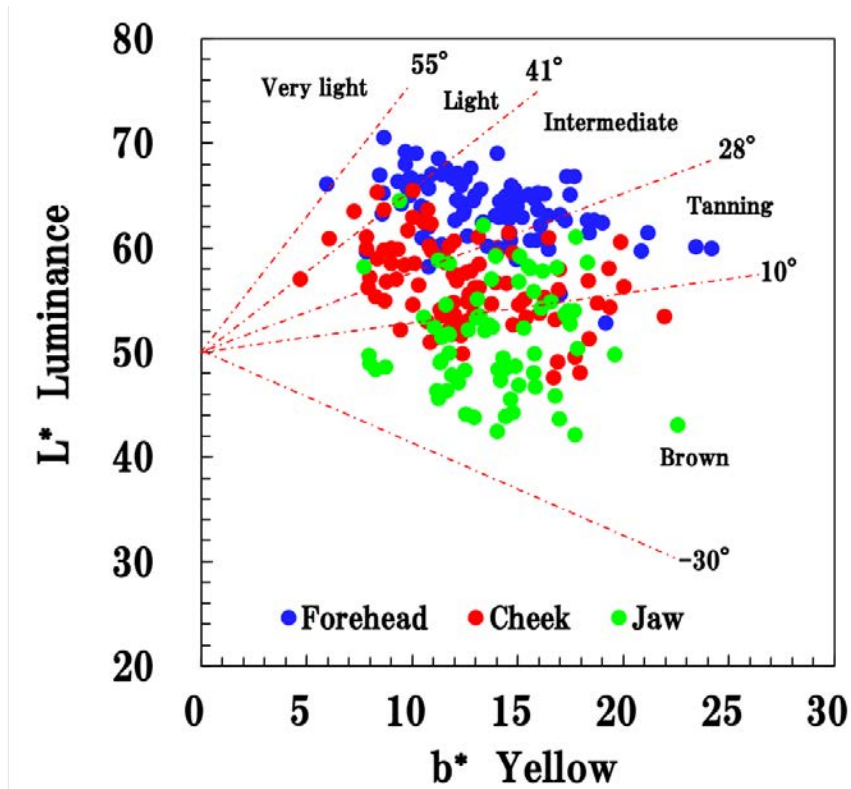


Figure 3.6: The ITA values of 91 subjects

significant difference was found between the forehead and cheek and between the cheek and chin, as was observed in the ITA ( $p < 0.01$ ).

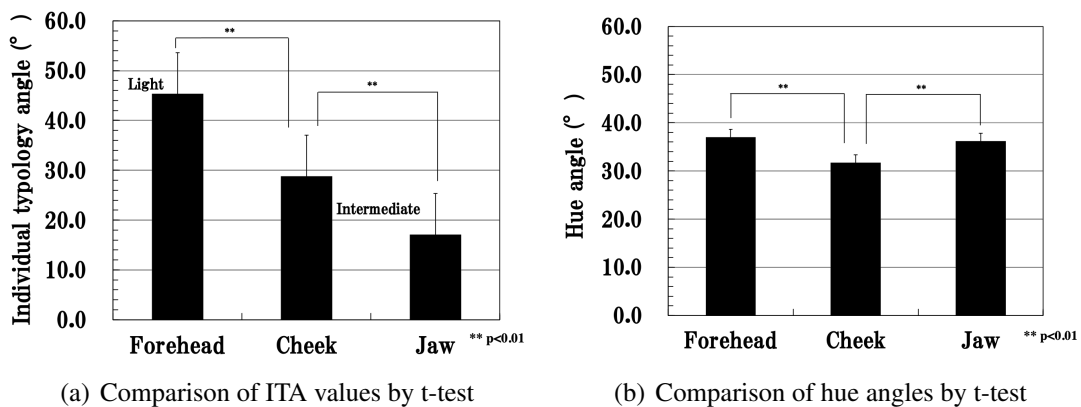


Figure 3.7: Skin color comparison of anatomical sites

### 3.3.4 Comparison of skin color by different instruments

The comparison of the hue angles determined based on an imaging analysis and by colorimeter (CR-13) is shown in Fig. 3.8. The hue angle values of the forehead and cheek

values determined by the imaging analysis were lower than those measured with a colorimeter (CR-13); the average difference was almost 20, which means that the a\* axis values determined from imaging analyses may be higher than those determined using a colorimeter.

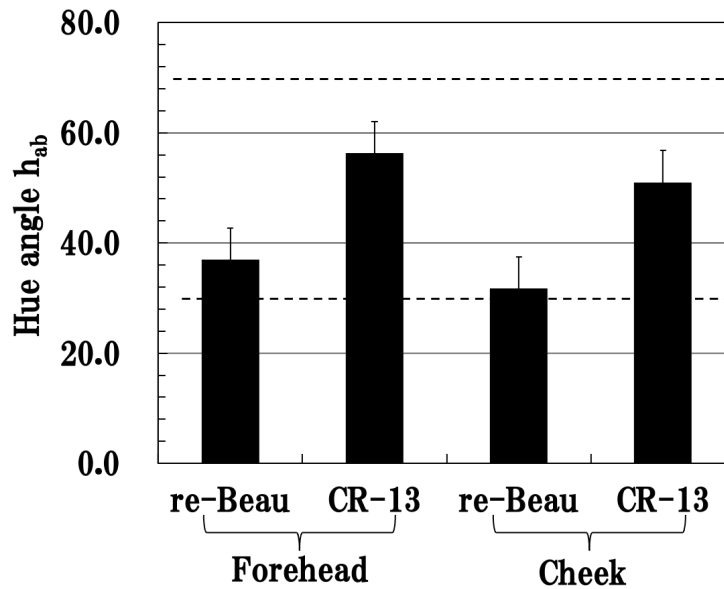


Figure 3.8: Comparison of hue angles by different devices

### 3.3.5 Comparison of skin color indexes

According to the Chardon skin color classification method, the facial ITA value-based classifications of females in Beijing and Tokyo were compared. As shown in Table 3.2, the intermediate skin color category was the main skin color in East Asian females, and the grade VI (dark) category was not observed in the East Asians examined in this study.

Table 3.2: Classification of female cheek skin color in East Asia

Geographic location	ITA classification					Total
	I	II	III	IV	V	
Beijing	8(2.2%)	148(41.1%)	165(45.8%)	37(10.3%)	2(0.6%)	360(100%)
Tokyo	0(0%)	6(7.2%)	48(57.8%)	29(34.9%)	0(0.0%)	83(100%)
Total	8(1.8%)	154(34.8%)	213(48.1%)	66(14.9%)	2(0.5%)	443

Among the two populations, the grade III skin color was the main skin color (more than 50%), but the most interesting aspect of the results was that the second most common skin color levels differed. Beijing individuals had a grade II (light) (41.6%) skin color as



the second most common category, similar to other East Asians. Tokyo individuals had a grade IV (tan) (34.9%) skin color as the second most common category. In addition, a much wider range of skin color categories was observed in Beijing than in Tokyo.

To assess skin color more objectively, 5 skin color indexes were measured and compared. The mean value  $\pm$  standard deviation of each index is shown in Table 3.3.

Table 3.3: Descriptive analysis of the skin color parameters of the cheek

	Beijing (mean $\pm$ SD)	Tokyo (mean $\pm$ SD)	Mean (mean $\pm$ SD)
L*	61.87 $\pm$ 3.23	59.25 $\pm$ 2.08**	61.38 $\pm$ 3.21
a*	14.65 $\pm$ 2.62	10.28 $\pm$ 1.34**	13.84 $\pm$ 2.97
b*	14.45 $\pm$ 2.26	15.40 $\pm$ 1.82**	14.63 $\pm$ 2.22
ITA	38.99 $\pm$ 9.16	31.06 $\pm$ 7.42**	37.51 $\pm$ 9.38
hue angle	44.73 $\pm$ 7.87	56.2 $\pm$ 4.11**	46.88 $\pm$ 8.58

\*\*p<0.01

L\* represents lightness, and its values ranged from 44.92~71.10 for East Asians in general; for the Beijing and Tokyo groups these values were 44.92~71.10 and 53.53~63.33, respectively. The redness, or a\* values, of East Asians ranged from 7.17~22.21, and these values were 8.04~22.21 in the Beijing group and 7.17~13.00 in the Tokyo group. The b\* is yellowness, and its values ranged from 8.83~23.12 in East Asia, and these values were 8.83~23.12 in the Beijing group and 11.77~21.93 in the Tokyo group. The ITA is the most common and comprehensive index expressing skin color, especially skin pigmentation. The ITA values ranged from -18.1~63.8 in East Asia, from -18.1~63.8 in the Beijing group and from 11.6~46.4 in the Tokyo group. The hue angle is often used as the index of erythema. In this study, the hue angle ranged from 25.83~64.62 in East Asia, from 25.83~64.62 in Beijing and from 43.93~64.21 in Tokyo. The differences in Beijing and Tokyo were compared using the independent simple t-test. Females in Tokyo showed significant differences for all indexes (p<0.01). The table below illustrates the main characteristics of the facial skin color of females in Tokyo, with lower lightness, lower redness, more darkness and higher yellowness.

### **3.3.6 Comparison of age-related skin color variations**

ANOVA was used to discuss the skin color variations with age. The data in Fig. 3.9 show the effect of age and geographic location on skin color. Except for the  $a^*$  values that tended to increase with age, the remaining indexes showed the same trend of decreasing with increasing age in East Asia. There was a clear trend and strong evidence of increasing  $a^*$  values, as shown in Fig. 3.9(b), and decreasing hue angles, as shown in Fig. 3.9(e), with significant differences ( $p=0.000$ ), which indicated that skin erythema looks more obvious with increasing age. The change in lightness also showed a significant difference with age ( $p = 0.038$ ), which revealed that the skin appears darker with age. The changes in all of the indexes between Beijing and Tokyo were significantly different. In Beijing, the  $L^*$ , ITA and hue angle decreased, while  $a^*$  increased, all with significant age-based differences. However, the  $L^*$  and ITA data in Tokyo showed different trends from those in Beijing, and no significant differences were observed.

## **3.4 Discussion**

Human skin color is influenced by both genetics and the environment. Usually, genetics is the most important reason why different ethnicities exhibit a unique skin color.

When evaluating skin color, it is essential to assess pigmentation and erythema at the same time, especially in Asian people, whose skin color is yellowish, rather than deeply melanized. It was found that the ITA and hue angle shown in this study are extremely useful as indexes for the evaluation of skin color.

In this study, we developed a method that measures skin color on imaging in which the measured part could actually be seen on the monitor and the region of interest (ROI) can be selected. The skin color is usually evaluated based on different methods of analyzing the light reflected by skin, such as measurement by the colorimeter that we used for the purpose of comparison in this study or the skin colorimeter CL 400 (Courage+Khazaka Electronics, Germany). This method requires a professional operator to hold the device against the measured sites [45]. This may cause the measurement part to become anemic

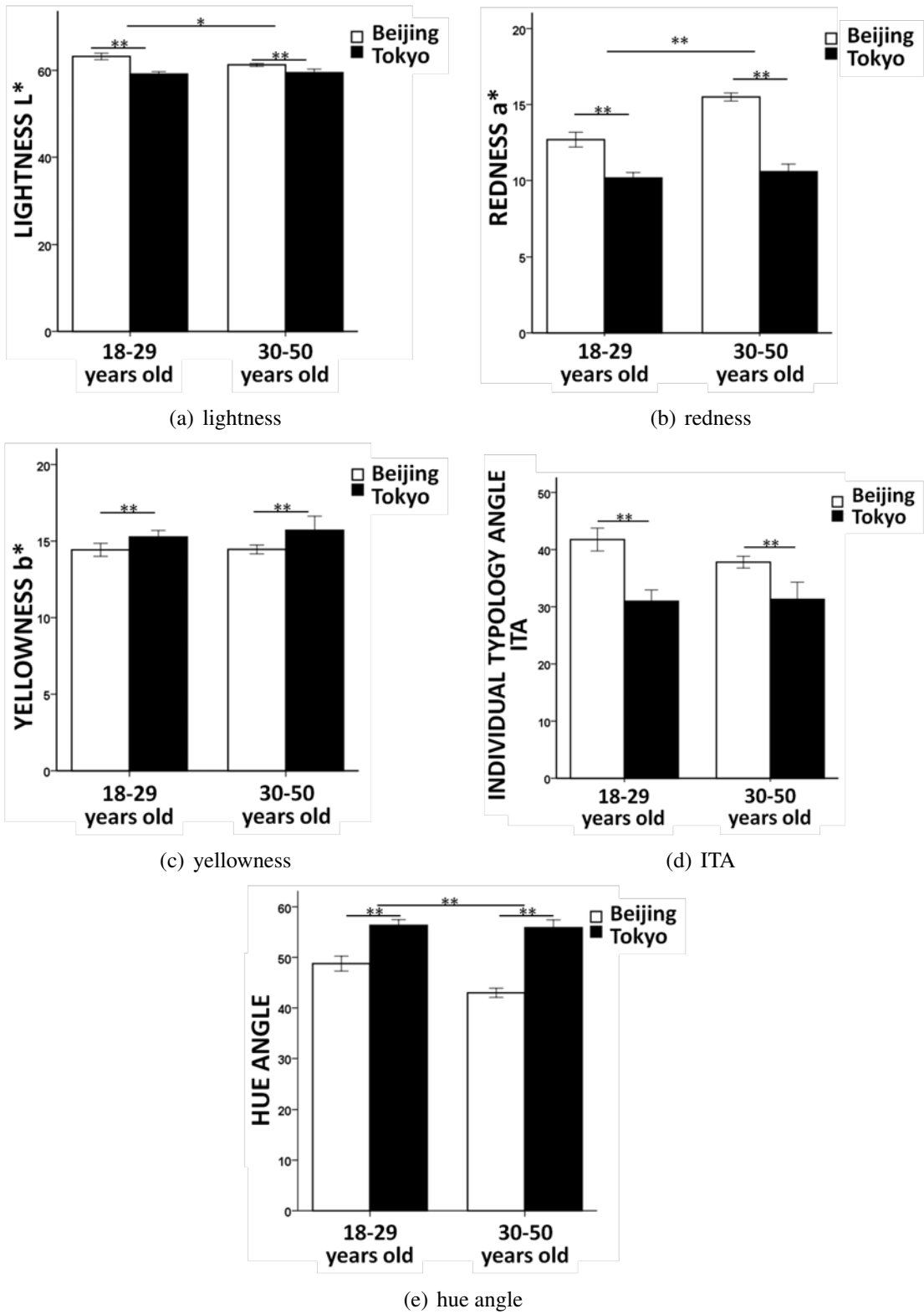


Figure 3.9: Effect of geographic location and age on skin color

due to the pressure of applying the measurement head to the measurement part, which will cause the color to change. Thus, evaluated skin color on imaging. With this method, the skin color can be evaluated on the screen, even if the operators differ. Anyone can use this method and obtaining constant values does not require expert skills.

In a previous study, the individual typology angle values of the cheeks of Japanese female subjects showed that skin types were light, intermediate and tan [46], which is similar to the results in this study. Facial skin exhibits unique biophysical properties, which are influenced by anatomical sites [47]. Thus, we evaluated three anatomical sites to comprehensively assess the facial skin color of Japanese female subjects and found that the ITA range was wider, from light to brown, because the skin color of the jaw was darker than that of the forehead and cheek.

On the other hand, the hue angle measured on imaging was lower in comparison to the values measured by the colorimeter. Similarly, the values were lower than the normal values in other studies [48,49]. The usage of white LED lamps might be the reason for the low hue angle. In recent years, white LED lamps have been used not only to improve the efficiency of indoor lighting but also for measurement technology. There are two types of methods for obtaining white light: (i) red LED + green LED + blue LED and (ii) blue LED + yellow phosphor. Blue LED + yellow phosphor has been most frequently applied due to its simple process and low cost [50]. However, this type of LED is associated with a problem in that the red component is insufficient and the color reproduction of the skin color is not optimal. Table 1.5 demonstrates the calculated color rendering index values of 15 color samples of color rendering property evaluation test colors (JIS, 1990). As the numerical value of the color rendering index becomes closer to 100, the color rendering properties become better. However, the evaluations of red color or Japanese skin color are considered to be poor. It is understood that the color rendering property of skin color is low. Accordingly, we considered that the color rendering property of this white LED lamp was the reason for the low hue angle. We considered that the use of white LED lamps with high color rendering ability would improve this issue. Furthermore, the color gamut

area of sRGB on the display is narrower than the NTSC television standard. However, the use of such standards is considered advantageous because it is not necessary to consider differences in display devices.

Based on the convenience of operation and the unique feature that the region of interest (ROI) can be selected and that it does not require the application of pressure, this method could be utilized in an aesthetic and dermatological diagnosis support system. E. Cinotti et al. [51] used videodermoscopy to diagnose the variations of skin erythema, yellowness, pigmentation, color variance and xerosis induced by seasonal effects. They applied the CIE-L\*a\*b\* color space and used the individual typology angle (ITA) of the image as an index of pigmentation, and reported seasonal changes in erythema, pigmentation, xerosis and yellowness based on the analysis of images. Specifically, erythema, pigmentation and xerosis increased and yellowness decreased after summer. In addition, X. Delpueyo Español [52] developed a spectral imaging system to improve the diagnosis of skin cancer. The individual typology angle and hue angle were applied as indexes to compute the difference between the segmented lesion and the averaged surrounding skin. This diagnosis system attempted to detect melanomas and provided 100% sensitivity and 72.2% specificity.

Besides the diagnosis, when judging the therapeutic effect, it is easy to compare clinical photographs side-by-side after the completion of treatment. However, it is necessary to remember the previous condition for each trial and to determine the effect. Even with a proficient dermatologist, the longer the observation period is, the harder it is to compare. Confirming the effect based on numerical values measured by a skin color measuring device was considered effective because it facilitates objective judgment.

This method would also become a powerful source of information that can be used to explain the course of treatment to patients using images. It is also possible to compare the changes of the lesion part over time or to compare individual diseases or treatments, suggesting its possible application in dermatology and cosmetics.

Many studies have focused on comparisons among ethnicities [39, 43, 53, 54], while studies on skin color differences in the same ethnic group due to environmental factors are scarce studies. This study aimed to objectively assess the subtle skin color variety in East Asians and explore age-related color variations.

Prior studies that have noted prominent differences in skin color in the same ethnic group as a consequence of geographic location [53, 55]. Chinese and Japanese women showed similar proportions of individuals with skin color in the intermediate (III) ITA category, which was also the main category. Nevertheless, the second most common ITA category in Chinese and Japanese women was light (II) and tan (IV), respectively. In addition, an extensive range of categories from very light (I) to brown (V) was observed in Chinese women but not in Japanese women. This finding suggests that the main categories are light (II), intermediate (III) and tan (IV) in East Asians, while the dark (VI) category was not observed. Likewise, C. Cho et al [55] reported that the light and intermediate skin color categories were the most common in both Korean and Cantonese (people living in Guangdong, China) people.

In the current study, comparing the skin colors of Chinese and Japanese individuals indicated that Chinese females had brighter and more reddish skin than Japanese females, while Japanese women have a more yellowish complexion. This result may be explained by the geographic locations, UV radiation and consumer skin care habits.

The geographical locations and climatic conditions of Beijing and Tokyo are different. Beijing belongs to the temperate continental climate, where it is cold in winter and hot in summer. The annual temperature difference is large, and the precipitation is concentrated. Additionally, Beijing has four distinct seasons, and the annual rainfall is low. Relatively speaking, Tokyo has a subtropical marine monsoon climate and is deeply affected by the marine air mass. There is no extreme cold in winter or extreme heat in summer. The average temperature of the coldest month is above 0 °C, and that of the hottest month is below 22 °C. The precipitation occurs throughout the year. On the other hand, UV exposure plays a significant role in skin color [56], as shown in Fig. 3.10. C. Battie et al [56]

reviewed the relationship between skin type and UVA radiation and found that UVA radiation in major East Asian cities showed the following trend: Tokyo>Seoul>Beijing. UVA radiation is responsible for the early signs of photoaging, such as skin pigmentation. UVB radiation is responsible for the occurrence of skin erythema. S. Shono et al [57] studied the relationship between skin color, delayed erythema and delayed tanning (DT) caused by exposure to UVB and proved that skin erythema was mainly caused by UVB radiation. In addition, latitude and longitude could affect the sunshine time and sunshine intensity, and the geographical latitude of Beijing is higher than that of Tokyo, thus the ultraviolet radiation level is low. Therefore, Chinese people are more likely to have lighter skin color and to develop a sunburn under ultraviolet light. C. Cho et al [55] also found a similar conclusion by comparing the differences in skin color between Korean and Cantonese people, revealing that Koreans living in a higher latitude and a relatively less sunny environment are lighter than Cantonese people who are exposed to more ultraviolet light. Koreans are also more susceptible to sunburn.



Figure 3.10: UVA dose received in main Asian cities

In addition, because Beijing and Tokyo are the capitals of China and Japan, respectively, many economic and cultural parameters are similar. Both locations are international metropolises with large populations. The people generally exhibit a yellowish skin tone and have similar genetic backgrounds and are willing to pay a certain degree of attention to skin care. Foundation makeup is generally applied, and the sunscreen ingredients in foundation help to prevent tanning of the skin.

As an irreversible influence, age impacts facial skin color and pigmentation visibly. Comparing the variations in skin color in the 18- to 29-year-old and 30- to 50-year-old groups, there was a significant difference in  $L^*$ ,  $a^*$  and hue angle. Skin color became darker and more reddish with age. Both Chinese and Japanese women showed the same age-related trends. On the other hand, the comparison of Chinese and Japanese women in both age groups revealed that Chinese skin is less yellowish, much brighter and more reddish than Japanese skin. A possible explanation for these results may be related to intrinsic as well as photoaging. L. Wang et al [58] demonstrated skin color darkened with age due to a decrease in the modified ITA. This study found similar findings in Chinese women but different trends in Japanese women. This may be because of the smaller sample size in Japan. K. Kikuchi et al [40] also found that pigmented spots in Japanese people increased with age. F. Flament et al [59] reported that skin pigmentation was observed with age in Caucasians. In addition, C. Cho et al [60] researched the age-related skin color changes in the epidermal and dermal skin in Koreans and discovered that skin transparency and brown spots showed a rapid change at the ages of the early 30s and late 50s.

In this study, skin color differences in East Asians were observed by direct comparison under the same controlled protocol. However, these results were limited by the small sample size, especially in Tokyo. Due to common makeup habits, it was more difficult to persuade volunteers to remove their makeup for skin color assessment in Tokyo than in Beijing. A further study could assess the skin color variety with more samples and more cities in East Asia to confirm these results.



Overall, this study strengthens the idea that East Asian facial skin color is varied, becoming darker and more reddish with age, and that yellowness is related to geographic location. These results confirmed that different skin color characteristics occurred in the same ethnic group. In addition, we presented an imaging analysis method that quantifies the properties of skin color. The improvement of software programs and camera technology has made imaging analysis useful for the quantitative assessment of the properties of skin color. The ITA and hue angle were found to be extremely useful for the evaluation of skin color. The results of the present study demonstrate the potential application of an imaging system as a research and clinical tool. These findings have significant implications for the understanding of how to develop precision skin whitening and antiaging products for specific consumers.

For skin color extraction, it is the first time we applied the individual typology angle and hue angle in image processing, which inspire the consideration of color component on human skin image processing.

## **Chapter 4**

# **Quantitative Evaluation of Skin Porphyrins**

## 4.1 Skin porphyrin introduction

Skin is the largest and outermost organ of the human body, which has a pivotal role in protecting the body from potential risks of external environmental factors. Investigating skin conditions monitoring is a continuing concern both in dermatology and aesthetics. For dermatologists and researchers, it would be valuable research data in the field of exploring a pathogenesis or treatment plans targeting long-term chronic skin diseases and confirming therapeutic effects. Besides, for ordinary consumers, who have already paid more attention to their skin health, it could also be a guiding tool in daily skincare and cosmetics choosing. Nevertheless, skin health conditions are quite complex and can be influenced by many internal and external factors, such as bacteria. As we know, the skin is an ecosystem supporting abundant microorganisms, inclusive with bacteria, fungi, and viruses on the surface, most of which are harmless and even beneficial [61]. When the delicate balance between the host and microorganism is stable, it is seen as healthy skin, on the contrary, disturbing the balance on either side would lead to skin health hazards [62], and several skin biophysical properties would be damaged, such as skin barrier function destruction [63]. Unhealthy skin conditions have a huge impact both physically and mentally. *Propionibacterium acnes* (*P. acnes*) is one of the commensal bacterium covering the skin surface, which not only prevents colonization from other harmful pathogens, but also destroy the skin health, leading to skin diseases, such as *acne vulgaris* [64], the most common and chronic inflammatory follicle disorder worldwide, or *Progressive macular hypomelanosis* (PMH) [65], which causes hypopigmentation in a variety of skin types.

Previous research has established numerous objective and professional evaluation devices for skin properties, such as probe types and image processing types. However, some limitations exist, for example, most of the devices were expensive and designed to assess a single property, the operation needed professional researchers finished training.

As M. Shu et al. [66] reported, porphyrins are series of organic compounds and pigmented compounds, which play important roles in diverse process as oxygen transportation and photosynthesis. Porphyrins have the capacity on exposing red fluorescence when exposed to long-wavelength ultraviolet light near 400 nm [10, 67]. Usually, it is believed that *P. acnes* produce porphyrins and with the discovery of wood’s lamp, fluorescent porphyrins become visible, which can be observed as the red fluorescence on Wood’s light excitation. Most of the prior researches focused on acne diagnosis applying the relationship between porphyrins and *P. acnes* [68–70], which has been reported since 1967. L. C. Luchina et al. [70] graded their observations on a fluorescence scale, grade 0 to 3 representing acne scale none to extensive. Application in skin acne vulgaris diagnosis was explored accordingly.

There is a growing development of fluorescent porphyrin image analysis, and a large series of methods about porphyrin segmentation and acne classification have been proposed [71–73]. Table 4.1 lists out several existed methods of porphyrin segmentation. J. R. Balbin et al. [74] used image processing to detect acne region and map the facial fluids. G. Peris Fajarnés et al. [71] applied a k-means algorithm to count acne lesions automatically. F. S. Abas et al. [75] used discrete wavelet frames and gray-level co-occurrence matrix to classify the acne lesion types. However, most image data consists of the whole face, which implies that the device needed is huge and more fit for professional research institutions, aesthetic salons, rather than usual consumers.

Table 4.1: Related work of skin porphyrin evaluation

Author	Year	Image data	Algorithm	Extracted features
Manita Khongsuwan [72]	2011	Partial fluorescence image	Adaptive histogram equalization+ extended maxima transform	Number of <i>P. acnes</i> points
Jessie R. Balbin [74]	2017	Whole facial image	Convert to the binary image by automatic threshold value by Otsu’s method + subjective threshold value determination by morphological structuring element	Porphyrin number and region
Guillermo Peris Fajarnes [71]	2020	Whole facial image	K-means segmentation + fuzzy c –means algorithm	Number of points

In this chapter, we proposed a quantitative and convenient assessment of porphyrins from fluorescence images in the cheek site taken by portable devices using image processing and applied the algorithm in studying porphyrins characteristics changing trends with age.

## 4.2 Methods and materials

### 4.2.1 Skin fluorescence image captured device

In this study, fluorescence images were taken by an integrated portable device, Smart Skin Care<sup>®</sup> (IT Access Co., Ltd, Yokohama, Japan) with a UV-LED illumination system (Fig. 4.1). A fiber input multichannel spectrometer (USB2000+, Ocean Optics, U.S) was used to measure the spectral characteristics of the UV-LED lamps built-in Smart Skin Care<sup>®</sup>. The spectral intensity was measured at intervals of 5 nm in the measurement wavelength range from 340 nm to 420 nm. The relative emission intensity diagram of UV-LED lamps was displayed in Fig. 4.2, which implied that the wavelength of these UV-LED lamps was near 375nm, on behalf of specific UVA light. There were 8 UV-LED lamps arranged as a circle (diameter 40mm) with 40 degrees inwards apiece, which kept the certain 68mm distance between the lens of the device and the assessed skin area, and which ensured the uniform irradiation with an average power of density of 44.4 mW/cm<sup>2</sup>. A long-wavelength filter (>515nm) with a diameter of 10 mm was in the front position of the CMOS RGB sensor to enhance the detection of fluorescence emission and to prevent the detection of UV-LED emission at the same time. Figure 4.3 presents the fluorescence images observed before and after using the filter.



Figure 4.1: Smart Skin Care<sup>®</sup> device illustration [3]

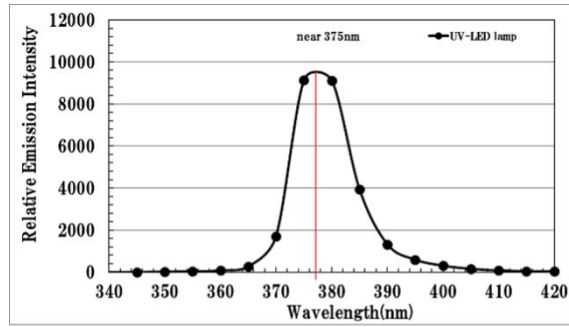
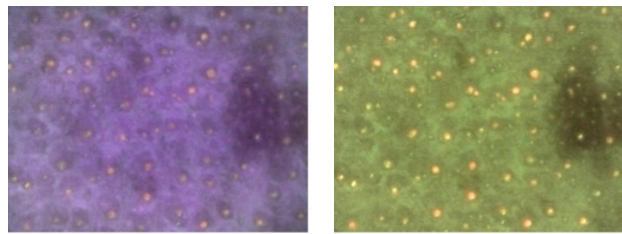


Figure 4.2: UV-LED lamps' spectrum characteristics

The CMOS RGB image sensor with a resolution of  $1280 \times 960$  pixels was utilized in fluorescence image attainment. Compared to the other main electronic image sensor CCD sensor, the CMOS sensor is much faster in the readout and less power usage. The magnification of the lens is  $\times 23.7$ .



(a) captured without the filter (b) captured with the filter

Figure 4.3: Fluorescence images

## 4.2.2 Image processing

In-vivo skin fluorescence images of the cheek were recorded in RGB color space and consisted of  $1280 \times 960$  pixels with the resolution, which represent the skin surface area with the relevant size of  $12 \times 9$  mm. Image processing was enabled by the OpenCV and Python software. The flowchart of image processing is shown in Fig. 4.4.

As we know, skin in the cheek is curved because of the cheekbone, it is easy to obtain the image with uneven light, especially at the edges of the image. Therefore, prior to processing the image, uniform distribution of light on all of the images is essential.

Choosing the central  $800 \times 800$  pixels of the image as the region of interest (ROI) is the simplest and the most effective approach. Once ROI was determined, one more step was implemented as the preprocessing, which is noise removes. In the algorithm

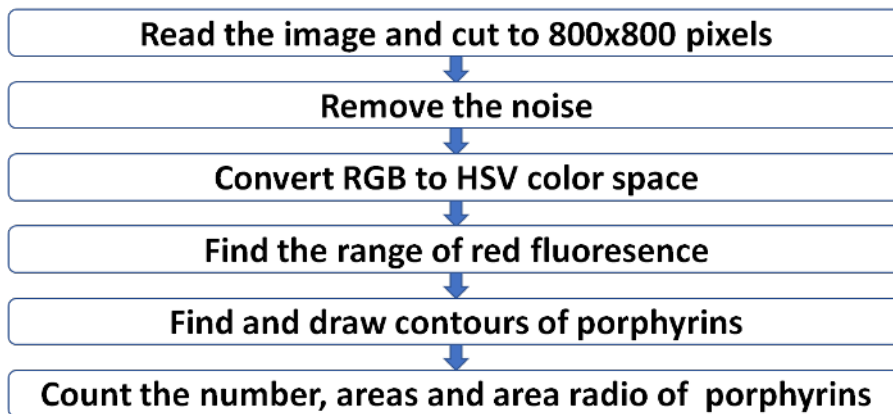


Figure 4.4: Flowchart of skin fluorescence image processing

proposed, a Gaussian filter was operated to remove the noise. Following the correction of ROI, the RGB color model was converted to the HSV color model. The original image was performed in RGB color space, which is more suitable for computer vision rather than human vision. The RGB color model is an additive combination of three primary colors, red, green, and blue. They represent three different frequency bands in the visible spectrum, however, some properties cannot be separated from RGB color model, like the color's lightness. In consequence, HSV color model was selected, where the color is defined by the dimension "hue", "saturation", and "value", showed as Fig. 4.5.

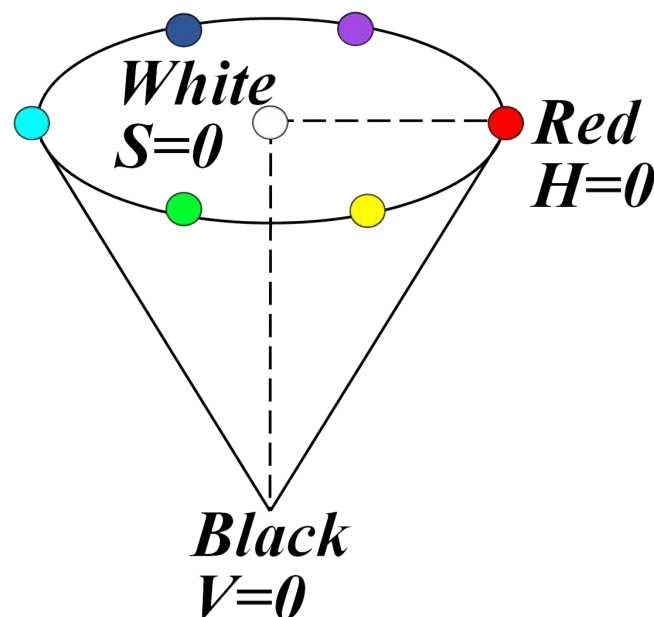


Figure 4.5: HSV color model illustration

The RGB to HSV conversion formula is as follows:

$$R' = \frac{R}{255} \quad (4.1)$$

$$G' = \frac{G}{255} \quad (4.2)$$

$$B' = \frac{B}{255} \quad (4.3)$$

$$C_{max} = \max(R', G', B') \quad (4.4)$$

$$C_{min} = \min(R', G', B') \quad (4.5)$$

$$\Delta = C_{max} - C_{min} \quad (4.6)$$

H, S, and V represent hue, saturation, and value, respectively in the HSV color space.

The calculation formula of H, S, and V is showed as follows:

$$H = \begin{cases} 0^\circ, & \text{if } \Delta = 0 \\ 60^\circ \times \left( \frac{G' - B'}{\Delta} \bmod 6 \right), & \text{if } C_{max} = R' \\ 60^\circ \times \left( \frac{B' - R'}{\Delta} + 2 \right), & \text{if } C_{max} = G' \\ 60^\circ \times \left( \frac{R' - G'}{\Delta} + 4 \right), & \text{if } C_{max} = B' \end{cases} \quad (4.7)$$

$$S = \begin{cases} 0, & \text{if } C_{max} = 0 \\ \frac{\Delta}{C_{max}}, & \text{if } C_{max} \neq 0 \end{cases} \quad (4.8)$$

$$V = C_{max} \quad (4.9)$$

On one hand, porphyrins showed fluorescent orange-red spots visibly under the UVA lights, H dimension was picked as one index, on the other hand, the edges of fluorescent spots are compulsory, V dimension was chosen as the other index to classify and segment the fluorescence. The mouse click programming was used to measure the HSV values of fluorescence images 10 times randomly and the resultant range of H and V values we got were 11-34 and 230-255, respectively. Since S does not matter with fluorescence, its range is 0-255. Finally, the contours of fluorescence were certified and extracted, except for those less than 20 pixels in case of being over-segmentation.



For skin condition analysis, three series of parameters were adopted, the number of fluorescent porphyrins, the area of fluorescent porphyrins, and the mean intensity of fluorescent porphyrins. The following expression was applied:

$$\text{mean intensity} = \text{area of fluorescent porphyrins} / (800 \times 800)$$

### 4.2.3 Age-dependent changes in cheek porphyrins

There are 3595 healthy Japanese aged 16-85 years enrolled in the study. The people who were diagnosed as acne or other dermatitis in the last 6 months were not included. They were divided into 8 groups and per 10 years were a group (Table 4.2). Fluorescence images were collected from the cheek anatomical site and processed using the algorithm performed. The study was conducted according to the principles of the Declaration of Helsinki. Statistical analysis was carried out using SPSS 21.0 software (SPSS Science). The one-way analysis of variance (ANOVA) was assessed among different age groups. The statistical tests were two-tailed with the following significance levels:  $p < 0.05$  and  $p < 0.01$ .

Table 4.2: Age distribution of study subjects for skin porphyrin measurement

Age	10s	20s	30s	40s	50s	60s	70s	80s	Total
number	22	1422	563	1001	365	152	56	14	3595

## 4.3 Skin red fluorescence of porphyrins evaluation results

For extracting fluorescent porphyrins, the implemented algorithm segments the fluorescent image and indicates number, area and mean intensity output parameters. As can be seen from Fig. 4.6, main porphyrins were classified and extracted well, especially the obvious and large ones. Unlike the T zones, there are few porphyrins on the cheek. However, four grades were established on the cheek site as a parameter to imply the skin health hazards, such as comedogenic potential.

As we know, algorithm evaluation methods must adhere to rigorous standards of statistical reliability. Three parameters were chosen to verify the proposed algorithm which

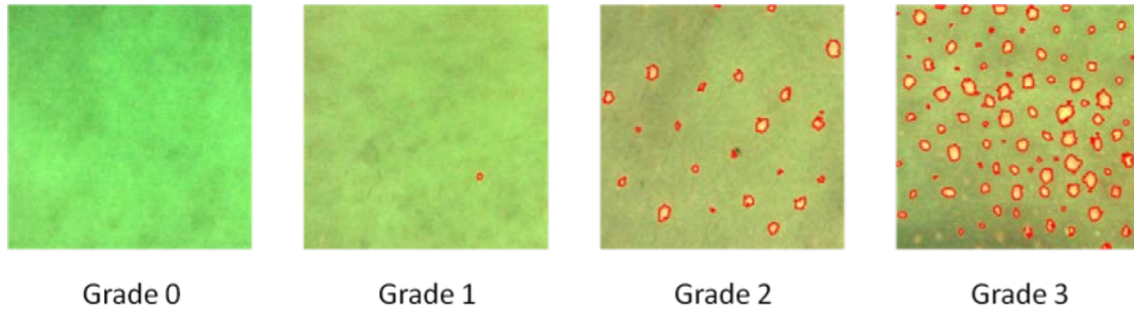


Figure 4.6: Processed porphyrin images with contours

includes accuracy, sensitivity, and precision in this study. Statistical measurements of accuracy and precision demonstrate the basic reliability of the test. Accuracy means the percentage of measuring the true amount. Precision represents similar results provided on the same sample when the test repeats. Sensitivity reveals the likelihood of false negatives and false positives.

To verify the accuracy, sensitivity, and precision of the proposed algorithm, four parameters were applied, which are (i) true positive (TP) rate (number of the fluorescence detected correctly), (ii) false negative (FN) rate (number of the fluorescence not detected), (iii) false positive (FP) rate (number of the non-fluorescence wrongly detected as fluorescence) and (iv) true negative (TN) rate (number of the non-fluorescence correctly detected as non-fluorescence). And the formulas are as follows.

$$\text{Accuracy} = (\text{TP} + \text{TN}) / (\text{TP} + \text{FN} + \text{FP} + \text{TN})$$

$$\text{Sensitivity} = \text{TP} / (\text{TP} + \text{FN})$$

$$\text{Precision} = \text{TP} / (\text{TP} + \text{FP})$$

Ten random images were selected and counted by both the proposed algorithm and the human eye. Table 4.3 below illustrates the comparison results, where sample images are selected randomly by randomized algorithm and human counting results are calculated by three test people and the median values are chosen as the result. It can be found out that the accuracy, sensitivity, and precision were 71%, 72% and 88%, respectively. It can be seen from the data in Table 4.3 that the algorithm showed great accuracy and sensitivity when there are a lot of porphyrins in the image, which indicated that the proposed algorithm is sensitive to detect the porphyrins and has the strong ability to calculate the porphyrins

Table 4.3: Verification of porphyrin image processing

Sample images	Human counting	Image processing	TP	FP	TN	FN	Accuracy	Sensitivity	Precision
1	51	52	51	1	0	0	0.98	1	0.98
2	20	8	8	0	0	12	0.4	0.4	1
3	4	3	3	0	0	1	0.75	0.75	1
4	2	0	0	0	0	2	0	0	0
5	68	67	67	0	0	1	0.99	0.99	1
6	2	1	1	0	0	1	0.5	0.5	1
7	31	20	20	0	0	11	0.65	0.65	1
8	2	2	2	0	0	0	1	1	1
9	21	22	21	0	0	1	0.95	0.95	1
10	56	66	56	10	0	0	0.85	1	0.85
Average							71%	72%	88%

correctly. However, it would miss some information when there are fewer porphyrins. In some cases, the percentage of discrepancy between human counting and image processing did not exceed 1%.

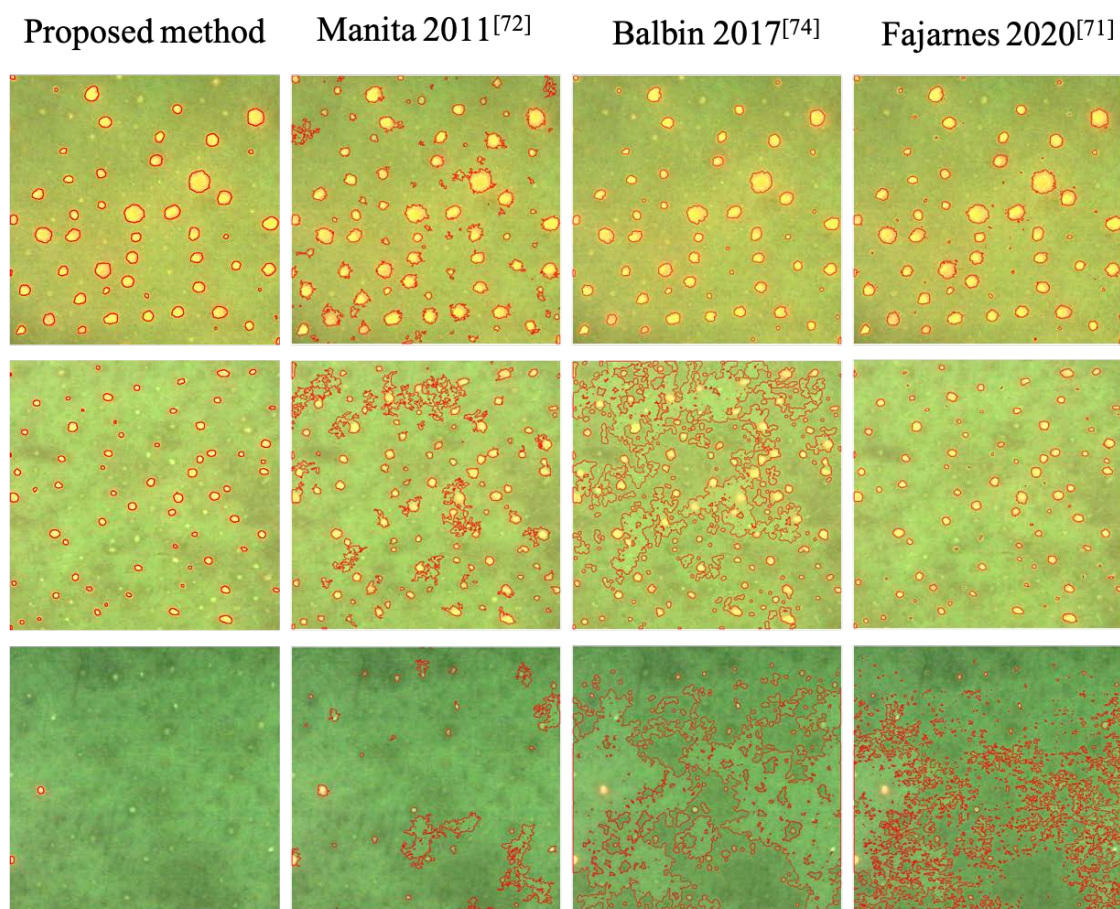


Figure 4.7: Comparison results of extracted skin porphyrins

Table 4.4: Comparison with other methods

Algorithm	Accuracy	Sensitivity	Precision	Merit	Limitation
Proposed method	71%	72%	88%	No over-segmentation happens in all kinds of images. Only extract porphyrins without hair follicles.	Sometimes cannot detect porphyrins, especially when there are few porphyrins.
Manita 2011 [72]	11%	100%	11%		Over segmentation, especially when there are few porphyrins. (Image data is different. )
Balbin 2017 [74]	18%	100%	18%	Perform well when porphyrins are obvious and big.	
Fajarnes 2020 [71]	21%	100%	20%	Perform well in images with lots of porphyrins.	

By compared to other three existed method shown in Table 4.4 , the results show in Fig. 4.7. Other than proposed method, other methods all show some over segmentation. Continually, the accuracy, sensitivity, and precision are calculated and compared, which turns out the proposed method has the highest accuracy and precision. It has the merit that no over segmentation happens in all kinds of images. Also, only porphyrins are extracted without hair follicles.

#### 4.4 Age-dependent changes in facial porphyrins

Age-dependent changes in porphyrins were examined applied the algorithm proposed and Fig. 4.8 provides some examples of different ages.

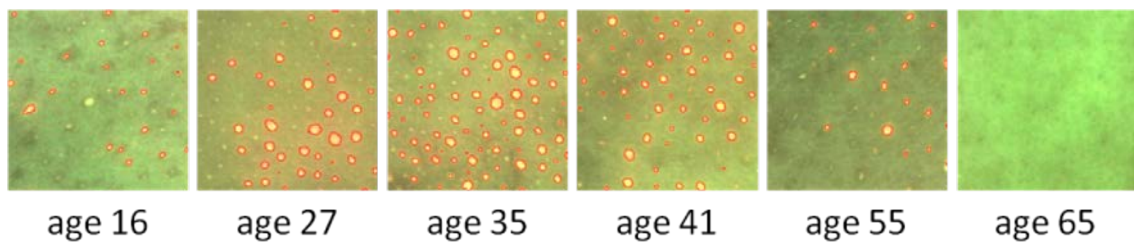
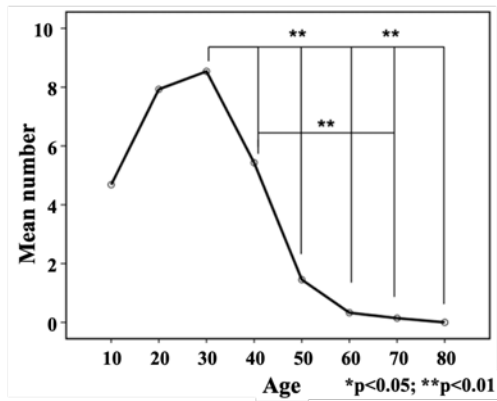


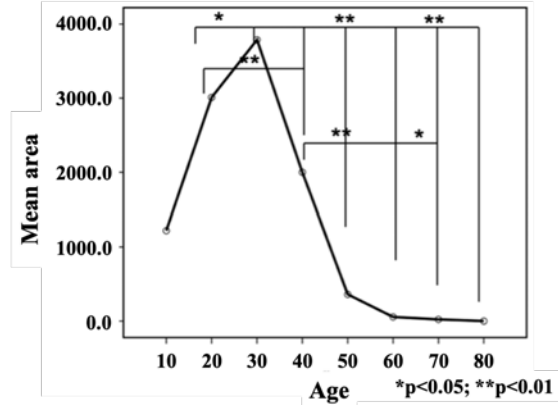
Figure 4.8: Porphyrin trends with age examples

The change in porphyrin number with age is shown in Fig. 4.9(a). It indicated that porphyrin numbers increased with age and rose to the peak at 30 years old and then decreased at a high rate with age. It came to almost zero when people were 60 years old. And the values among different age groups showed a significant difference( $p < 0.01$ ), except for the 10s and 20s age groups. Likewise, the change of porphyrin area and mean intensity with age implied similar trends, but with a sharper slope (Fig. 4.9(b), Fig. 4.9(c)). For

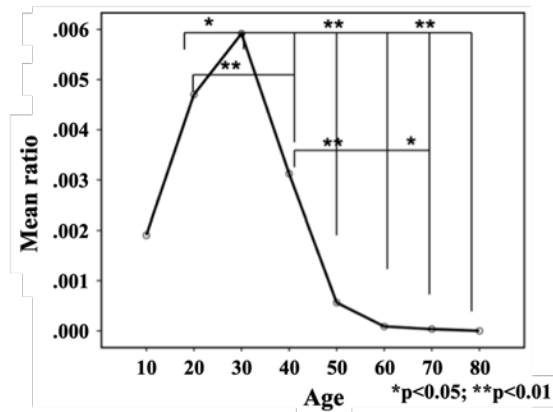
porphyrin area and mean intensity, the significance difference started earlier from 20 years old. From the graph we can see that after 50 years old, there was no significant difference anymore, which may be due to lack of sebum.



(a) Porphyrin number change with age



(b) Porphyrin area change with age



(c) Porphyrin mean intensity change with age

Figure 4.9: Porphyrin variation with age

## 4.5 Discussion

In this research, we developed a new quantitative algorithm to classify and extract the porphyrins features from skin fluorescence images which had the potential to monitor skin health. Furthermore, age-related changes with porphyrins in healthy skin were conducted applying the algorithm proposed. The range of fluorescence is the key point for the proposed approach so that precise and numerical parameters like fluorescence number, area and mean intensity can be used to reflect skin conditions quantitatively.

Prior studies have noted the importance of fluorescence images in skin acne evaluation, like skin acne grade classification, skin acne lesion segmentation. Several fluorescent image processing algorithms have been performed until now for skin acne or sebum evaluation in general. The proposed algorithm utilized the feature in different color models to extract the fluorescence number, area and mean intensity at the same time. M. Khongsuwan et al. [72] used the extended maxima transform to extract porphyrin numbers. However, it might cause over-segmentation and only calculated the number. Assessing the porphyrin number and area at the same time is more accurate because situations often happen with little number but large areas. Other research [71] used the whole facial images as the original data, where fluorescence shows too small and is hard to count the number.

The correlation of fluorescence and age was performed under large-scale samples from Japan, which presented human skin porphyrin was increasing with age until 30 years old when it got to the highest level. Later porphyrin decreases rapidly until 50 years old. There is no significant variation after 50 years old. All the three fluorescence indexes showed similar trends, which was also reported by K. J. McGinley et al. [76]. There are several possible explanations for this result. First of all, porphyrins evaluated in the study are mainly produced by *P. acnes*, and *P. acnes* change with age. J. J. Leyden et al. [77] found out *P. acnes* levels increase with age and get to the peak around 30 years old, which confirms the association between fluorescent porphyrins and *P. acnes*. The second reason may be related to sebum secretion. H. Dobrev et al. [68] explored the relationship between fluorescence intensity and sebum level in patients with acne and found out the strong correlation with the parameters, number, and percentage of the area, which were similar to our study. S. W. Youn et al. [78] investigated that porphyrins were affected by not only *P. acnes* but also sebum secretion. However, this relationship is contrary to that of D. T. Xu et al. [79] who found that the ultraviolet-induced red fluorescence is emitted by resident bacteria, rather than by sebum. These results should be interpreted with caution because sebum secretion might be the major factor determining *P. acnes* populations.

In addition, people usually feel more stressed both at work and home after they graduate from university and start to work even build a family. M. Tanida et al. [80] demonstrated the subjects with higher sebum levels and high *P. acnes* populations in the facial skin were more sensitive to stress.

More information existing in fluorescence images is waiting to be discovered, as shown in Fig. 4.10, other than red-orange fluorescence spots, there are white spots, black areas, and bright blue substances, representing sebum secretion, pigmentation and exogenous substances to each. It would be more effective to predict skin health if all this information can be extracted and segmented directly from the fluorescence images using image processing or machine learning. A. Lihachev et al. [81] used the fluorescence images to differentiate seborrheic keratosis, basal cell carcinoma, nevi and melanoma. K. Tsuchida et al. [82] found out the positive correlation between oxidative stress and skin porphyrins, which also indicated skin porphyrins are related to skin aging.

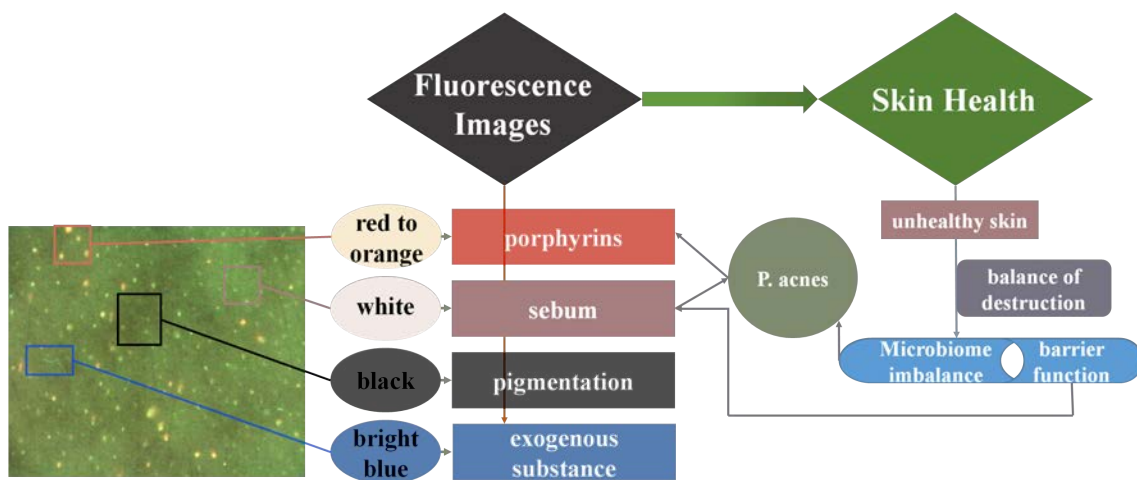


Figure 4.10: Information illustration of the skin fluorescence image

The utilization of fluorescence images is not only in the field of skin conditions, but also in the product quality appraisal. G. Sauermann et al. [83] analyzed comedogenic possibility of raw materials and consumer products by comparing the fluorescent images before and after using them. The parameters they chose were the number of fluorescent spots/area, size of individual glands and fluorescence intensity, which were similar to the parameters selected in the study.



The proposed method focused on the fluorescence attribute in normal skin. Most studies compared the frequency zone of fluorescence, like nose, head, however, cheek site would also have strong fluorescence intensity when skin becomes unhealthy in daily life, such as keratotic plugs.

On the other hand, when there are a lot of people with different skin disorders, like acne vulgaris with different visual types and severity, the therapeutic effect in porphyrins may need more time than visual improvement. There are several algorithms proposed to assess and classify the acne vulgaris with optical images [74, 84, 85]. It would be better to diagnose and follow up on the effect combining the results of fluorescence images and optical images.

## **4.6 Conclusions**

In conclusion, the convenient and quantitative evaluation algorithm of fluorescence proposed in this study has the potential to be an effective assisted tool to monitor skin health and support skin acne diagnosis. The study figured out the variation trends of porphyrin fluorescence in cheek site with age, which it shows level up from 10 years old and got the peak in 30 years old, and then level down from 30 years old. These variation trends provide the fiducial values for skin condition evaluation.

For skin porphyrin extraction, it is hard to extract porphyrin accurately without over segmentation, especially when there are few porphyrins. Proposed method focused on the color information of porphyrins, and found out the most suitable color space HSV, and the most appropriate ranges, which prevent the possibility of over segmentation.

In the future, combined with the fluorescence extraction algorithm, more segmented methods should be designed for more information extraction from fluorescence images, such as comedogenic possibility, the sebum level quantification, pigmentation analysis, and so on.



## **Chapter 5**

# **Quantitative Evaluation of Skin Barrier Function: a Preliminary Study**

## 5.1 Introduction of Skin barrier function

As the outermost organ of human body, skin takes a momentous role in defending against the harmful external factors owing to its complex structure and physicochemical properties. Therefore, skin barrier function is one of the prior research areas in the field of dermatology and cosmetics, which is formed mainly by a unique structure of lipids and corneocytes from the Stratum corneum (SC), the most external layer of epidermis.

The state of the skin barrier is determined by its physical properties, such as epidermal hydration, transepidermal water loss (TEWL), the pH values, and sebum amount. Healthy skin has acidic pH values, oscillating between 4.0 and 6.0. A hydro-lipid film covers the surface of SC, which mainly consists of sebaceous gland lipids as the biochemical barrier. Epidermal hydration is thus preserved inside without loss. A sufficient quantity of water is a prerequisite for maintaining normal structure and function of the SC [86–90]. Two characteristic parameters are used to represent the water content, skin surface hydration content, and TEWL. Impairment of skin barrier function usually accompanies with low levels of SC hydration and high levels of TEWL.

There are a number of individual and environmental factors that would influence these properties and further on skin barrier function, like the environmental humidity, temperature, seasons, race, gender, age, anatomical sites, and so on. Consequently, objective and quantitative measurement of these properties is quite important for monitoring skin barrier conditions. A variety of measurement has been developed recently including invasive and non-invasive methods.

According to the revised EEMCO guidance [91], non-invasive skin hydration evaluation is usually based on electrical methods, including capacitance and conductance. Mainstream electrical evaluation has already made commercial instruments come true. Probes are designed to measure skin hydration. Skico-200EX (I.B.S. Co., Ltd., Japan) is developed utilizing the principle of skin electrical conductance. In addition, one more popular commercial instrument is Corneometer CM825 (Courage Khazaka Co., Ltd.,

Germany), which applies electrical capacitance as measuring principle. Both of these instruments represent high levels of skin hydration positively.

Within rapid development of image technology, it has been possible to measure skin hydration by images. Mapping of skin hydration by electrical capacitance multisensor is one of the methods to make variation of skin hydration visualization [92–94]. This measurement is based on capacitance imaging and the sensor measures the penetration of the electromagnetic field. Water reflect the signal making the resulting pixel darker while non-conductive material makes the signal go farther inside and the resulting pixel would be lighter on a scale of 255 grey levels [86,95]. Thus, high levels of skin hydration are represented by grayscale values negatively. The MoistureMap (Courage Khazaka Co., Ltd., Germany) has been available commercially. Furthermore, skin hydration image captured under near-infrared (NIR) light source has also been developed to visualize water distribution [96,97]. This method applies the water OH band centered near 1920nm to evaluate skin hydration. High levels of skin hydration are characterized by lighter pixels.

In addition, hydration measurement based on spectroscopy data is also developed recently. B. P. Yakimov et al. [98] used diffuse reflectance spectroscopy data to assess skin water content.

However, traditional methods have plenty of flaws that need to be addressed. For probe used methods, the operation usually needs professional trained operators, and it is easily influenced by pressing strength. Also they can only measure the partial area of the skin due to the small area of the probe, which makes skin hydration mapping difficult. For capacitance image based methods, it forms the non-optical image eventually still with the probe integrated multi-sensors, which is expensive and regionally. Until now skin hydration evaluated by images are mainly focused on their electrical properties or optical properties of water on the wavelength of near infrared area, and the details show in Table 5.1. For NIR image methods, it is effective but needs professional light source, which is inconvenient and costly.

As a matter of fact, skin surface optical properties are highly influenced by skin hydration conditions. T. Y. Masahiko Ooe et al. [99] explored the influence of SC hydration for optical properties and found out the adequate hydration contents (up to 38%) in the SC showed gradually to increase the transmission, while excess hydration conversely decreased. Z. X. Jiang et al. [100] studied the appearance benefits of skin moisturization and their research revealed that the optical heterogeneity of skin surface decreases when skin hydration levels up. Both the skin spectral reflectance and the skin scattering coefficient decreased as skin was hydrated.

Table 5.1: Related work of skin hydration evaluation

Approach	Image capture device	Image data	Algorithm	Extracted features
D. Batisse [94]	Capacitance device	Partial skin image	Calculate the mean gray level and mean thresholded histogram 20	Grayscale value (darker means high content)
H. Arimoto [97]	NIR device	Partial skin image	Calculate the area of light grayscale region	Grayscale value (lighter means high content)
M. Egawa [96]	NIR device	Whole facial image	Mesh partition analysis algorithm	Grayscale value (lighter means high content)

In this chapter, based on skin optical properties with skin hydration conditions, we proposed a new method to evaluate skin hydration objectively and quantitatively from optical skin images. Reflectance intensity is extracted as the feature to evaluate skin hydration. Skin hydration values evaluated by Corneometer and Skicon are set as ground truth to be compared.

## 5.2 Methods and materials

### 5.2.1 Skin hydration evaluation instruments

#### Skin hydration evaluation instruments based on electrical measures

Two common evaluation instruments of skin hydration were applied in the study, which are Corneometer® CM825 (Courage Khazaka, Germany) and Skicon-200EX (I.B.S. Co., Ltd, Japan).

### **Skin image capture device**

The optical skin image was captured by EPISCAN (CBON Co., Ltd., Tokyo, Japan) with a camera, white LED lamps and blue LED lamps (Fig. 5.1). The whole facial image could be captured and the resolution of it is  $980 \times 1307$  pixels.



Figure 5.1: The whole facial skin image capture instrument: EPISCAN [4]

### **5.2.2 Database of skin hydration**

As a prior study, two healthy Japanese female volunteers aged 30s were enrolled. The study was conducted according to the principles of the Declaration of Helsinki. Informed consent was obtained from all the subjects after the subjects were providing a complete explanation of the protocol. As shown in Fig. 5.2, three facial sites of skin surface hydration from two volunteers were evaluated three times as the database of skin hydration, which include before using the moisture cream, after using the moisture cream for 15 minutes, and after using the moisture cream for 60 minutes. Three instruments were applied to record the skin hydration inclusive of skin image capture machine, EPISCAN, and common skin hydration evaluation instruments, Corneometer and Skicon. Measured skin hydration values from Corneometer and Skicon are set as ground truth. During the measurements, the device was put gently and fully on the measured area to avoid any pressure or outside light. The ground truth data was all operated for three times and the mean values represented facial skin hydration for each subject.

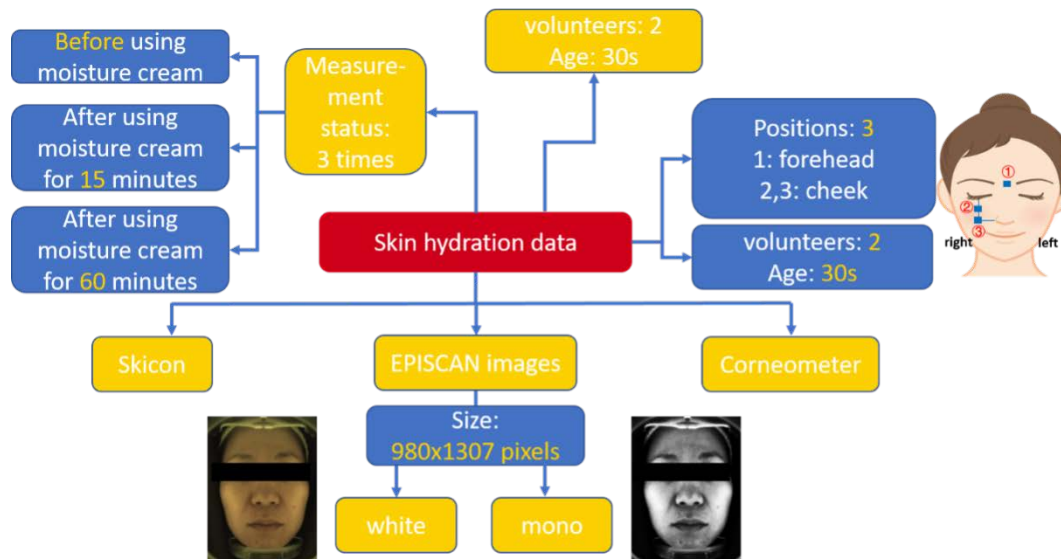


Figure 5.2: Skin hydration database

### 5.3 Image processing

The flowchart of skin hydration extraction algorithm is shown in Fig. 5.3. Image processing was enabled by MATLAB software. There are two series of original images from EPISCAN and the white image was chosen as the original image to be processed, which were recorded in RGB color space and consisted of  $980 \times 1307$  pixels pixels with the resolution.

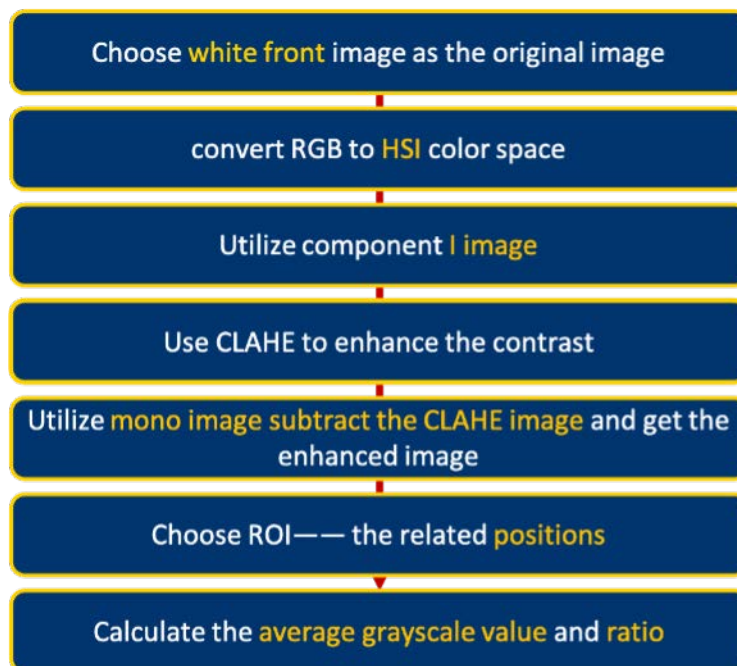


Figure 5.3: The flowchart of skin hydration extraction

Since RGB color model is more fitted in computer vision instead of human vision, conversion of color model is necessary. There are plenty of color models such as CIE- $L^*a^*b^*$  color space, which is usually applied in skin color evaluation, CMY color model, which is commonly used in color printing. In the study, HSI color model was selected, where each color represented by three components: hue (H), saturation (S), and Intensity (I).

Conversion formula from RGB to HSI is shown as follows.

$$\theta = \cos^{-1} \left\{ \frac{\frac{1}{2}[(R - G) + (R - B)]}{[(R - G)^2 + (R - B)(G - B)]^{1/2}} \right\} \quad (5.1)$$

$$H = \begin{cases} \theta, & B \leq G \\ 360 - \theta, & B > G \end{cases} \quad (5.2)$$

$$S = 1 - \frac{3}{(R + G + B)}[\min(R, G, B)] \quad (5.3)$$

$$S = 1 - \frac{3}{(R + G + B)}[\min(R, G, B)] \quad (5.4)$$

Figure 5.4 displays the illustration of HSI color model.

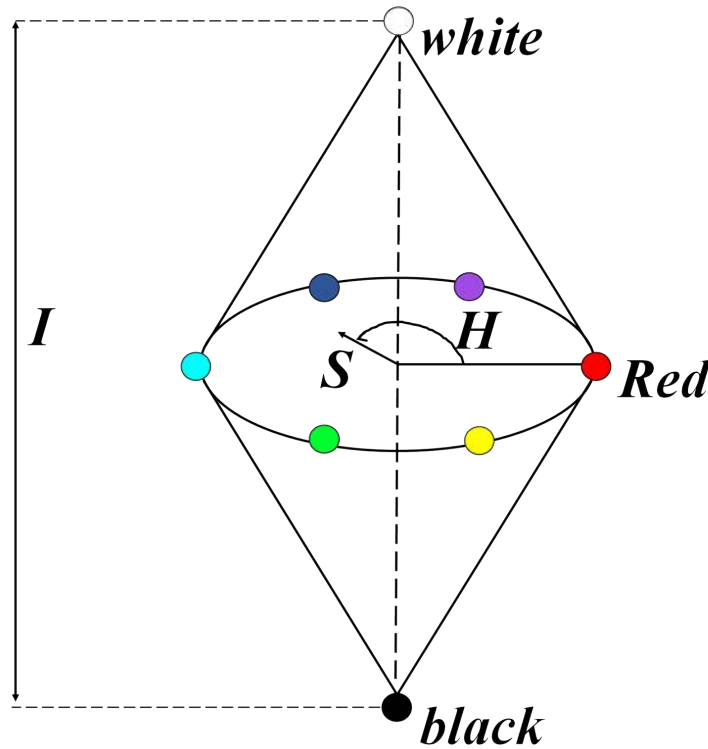


Figure 5.4: The illustration of HSI color model

After conversion to HSI color space, component I (intensity) was extracted for further processing. For the purpose of contrast enhancement, contrast limited adaptive histogram equalization (CLAHE) algorithm was utilized to obtain enhanced skin image. Contrast enhancement is always applied to make the reflectance of light more obvious, where brighter area represents high reflectance. In contrast with ordinary histogram equalization tending to overamplify the contrast in near-constant regions, contrast amplification is limited in CLAHE making noise reduction possible [101]. Contrast enhancement in the neighborhood of a given pixel value is given through the slope of the transform function, which is proportionate to the slope of the cumulative distribution function of neighborhoods (CDF) and hence to the histogram value at this pixel value. Predefining value before computing the CDF is the principle to make the limitation come true, which restricts the slope of the CDF and thus of the transform function.

Large information details of skin have a bad effect on skin reflectance computing, which both exist in mono and CLAHE images, such as skin spots, color, and texture. These influences can be diminished by subtracting the CLAHE image from the mono image and the skin reflectance image was obtained.

The next step is to evaluate skin hydration content in specific region. Therefore, region of interest (ROI) was selected as same as the sites measured by Corneometer and Skicon. All of ROI are 101 x 101 pixels. Due to the skin color and human facial size, the overall intensity degree is different. Therefore, the grayscale value ratio (GVR) is also computing besides the average grayscale value (AGV). The formula of grayscale value ratio is performed as follow.

$$\text{Grayscale Value Ratio (GVR)} = \frac{\text{average grayscale value of ROI}}{\text{sum gray value of whole image}} \quad (5.5)$$

### 5.3.1 Statistical analysis

SPSS 21.0 (SPSS Science, Chicago, IL) software was used for all statistical analyses. The variation trends of skin hydration content before and after using moisture cream were



illustrated by folded line chart. Pearson correlation coefficients were assessed among the hydration values measured by Corneometer and Skicon and grayscale value ratio calculated by proposed algorithm, in which lower than 0.3 representing weak correlation, 0.4-0.6 representing mediate correlation and higher than 0.6 representing high correlation. The linear regression was applied to explore the relationship among the skin hydration value by Corneometer and Skicon and grayscale value ratio, respectively. The statistical tests were two-tailed with the following significance levels:  $p < 0.05$  and  $p < 0.01$ .

## 5.4 Results of skin hydration evaluation

### 5.4.1 Image processing results

Color model conversion results were shown in Fig. 5.5 and intensity (I) component was extracted successfully.

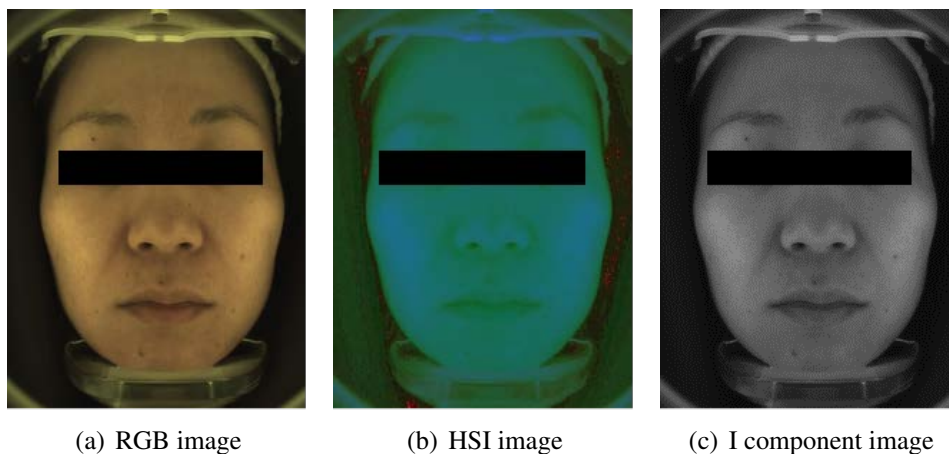


Figure 5.5: Color model conversion example

Continually CLAHE was applied to enhance the contrast of I component, which can be found out in Fig. 5.6. Skin reflectance was separated from mono image by subtracting the CLAHE image, where there was more reflectance on the cheek site over other positions. The reason of this phenomenon is not only the skin hydration content, but also the skeletal structure of the face, such as zygomatic bone.

The ROI of different positions was displayed in Fig. 5.7 both on original and reflectance images.

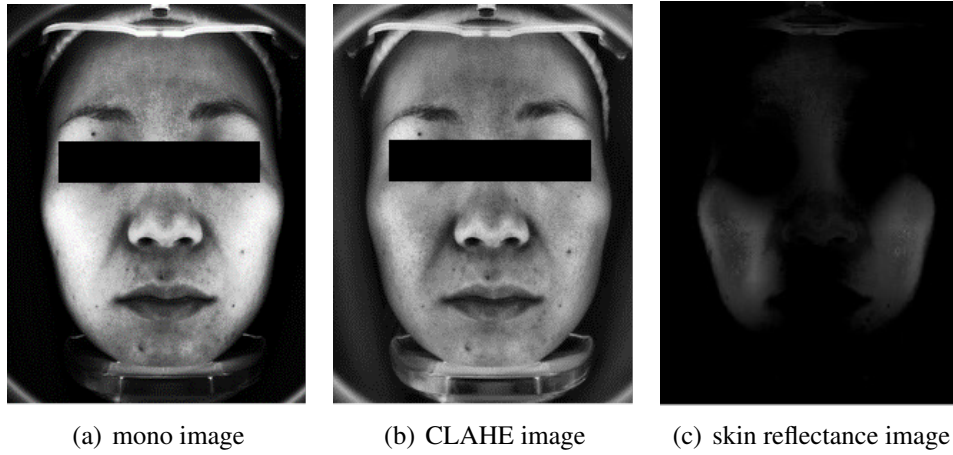


Figure 5.6: The example of mono image, CLAHE image, and skin reflectance image

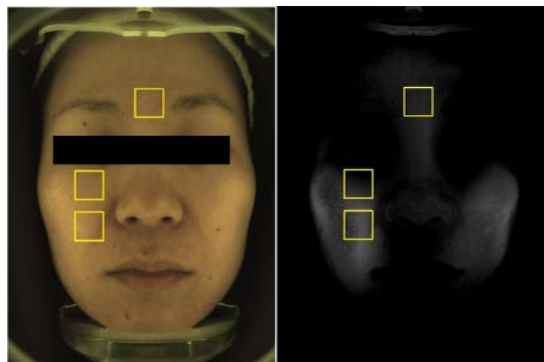


Figure 5.7: ROI comparison in original image and skin reflectance image

### 5.4.2 Before-after variation trends of skin hydration

The changes of skin hydration content before and after using the moisture cream evaluated by different instruments are shown in Fig. 5.8, which found out the variation trend of average grayscale value ratio was similar to the ground truth (both skin hydration content measured by Corneometer and Skicon), while average grayscale value had the totally different trend from the ground truth. Later the one-way analysis of variance (AVONA) was

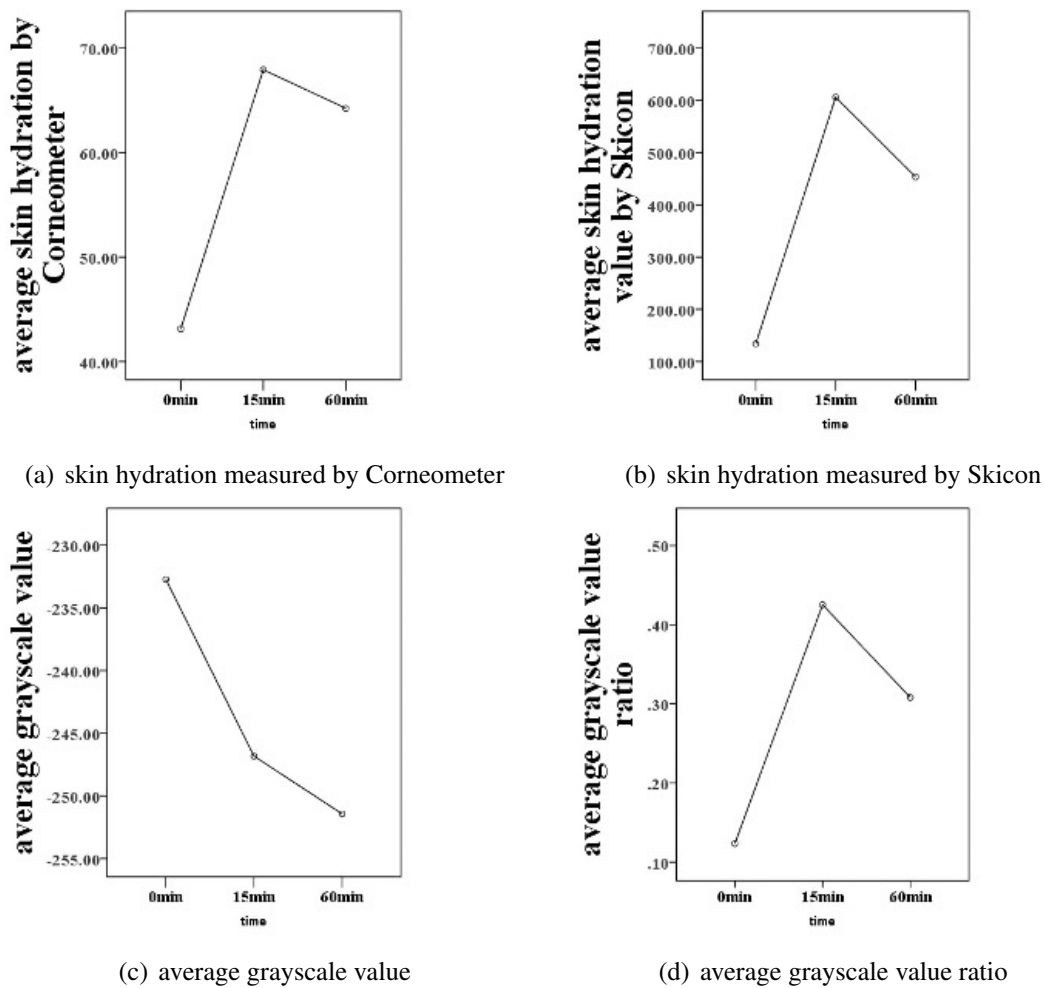


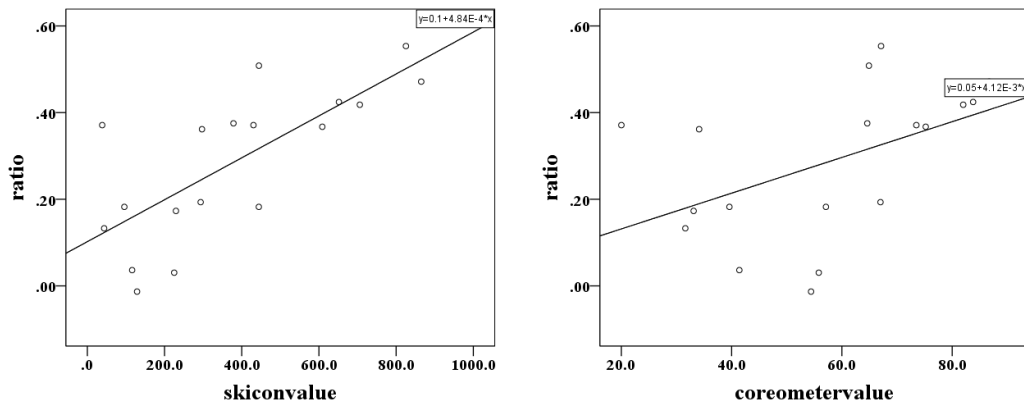
Figure 5.8: Before-after skin hydration content variation trends

applied among before and after using the moisture cream, which improved that for ground truth, there was a significant difference ( $p < 0.01$ ) of skin hydration content between 0 min and 15 min. also there was a significant difference between 0 min and 15 min, while no significant differences showed between 15 min and 60 min. Same correlation has been embodied in the average grayscale value ratio with significant differences. So far, the

average grayscale value ratio indicated same variation trend and significant correlation as same as the ground truth.

### 5.4.3 Correlation with skicon and corneometer

It was implied that average grayscale value ratio had more relationship with ground truth from before-after experiment. Therefore, the correlation of GVR with Skicon values and Corneometer values were explored by pearson correlation coefficients and linear regression, which is shown in Fig. 5.9. A positive correlation was found among GVR, Corneometer values and Skicon values.



(a) Linear regression of GVR and Skicon value (b) Linear regression of GVR and Corneometer value

Figure 5.9: Linear regression among GVR, Corneometer, and Skicon

On the other hand, it is apparent from Table 5.2 that there was medium correlation between GVR and Corneometer values. In addition, strong correlation between GVR and Skicon values were also figured out.

Table 5.2: Pearson correlation coefficient

		ratio	corneometer	skicon
ratio	Pearson correlation coefficient	1	0.477*	0.736**
	Significant difference		0.046	0
corneometer	Pearson correlation coefficient		1	0.830**
	Significant difference			0

\*p<0.05; \*\*p<0.01.

## 5.5 Discussion

In this chapter, we developed a novel algorithm using image processing to assess skin hydration quantitatively from visible optical skin images. GVR, as the feature value, has been proved to highly relate to skin hydration ground truth. The reflectance intensity image is the key point for the proposed approach since skin color, texture, and spots have large effect on skin hydration evaluation.

A lot of color model has been tried out, like the skin color represented CIE-L\*a\*b\* color model, which has been proved without any effect. At last, HSI color model was selected since the original image is low-light image, which enhancement algorithm would be more effective and without over enhancement based on HSI color space [102].

Contrast enhancement is the regular operation for most image processing algorithms. However, choosing different algorithm would obtain totally different results. In this research, what we need is non-reflectance images with high contrast. Plenty of enhancement algorithms were attempted, and the results showed that CLAHE was the most fitted algorithm in the study.

Non-invasive skin hydration measurement has been researched and developed for many years. Researchers are not content with conventional probe measurement, since the evaluation area is small and it is easily influenced by pressure. Skin hydration measurement based on image processing and machine learning is state of the art. K. Koseki et al. [88] applied topological data analysis to measure the TEWL with skin images and predicted TEWL using machine learning. It is surprising to develop the rational algorithm to represent parameters related to skin barrier function. S. Liaqat et al. [103] also applied machine learning to detect skin hydration level, whose dataset is from collecting skin conductance data by the non-invasive wearable sensor. However, in this research, tradition image processing was utilized and skin hydration related optical properties were under consideration, which is also proved effective. Most comprehensive skin measurement instruments are optical system, no matter the professional instruments, like VISIA and SmartSkinCare, or convenient instruments, like mobile applications, most of which

use smartphone's lens directly. Therefore, the development hydration measurement of visible optical skin images has a board prospect of adapting these existing instruments.

## **5.6 Conclusion**

In conclusion, this novel algorithm was undertaken to design a quantitative and objective measurement for skin surface hydration evaluation from visible optical skin images. Although it is a prior study until now, it is observed that this algorithm has the great potential to be an effective evaluation method to measure skin hydration directly from visible optical images and may even visualize skin hydration mapping. The study explored a feature value to represent skin hydration and extracted the GVR parameter which has strong positive correlation with skin hydration values measured by Skicon and medium positive correlation with Corneometer values.

For skin hydration estimation, it is the first time that skin hydration related features are extracted from visible optical images with strong correlation, which provides the potential of evaluating skin hydration from images directly and mapping the variation of skin hydration.

In the future, more image data should be collected to verify the proposed algorithm. In addition, there are a variety of whole facial skin image by different instruments, and some modification may also need to be considered.

## **Chapter 6**

# **Comprehensive Evaluation System of Skin Conditions**

## 6.1 Introduction

The skin condition is full of changes and complexity, which results in a simplified measurement unsatisfied with the diagnosis of the condition of the skin in practice. Skin condition is not influenced only by one parameter, but the synthesis of various indicators. Therefore, the establishment of a comprehensive skin condition measurement system is necessary and significant.

## 6.2 Comprehensive skin evaluation system structure

### 6.2.1 Radar chart introduction

There are many types of diagrams to demonstrate the data status. Radar chart is one of the clear approach to exhibit multiple variables at the same time visibly. Due to the similarity to the graphics of radar chart in navigation radar screen, radar chart is called so and as a geometric projection method to articulate the data points in the multiple dimension. Radar chart is a visual method which has the ability to plot the point of a multidimensional space to the two-dimensional space and put into use the attribute values using two-dimensional graphics [104].

In this study, radar chart is plotted by MATLAB and the drawing method for multidimensional data is pointed out.

$X = X_1, X_2, \dots, X_j, \dots, X_n$  is a multi-dimensional data set, and  $X_i X_{i1}, X_{i2}, \dots, X_{in}$  is a N-dimensional vector. Use the radar chart when  $N \geq 3$ .

- (1) Draw a circle and divide it in N parts equally.
- (2) Connect the center and individual points. The radius is defined as the coordinate axis of the aimed attribute and marked with apropos calibration.
- (3) Mark the values of indicator N of the values observed on the corresponding axis and connect them in a form of N-sides.
- (4) Observation data N can be formed as N-sides.



## **6.2.2 Five-level evaluation rating scales design**

Rating scales has been applied prevalently in many fields. The purpose of a rating scale is to allow respondents to express both the direction and strength of their opinion about a topic [105]. With the development of rating scales, it is also used for system evaluation. Investigation of the choice and functioning of rating scale categories has a long history. Rating scale categorizations should be well-defined, mutually exclusive, univocal and Exhaustive [106].

Five-level rating scales has a widespread application on skin related evaluation. D. J. Day et al. [107] set up the 5-grade wrinkle severity rating scale and it is proved as a useful clinical tool to assess the effectiveness of soft-tissue augmentation and other facial contouring procedures. J. I. Silverberg [108] proposed a 5-level numeric rating scale to measure the skin-pain with atopic dermatitis in adults, including clear, mild, moderate, severe, and very severe. Similarly, E. K. Yeoung et al. [109] improved burn scar evaluation by developing a scar rating scale, which also has 5 levels by increasing severity, ranging in whole numbers from -1 to 4, representing smooth to rough.

In this chapter, 5-level skin condition rating scale is proposed, where 5 represents the best condition, and 1 represents the worst condition.

## **6.2.3 Evaluation index chosen standards**

The definition of beautiful and healthy skin varies among different countries and culture. White skin tends to be preferred in Asian countries, while people prefer tanning skin in western countries. There is a slight difference in skin tone even within the Asian regions, like China and Japan, not to mention the standard of skin beauty and skin concern. S. Kasolang et al. [110] reviewed the common skin disorders and found out that majority of the global population is affected by skin disorders mainly including three categories namely dry skin, acne and hyperpigmentation.

In this thesis, we define some skin indexes to assess skin condition based on the majority of common skin concerns, which includes skin health, skin aging, skin roughness, skin pores, and skin color.

The example of skin assessment result is shown in Fig. 6.1, which includes 5 dimension, and 5 levels in each dimension, ranging from 1 to 5. Higher number represents better condition. The blue section of the radar chart is the average skin condition of the era, which is set as level 3 in all dimensions.

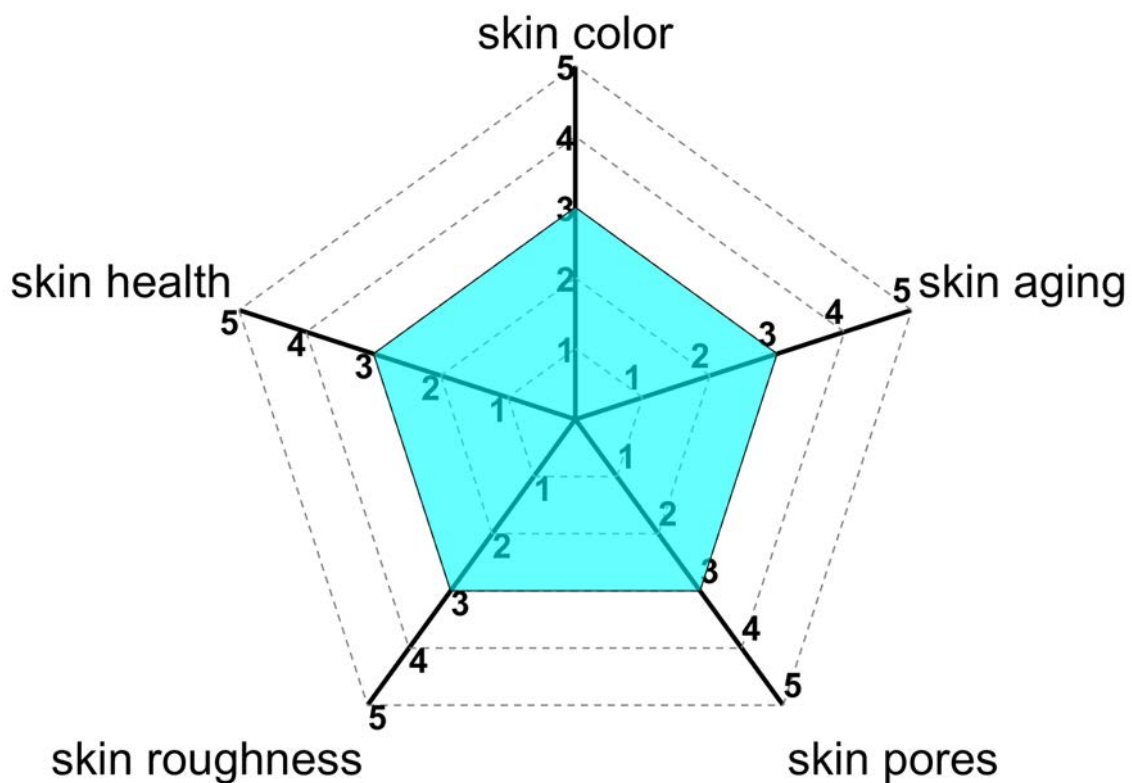


Figure 6.1: Skin evaluation score of average level

## 6.3 System algorithm design

### 6.3.1 Skin health algorithm design

As we known, skin health is highly related to skin surface flora. And *P. acnes* is one of them, which produce porphyrins with fluorescence under ultraviolet light. Therefore, the status of porphyrins is possible to imply skin health. Three features about porphyrins are

extracted well from Chapter 4, including porphyrin number, porphyrin area, and mean intensity of porphyrins. Two of them of selected to calculate skin health by the following formula (6.1).

$$\text{skinhealthlevel} = \min[\text{level}(\text{porphyrinnumber}), \text{level}(\text{meanintensityofporphyrins})] \quad (6.1)$$

According to the samples in Chapter 4, it is figured out that both porphyrin number and mean intensity of porphyrins change with age, which reveals that the rating scale needs to be set differently with age. Table 6.1 calculated the number of level 3 firstly, which are the average value among age groups. And then other levels' values are also determined based on the percentage.

Table 6.1: Level standard of porphyrin number among age groups

Level	10s	20s	30s	40s	50s	60s	70s
5	0	0	0	0	0	0	0
4	4	2	2	2	1	1	1
3	10	8	7	8	4	2	2
2	20	21	21	23	17	5	4
1	21	22	22	24	18	6	5

Table 6.2 is calculated in the same way. According to formula (6.1), the maximum level is chosen as the final level of skin health.

Table 6.2: Level standard of mean intensity of porphyrins among age groups

Level	10s	20s	30s	40s	50s	60s	70s
5	0	0	0	0	0	0	0
4	0.12%	0.08%	0.09%	0.04%	0.03%	0.02%	0.01%
3	0.31%	0.27%	0.28%	0.15%	0.07%	0.04%	0.02%
2	0.61%	1.05%	0.97%	0.72%	0.20%	0.07%	0.03%
1	0.61%	1.05%	0.97%	0.72%	0.2%	0.07%	0.03%

### 6.3.2 Skin aging algorithm design

Skin aging is a huge project, which is effected by internal and external factors at the same time. Skin aging appearance gives expression to many prospects, mainly focused on skin micro-relief. Four related indexes are chosen to imply the skin aging.

Contrast is one of the features extracted by Tamura Features in Chapter 2, which disclosed the depth of skin furrows and the higher the contrast, the deeper the skin furrows, as well as the older skin. Skin contrast has strong correlation with age, and according to the formula of skin contrast variation with age (6.2), average contrast values among each age group are computed as level 3.

$$y = 0.05x + 11.26 \quad (6.2)$$

Later other levels are calculated based on the percentage as shown in Table 6.3.

Table 6.3: Level standard of contrast among age groups

Level	0s	20s	30s	40s	50s	60s
5.0	8.0	9.0	9.0	9.0	10.0	10.0
4	10.0	11.0	11.0	11.0	12.0	12.0
3	11.5	12.5	13.0	13.5	14.0	14.5
2	13.0	14.0	15.0	15.0	16.0	18.0
1	15.0	16.0	17.0	18.0	18.0	20.0

Furrow state is highly correlated with skin aging. Furrow has primary lines and secondary lines. In chapter 2, we found out furrow length (FL) decreases with age and furrow width (FW) increases with age. Therefore, the shorter furrow length, the older skin. The wider furrow width, the older skin, which forms the level values in Table 6.4 and 6.5 calculated by the formula of furrow length with age (6.3) and furrow width with age (6.4).

$$y = -108x + 3.26E4 \quad (6.3)$$

$$y = 0.02x + 4.47 \quad (6.4)$$

Table 6.4: Level standard of furrow length among age groups

Level	0s	20s	30s	40s	50s	60s
5	40000	40000	40000	40000	35000	35000
4	36500	35000	35000	33870	30830	30290
3	33140	29900	28820	27740	26660	25580
2	28000	22500	20000	18870	18330	17790
1	23000	15000	10000	10000	10000	10000

Table 6.5: Level standard of furrow width among age groups

Level	0s	20s	30s	40s	50s	60s
5	2.5	2.5	2.5	2.5	2.6	2.8
4	3.5	3.7	3.8	3.9	4.1	4.3
3	4.6	5.0	5.2	5.4	5.6	5.8
2	6.0	6.3	7.6	7.7	7.8	9.1
1	7.5	7.5	10.0	10.0	10.0	12.5

In addition, closed polygon is also related to skin aging. The formula of average area of closed polygon (ACP) with age is as follows (6.5).

$$y = 6.67x + 1.22E3 \quad (6.5)$$

According to the formula (6.5), skin closed polygon increases with age, and average value among age groups is calculated as level 3. Other level values are computed by percentage, which is shown in Table 6.6.

Table 6.6: Level standard of average area of closed polygon among age groups

Level	0s	20s	30s	40s	50s	60s
5	900.0	850.0	850.0	800.0	800.0	800.0
4	1076.5	1118.4	1151.7	1160.1	1193.4	1226.8
3	1253.4	1386.8	1453.5	1520.2	1586.9	1653.6
2	1626.5	1843.4	1976.7	2110.1	2293.4	2326.8
1	2000.0	2300.0	2500.0	2700.0	3000.0	3000.0

Each parameter's evaluation rating scale is calculated and in conclusion, skin aging is the average level of all these parameters, whose formula is shown as follows (6.6).

$$\text{skin aging} = \text{round}\left(\frac{\text{level}(\text{contrast}) + \text{level}(\text{FL}) + \text{level}(\text{FW}) + \text{level}(\text{ACP})}{4}\right) \quad (6.6)$$

### 6.3.3 Skin color algorithm design

Skin color is effected by ITA value and hue angle at the same time. ITA has a bias on the lightness and melanin content, while hue angle represents erythema and yellowish more. The combination of ITA and hue angle has the capacity on skin color in an all-round way. ITA has its level already according to the ITA values. Since there is no significant

difference between age and skin color, the related level of ITA and hue angle is shown in Table 6.7 without comparison among age groups.

Table 6.7: Level standards of skin color

Level	ITA	Hue angle
5	55° (very light)	40
4	41° (light)	45
3	28° (immediate)	50
2	10° (tan)	55
1	-30° (brown)	60

The formula of skin color calculation is as follows.

$$\text{skin color} = \text{round}\left(\frac{\text{level}(\text{ITA}) + \text{level}(\text{Hueangle})}{2}\right) \quad (6.7)$$

### 6.3.4 Skin roughness algorithm design

Skin roughness is also called skin coarseness, which is extracted directly in Chapter 2. Skin roughness reveals skin hydration, skin texture, and skin smoothness, playing a vital role in skin evaluation visually. The relationship between coarseness and age is exhibited in following equation (6.8).

$$y = 0.03x + 18.79 \quad (6.8)$$

Same method as above was utilized, level standards of skin roughness are shown in Table 6.8.

Table 6.8: Level standards of skin roughness among age groups

Level	0s	20s	30s	40s	50s	60s
5	15	16	16	16	16	16
4	17	19	19	19	19	19
3	19	20	20	21	21	21
2	21	22	22	22	22	22
1	21	24	25	25	25	25

### 6.3.5 Skin pores algorithm design

Skin pores are affected by many factors, and due to the gravity and sebum secretion, skin pores become bigger and more obvious with age. In this evaluation system, average pore

area is the key index to affect skin pores. According to the formula (6.9), the values of level 3 among different age groups are calculated first, and other values are continually computed with percentage, as shown in Table 6.9.

$$y = 6.75x + 7.86E2 \quad (6.9)$$

Table 6.9: Level standards of average skin pores area among age groups

Level	0s	20s	30s	40s	50s	60s
5	500	500	500	500	500	500
4	650	700	700	700	700	700
3	820	955	1022	1088	1157	1225
2	950	1200	1200	1400	1400	1400
1	1000	1500	1500	2000	2000	2000

## 6.4 Application for skin conditions evaluation

After establishing the comprehensive skin evaluation system, some skin image samples from the volunteer aged 25 years old (Fig. 6.2) are captured using the microscope, including the images from canthus and forehead. Image processing algorithms from Chapter 2 to 4 are utilized to analyze the conditions of skin micro-relief, skin color, and skin porphyrins.

The skin parameters details are evaluated by equation 6.1 to equation 6.9, and the comparison results between canthus and forehead are shown in Table 6.10 to 6.12, which is found out that skin health level of canthus is 5 while the level of forehead is 4 because of the high value of porphyrin number in Table 6.10. Skin aging is decided by several parameters shown in Table 6.11, and the final level of skin in canthus arrives at 4, while the forehead skin only gets 2. In addition, the skin pore condition in canthus is also better than forehead. For skin roughness, canthus skin condition gets level 4, which is also higher than forehead skin according to the calculated values. Skin color condition is determined as the average value of ITA and hue angle levels, therefore, the final level of skin color in canthus and forehead is 4 and 3 separately shown in Table 6.12.

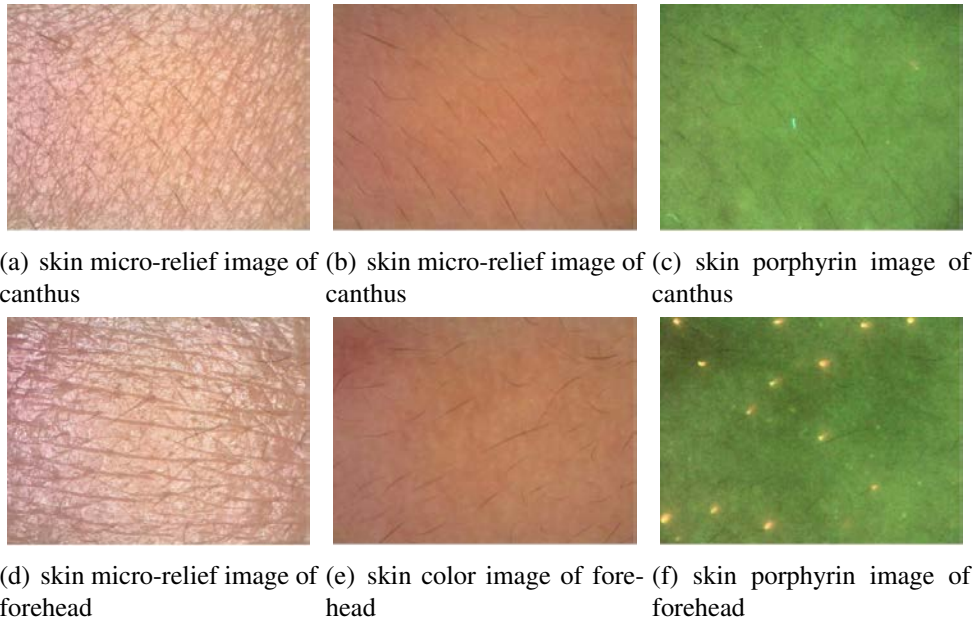


Figure 6.2: Skin samples captured by microscope

Table 6.10: Skin health level calculation

	Porphyrin number	Mean intensity of porphyrins	Level result
Canthus	0	0.00%	5
forehead	3	0.00%	4

Table 6.11: Skin aging, pores, and roughness calculation

	Contrast	FL	FW	ACP	Aging	Roughness	pore
Canthus	14.52	30914.6	4.22	1269.8		19.96	751
Level	2	3	4	4	4	4	4
forehead	15.47	18520	6.55	2219.5		20.93	1339.5
level	2	1	2	1	2	3	2

Table 6.12: Skin color calculation

	L	a	b	ITA	level	Hue angle	level	average
Canthus	56.65	20.95	25.53	31.7	3	48.1	4	4
forehead	35.38	12.05	15.6	21.8	2	49.3	4	3

Radar charts of these two anatomical sites are displayed in Fig. 6.3, which can be found out clearly that skin condition in crow's feet is better than forehead.



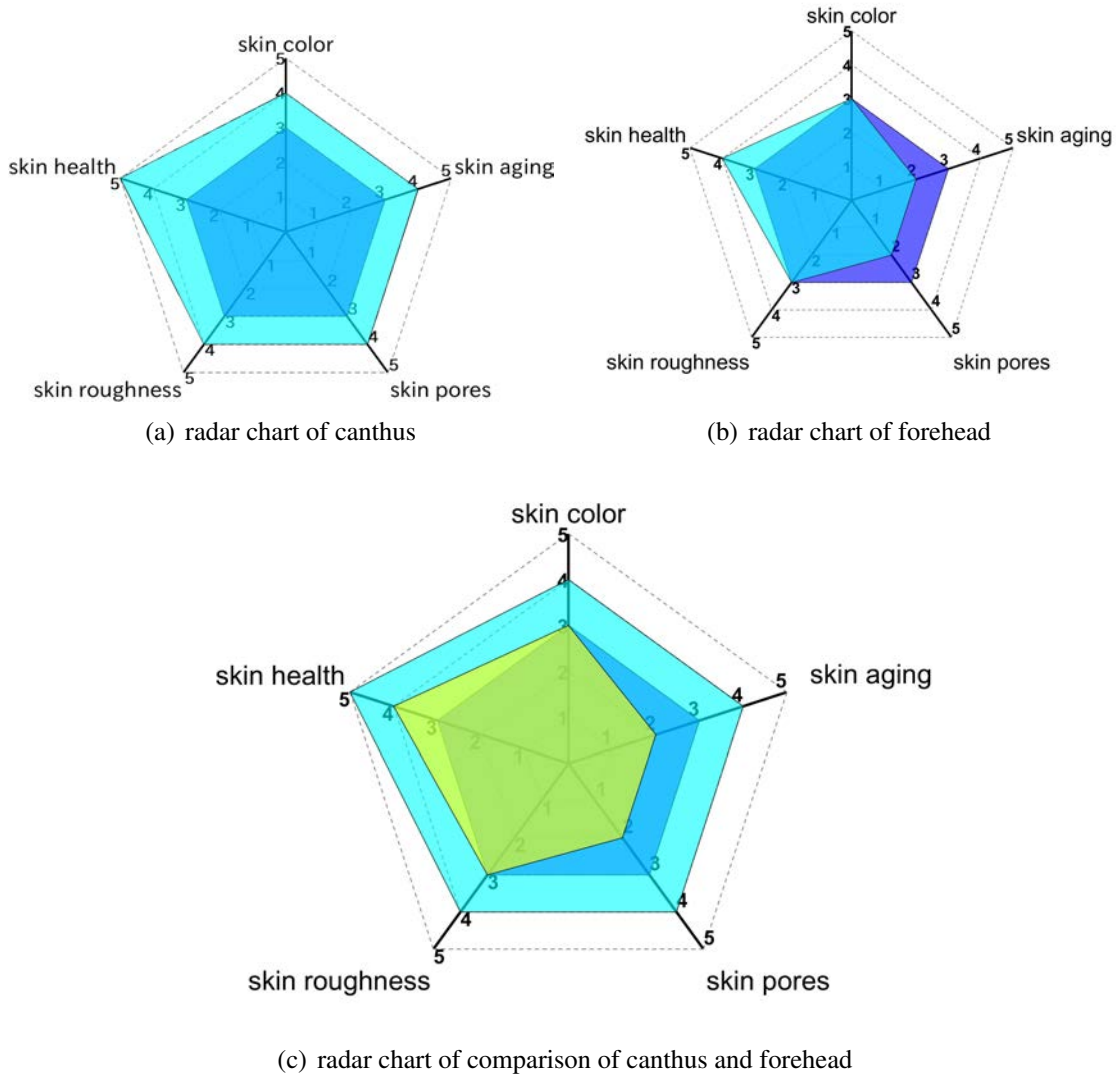


Figure 6.3: Radar chart of skin conditions

## 6.5 Discussion

In this chapter, comprehensive skin evaluation system was established, where five indexes are selected to represent skin condition synthetically. It is proved effectively and is easy to compare the results through the application of canthus and forehead.

In fact, this skin evaluation system is only the prototype and is not complete, which is built on account of the algorithms from Chapter 2 to 4. Some important skin parameters are not included yet, such as skin hydration and sebum.

On the other hand, radar chart is a common method to visualize composite indicator (CI). However, when involved in comparative evaluation of radial visualization solutions,

radar chart does not have the good performance [111]. As a CI, skin condition evaluation and visualization is complicate, especially when the skin condition changes over time, the comparison of this CI is more difficult to visualize.

## **Chapter 7**

### **Conclusions and Future Work**

The measuring of the skin is quite critical due to its function as a barrier to the human body. Within the complexity of human skin, most measurement can only measure the single property and small area. The evaluation methods presented in this thesis address this issue from four aspects by using image processing, including skin micro-relief, color, porphyrins, and hydration. In addition, the comprehensive skin evaluation system is established based on the extracted features. This chapter epitomizes the major contributions of this dissertation. Some perspectives are introduced for future research as well.

## 7.1 Conclusions

Objective measurement of skin micro-relief is proposed in Chapter 2, with four series of features extracted by image processing. Not only the skin surface property, but also the skin pores, furrows and closed polygons are segmented and calculated. Parameters variation of skin micro-relief with age is also explored, which provides the skin anti-aging advice.

Based on the comparison of skin color measurement by different instruments, Chapter 3 presents a quantitative skin color evaluation algorithm from digital images. ITA and hue angle are selected as standard indexes to represent skin color properties, including the information of brightness, melanin, and erythema. Skin color information is also proposed by comparing the anatomical sites and geographic regions.

Skin flora has momentous influence on skin health, and porphyrins by *P. acnes* are visible under the ultraviolet light, the properties of fluorescence produced by porphyrins are important. In Chapter 4, we propose a new algorithm to extract fluorescence and reveal the skin porphyrins variation with age.

Chapter 5 studies objective measurement of skin hydration from visible optical images, which is the first attempt and reached a great result by segmenting the skin reflectance of images.

According to several skin properties evaluated separately in Chapter 2 to 5, a comprehensive skin evaluation system is established in Chapter 6. Skin health, skin aging, skin

roughness, pores, and skin color are selected as representative indexes of comprehensive skin evaluation system, displayed as the radar chart.

## 7.2 Future research prospects

Skin surface characteristics include not only skin micro-relief, color, porphyrins, and hydration, but also other skin barrier function related parameters, such as skin sebum, TEWL values, and pH value. There are little research using optical images to extract them. Most of evaluation methods is to use the professional probes and tapes. Therefore, it would be great challenges to design the accurate algorithm, which needs not only image processing technology, but also optic simulation in skin and color science knowledge.

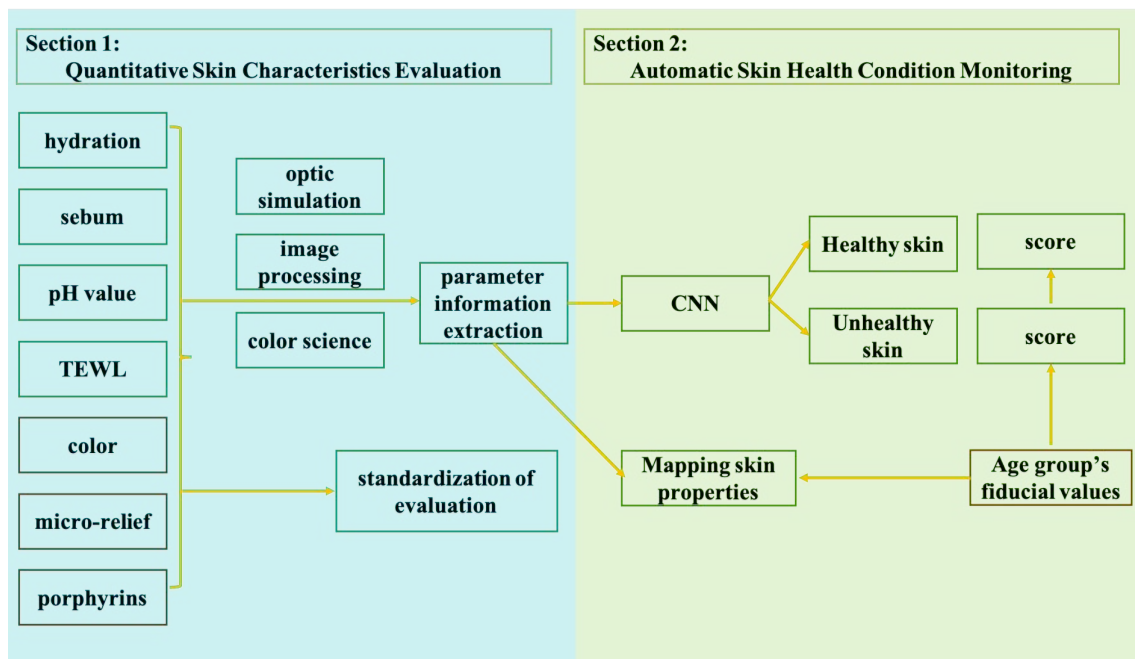


Figure 7.1: Future research perspectives

As shown in Fig. 7.1, eventually parameter information highly related to skin bio-physical properties would be extracted from optical images. Furthermore, these properties distribution in facial epidermal layers would be visualized and form the property map.

The future perspective is to develop an automatic skin health condition monitoring system using machine learning for cosmetic dermatology to detect skin health condition. First, classification algorithm would be chosen to detect if the skin is healthy or not, for

example, CNN. Combined with parameter's fiducial values of different age group, skin health score would also be calculated automatically, which has the potential to determine the effects of cosmetic procedures and treatments. In addition, the indirect goal is to contribute to the reduction of medical costs by compensating for the shortage of human resources among aesthetic dermatologists in the future.

# Lists of Author's Publications

## Journals

1. Yue Wu, Makio Akimoto, Hiroshi Igarashi, Yoshinao Shibagaki, Toshiyuki Tanaka. [Quantitative Assessment of Age-dependent Changes in Porphyrins from Fluorescence Images of Ultraviolet Photography by Image Processing], *Photodiagnosis and Photodynamic Therapy*, 35:102388, 2021. <https://doi.org/10.1016/j.pdpdt.2021.102388>.
2. Yue Wu, Toshiyuki Tanaka. [Objective and Quantitative Measurement of Skin Micro-relief by Image Analysis and Application in Age-dependent Changes], *Skin Research and Technology*, 00:1-9, 2021. <https://doi.org/10.1111/srt.13060>.
3. Yue Wu, Toshiyuki Tanaka, Makio Akimoto. [Utilization of Individual Typology Angle (ITA) and Hue Angle in Measuring Skin Color by Image Analysis], *Bioimages*, 28:1-8, 2020.
4. Yue Wu, Fan Yi, Makio Akimoto, Toshiyuki Tanaka, Hong Meng, Yinmao Dong. [Objective Measurement and Comparison of Human Facial Skin Color in East Asian Females], *Skin Research and Technology*, 26(4):584-590, 2020.

## Conferences

1. Yue Wu , Toshiyuki Tanaka. [Quantitative Evaluation of Skin Micro-relief in Different Age Groups by Image Analysis], [The 17th International Conference on Biomedical Engineering], [Singapore], [2019.12].
2. Yue Wu , Toshiyuki Tanaka, et al. [Dermatological Diagnosis Support System Based on Image Analysis Using Skin Digital Scope], [The 118th Annual Meeting of the Japanese Dermatological Association], [Japan/Nagoya], [2019.6].
3. Yue Wu , Makio Akimoto. [Comparison of Skin Color Measurements between Digital Imaging and Colorimeter], [The 65th Japan Society of Applied Physics Spring Meetings], [Japan/Tokyo], [2018].



# References

- [1] P. Humbert, F. Fanian, and H. I. Maibach, *Agache's measuring the skin*. Springer International Publishing, 2019.
- [2] U. Heinrich, U. Koop, M. C. Leneveu-Duchemin, K. Osterrieder, S. Bielfeldt, C. Chkarnat, J. Degwert, D. Häntschel, S. Jaspers, H. P. Nissen, M. Rohr, G. Schneider, and H. Tronnier, "Multicentre comparison of skin hydration in terms of physical-, physiological- and product-dependent parameters by the capacitive method (Corneometer CM 825)," *International Journal of Cosmetic Science*, vol. 25, no. 1-2, pp. 45–53, 2003.
- [3] IT Access Co.,Ltd. [Online]. Available: <https://www.sma-ski.com/>.(2021-07-23)
- [4] Episcan from CBON Co.,Ltd. [Online]. Available: <https://www.cbon.co.jp/company/news/companyinfo/detail/196>.(2021-07-23)
- [5] M. Venus, J. Waterman, and I. McNab, "Basic physiology of the skin," pp. 469–472, oct 2010.
- [6] P. A. J. Kolarsick, M. A. Kolarsick, and C. Goodwin, "Anatomy and Physiology of the Skin," *Journal of the Dermatology Nurses' Association*, vol. 3, no. 4, pp. 203–213, jul 2011.
- [7] D. E. Elder, *Lever's histopathology of the skin*. Lippincott Williams Wilkins, 2014.

- [8] W. D. James, T. G. Berger, and D. M. Elston, “Acne. Andrews’ Diseases of the Skin,” *Clinical Dermatology*, 10th ed. Philadelphia, PA: Saunders/Elsevier Inc, pp. 231–250, 2006.
- [9] A. N. Bashkatov, E. A. Genina, and V. V. Tuchin, “Optical properties of skin, subcutaneous, and muscle tissues: A review,” *Journal of Innovative Optical Health Sciences*, vol. 4, no. 1, pp. 9–38, jan 2011.
- [10] P. Asawanonda and C. R. Taylor, “Wood’s light in dermatology,” *International Journal of Dermatology*, vol. 38, no. 11, pp. 801–807, 1999.
- [11] B. Fink, K. Grammer, and R. Thornhill, “Human (Homo sapiens) facial attractiveness in relation to skin texture and color.” *Journal of Comparative Psychology*, vol. 115, no. 1, p. 92, 2001.
- [12] M. Q. Man, S. J. Xin, S. P. Song, S. Y. Cho, X. J. Zhang, C. X. Tu, K. R. Feingold, and P. M. Elias, “Variation of skin surface pH, sebum content and stratum corneum hydration with age and gender in a large chinese population,” *Skin Pharmacology and Physiology*, vol. 22, no. 4, pp. 190–199, 2009.
- [13] D. Trier and T. Taxt, “Evaluation of Binarization Methods for Document Images,” *IEEE Transactions on Pattern Analysis and Machine Intelligence*, vol. 17, no. 3, pp. 312–315, 1995.
- [14] N. Chaki, S. H. Shaikh, and K. Saeed, “A comprehensive survey on image binarization techniques,” *Studies in Computational Intelligence*, vol. 560, pp. 5–15, 2014.
- [15] M. Akimoto, N. Ikeda, S. Maeda, M. Watanabe, and K. M. Tokyo, “Evaluation method of skin surface condition using image analysis,” no. 16, pp. 3–5, 2016, (Japanese).
- [16] Y. Masuda, M. Oguri, T. Morinaga, and T. Hirao, “Three-dimensional morphological characterization of the skin surface micro-topography using a skin replica and

- changes with age,” *Skin Research and Technology*, vol. 20, no. 3, pp. 299–306, 2014.
- [17] S. Hurley, C. Messaraa, C. O’Connor, A. Metois, M. Walsh, D. Mc Namee, A. Mansfield, N. Robertson, L. Doyle, and A. Mavon, “DermaTOP Blue and Antera 3D as methods to assess cosmetic solutions targeting eyelid sagging,” *Skin Research and Technology*, vol. 26, no. 2, pp. 209–214, mar 2020.
- [18] P. M. Maia Campos, M. O. Melo, and D. G. Mercurio, “Use of advanced imaging techniques for the characterization of oily skin,” *Frontiers in Physiology*, vol. 10, no. MAR, 2019.
- [19] Y. Zou, E. Song, and R. Jin, “Age-dependent changes in skin surface assessed by a novel two-dimensional image analysis,” *Skin Research and Technology*, vol. 15, no. 4, pp. 399–406, 2009.
- [20] C. Bontozoglou, X. Zhang, and P. Xiao, “Micro-relief analysis with skin capacitive imaging,” *Skin Research and Technology*, no. September, pp. 1–6, 2018.
- [21] C. I. Moon and O. Lee, “Age-dependent skin texture analysis and evaluation using mobile camera image,” *Skin Research and Technology*, vol. 24, no. 3, pp. 490–498, 2018.
- [22] A. Humeau-Heurtier, “Texture feature extraction methods: A survey,” *IEEE Access*, vol. 7, pp. 8975–9000, 2019.
- [23] H. Pang, T. Chen, X. Wang, Z. Chang, S. Shao, and J. Zhao, “Quantitative evaluation methods of skin condition based on texture feature parameters,” *Saudi Journal of Biological Sciences*, vol. 24, no. 3, pp. 514–518, 2017.
- [24] P. S. Damanpreet Kaur, “Human Skin Texture Analysis using Image Processing Techniques,” *International Journal of Science and Research (IJSR)*, vol. 2, no. 5, pp. 17–20, 2013.

- [25] P. M. Arabi, G. Joshi, and N. Vamsha Deepa, "Performance evaluation of GLCM and pixel intensity matrix for skin texture analysis," *Perspectives in Science*, vol. 8, pp. 203–206, 2016.
- [26] R. Singh, P. Shah, and J. Bagade, "Skin texture analysis using machine learning," *Conference on Advances in Signal Processing, CASP 2016*, pp. 494–497, 2016.
- [27] H. Tamura, S. Mori, and T. Yamawaki, "Textural Features Corresponding to Visual Perception," *IEEE Transactions on Systems, Man and Cybernetics*, vol. 8, no. 6, pp. 460–473, 1978.
- [28] P. Howarth and S. Rüger, "Evaluation of Texture Features for Content-Based Image Retrieval," *Lecture Notes in Computer Science (including subseries Lecture Notes in Artificial Intelligence and Lecture Notes in Bioinformatics)*, vol. 3115, pp. 326–334, 2004.
- [29] J. Rew, H. Kim, and E. Hwang, "Hybrid segmentation scheme for skin features extraction using dermoscopy images," *Computers, Materials and Continua*, vol. 69, no. 1, pp. 801–817, 2021.
- [30] C. Bontozoglou, X. Zhang, and P. Xiao, "Micro-relief analysis with skin capacitive imaging," *Skin Research and Technology*, vol. 25, no. 2, pp. 165–170, 2019.
- [31] Q. Zhang and T. Whangbo, "Skin Pores Detection for Image-Based Skin Analysis," 2008, pp. 233–240.
- [32] N. Otsu, "THRESHOLD SELECTION METHOD FROM GRAY-LEVEL HISTOGRAMS." *IEEE Trans Syst Man Cybern*, vol. SMC-9, no. 1, pp. 62–66, 1979.
- [33] M. Uchida, R. Akaho, K. Ogawa-Ochiai, and N. Tsumura, "Image-based measurement of changes to skin texture using piloerection for emotion estimation," *Artificial Life and Robotics*, vol. 24, no. 1, pp. 1–7, 2018.

- [34] H. J. Jung, J. Y. Ahn, J. I. Lee, J. Y. Bae, H. L. Kim, H. Y. Suh, J. I. Youn, and M. Y. Park, "Analysis of the number of enlarged pores according to site, age, and sex," *Skin Research and Technology*, vol. 24, no. 3, pp. 367–370, aug 2018.
- [35] S. J. Lee, J. Seok, S. Y. Jeong, K. Y. Park, K. Li, and S. J. Seo, "Facial pores: Definition, causes, and treatment options," pp. 277–285, mar 2016.
- [36] J. H. Rabe, A. J. Mamelak, P. J. McElgunn, W. L. Morison, and D. N. Sauder, "Photoaging: Mechanisms and repair," pp. 1–19, jul 2006.
- [37] D. H. Kim, Y. S. Rhyu, H. H. Ahn, E. Hwang, and C. S. Uhm, "Skin microrelief profiles as a cutaneous aging index," *Microscopy*, vol. 65, no. 5, pp. 407–414, 2016.
- [38] B. Fink, K. Grammer, and P. J. Matts, "Visible skin color distribution plays a role in the perception of age, attractiveness, and health in female faces," *Evolution and Human Behavior*, vol. 27, no. 6, pp. 433–442, 2006.
- [39] K. Xiao, J. M. Yates, F. Zardawi, S. Sueeprasan, N. Liao, L. Gill, C. Li, and S. Wuerger, "Characterising the variations in ethnic skin colours: a new calibrated data base for human skin," *Skin Research and Technology*, vol. 23, no. 1, pp. 21–29, 2017.
- [40] K. Kikuchi, Y. Masuda, T. Yamashita, K. Sato, C. Katagiri, T. Hirao, Y. Mizokami, and H. Yaguchi, "A new quantitative evaluation method for age-related changes of individual pigmented spots in facial skin," *Skin Research and Technology*, vol. 22, no. 3, pp. 318–324, aug 2016.
- [41] P. Humbert, F. Ferial, P. Agache, and H. I. Maibach, *Agache ' s Measuring the Skin*, 2004.
- [42] L. Machková, D. Švadlák, and I. Dolečková, "A comprehensive in vivo study of Caucasian facial skin parameters on 442 women," *Archives of Dermatological Research*, vol. 310, no. 9, pp. 691–699, 2018.

- [43] J. de Rigal, I. Des Mazis, S. Diridollou, B. Querleux, G. Yang, F. Leroy, and V. H. Barbosa, "The effect of age on skin color and color heterogeneity in four ethnic groups." *Skin research and technology*, vol. 16, no. 2, pp. 168–78, may 2010.
- [44] A. Chardon, I. Cretois, and C. Hourseau, "Skin colour typology and suntanning pathways." *International journal of cosmetic science*, vol. 13, no. 4, pp. 191–208, aug 1991.
- [45] M. Wilkes, C. Y. Wright, J. L. du Plessis, and A. Reeder, "Fitzpatrick skin type, individual typology angle, and melanin index in an African population: steps toward universally applicable skin photosensitivity assessments," *JAMA dermatology*, vol. 151, no. 8, pp. 902–903, 2015.
- [46] S. Del Bino, S. Ito, J. Sok, Y. Nakanishi, P. Bastien, K. Wakamatsu, and F. Bernerd, "Chemical analysis of constitutive pigmentation of human epidermis reveals constant eumelanin to pheomelanin ratio." *Pigment cell melanoma research*, vol. 28, no. 6, pp. 707–17, nov 2015.
- [47] Y. Song, Y. Pan, H. Wang, Q. Liu, and H. Zhao, "Mapping the face of young population in China: Influence of anatomical sites and gender on biophysical properties of facial skin," *Skin Research and Technology*, no. November 2018, pp. 1–8, 2019.
- [48] L. Yang, M. Egawa, M. Akimoto, and M. Miyakawa, "An Imaging Colorimeter for Noncontact Skin Color Measurement," *Optical Review*, vol. 10, no. 6, pp. 554–561, 2003.
- [49] M. Akimoto, M. Miyazaki, H.-H. Lee, T. Nishimura, M. Tamura, and M. Miyakawa, "Using Fuzzy Reasoning to Support a System of Diagnosis of Skin Disease," vol. 17, pp. 9–18, 2009.
- [50] G. Stepniak, L. Maksymiuk, and J. Siuzdak, "Experimental comparison of PAM, CAP, and DMT modulations in phosphorescent white LED transmission link," *IEEE Photonics Journal*, vol. 7, no. 3, pp. 1–8, 2015.

- [51] E. Cinotti, J.-L. Perrot, B. Labeille, F. Cambazard, R. Vie, A. Delalleau, L. Tognetti, and P. Rubegni, “Season and anatomic site effect on skin color and xerosis quantified using an ultra-high definition videodermoscope,” in *2016 IEEE International Symposium on Medical Measurements and Applications (MeMeA)*. IEEE, 2016, pp. 1–6.
- [52] X. Delpueyo Español, “Development of a new spectral imaging system for the diagnosis of skin cancer,” 2017.
- [53] V. Hourblin, S. Nouveau, N. Roy, and O. de Lacharrière, “Skin complexion and pigmentary disorders in facial skin of 1204 women in 4 Indian cities,” *Indian journal of dermatology, venereology and leprology*, vol. 80, no. 5, pp. 395–401, 2014.
- [54] C. Galzote, R. Estanislao, M. O. Suero, A. Khaiat, M. I. Mangubat, R. Moideen, H. Tagami, and X. Wang, “Characterization of facial skin of various Asian populations through visual and non-invasive instrumental evaluations: influence of age and skincare habits.” *Skin research and technology*, vol. 19, no. 4, pp. 454–65, nov 2013.
- [55] C. Cho, P. Ruan, E. Lee, and J. Ha, “Comparison of skin color between two Asian populations: According to latitude and UV exposure,” *Journal of Cosmetic Dermatology*, vol. 14, no. 1, pp. 22–26, 2015.
- [56] C. Battie, S. Jitsukawa, S. D. Bino, and C. Marionnet, “New insights in photoaging, UVA induced damage and skin types,” vol. 23, pp. 7–12, 2014.
- [57] S. Shono, M. Imura, M. Ota, and K. Toda, “The relationship of skin color, UVB-induced erythema, and melanogenesis,” *Journal of Investigative Dermatology*, vol. 84, no. 4, pp. 265–267, 1985.
- [58] L. Wang, X. Wan, and G. Xiao, “Classification and influencing factors analysis of facial skin color in Chinese population,” *Skin Research and Technology*, vol. 25, pp. 693–700, 2019.

- [59] F. Flament, R. Bazin, S. Laquieze, V. Rubert, E. Simonpietri, and B. Piot, “Effect of the sun on visible clinical signs of aging in Caucasian skin.” *Clinical, cosmetic and investigational dermatology*, vol. 6, pp. 221–232, 2013.
- [60] C. Cho, E. Cho, N. Kim, J. Shin, S. Woo, E. Lee, J. Hwang, and J. Ha, “Age-related biophysical changes of the epidermal and dermal skin in Korean women,” *Skin Research and Technology*, vol. 25, no. 4, pp. 504–511, 2019.
- [61] E. A. Grice and J. A. Segre, “The skin microbiome,” *Nature Reviews Microbiology*, vol. 9, no. 4, pp. 244–253, 2011.
- [62] B. Dréno, S. Pécastaings, S. Corvec, S. Veraldi, A. Khammari, and C. Roques, “Cutibacterium acnes (propionibacterium acnes) and acne vulgaris: a brief look at the latest updates,” *Journal of the European Academy of Dermatology and Venereology*, vol. 32, pp. 5–14, 2018.
- [63] T. C. Wikramanayake, L. J. Borda, M. Miteva, and R. Paus, “Seborrheic dermatitis—looking beyond Malassezia,” *Experimental Dermatology*, vol. 28, no. 9, pp. 991–1001, 2019.
- [64] M. A. Suva, A. M. Patel, N. Sharma, C. Bhattacharya, and R. K. Mangi, “A Brief Review on Acne Vulgaris: Pathogenesis, Diagnosis and Treatment,” *Research & Reviews: Journal of Pharmacology*, vol. 4, no. 3, pp. 1–12, 2014.
- [65] E. Barnard, J. Liu, E. Yankova, S. M. Cavalcanti, M. Magalhães, H. Li, S. Patrick, and A. McDowell, “Strains of the Propionibacterium acnes type III lineage are associated with the skin condition progressive macular hypomelanosis,” *Scientific Reports*, vol. 6, no. 1, pp. 1–9, 2016.
- [66] M. Shu, S. Kuo, Y. Wang, Y. Jiang, Y.-T. Liu, R. Gallo, and C.-M. Huang, “Porphyrin Metabolisms in Human Skin Commensal Propionibacterium acnes Bacteria: Potential Application to Monitor Human Radiation Risk,” *Current Medicinal Chemistry*, vol. 20, no. 4, pp. 562–568, 2013.



- [67] I. Seo, S. H. Tseng, G. O. Cula, P. R. Bargo, and N. Kollias, “Fluorescence spectroscopy for endogenous porphyrins in human facial skin,” *Photonic Therapeutics and Diagnostics V*, vol. 7161, no. February 2009, p. 716103, 2009.
- [68] H. Dobrev, “Fluorescence diagnostic imaging in patients with acne,” *Photodermatology, Photoimmunology Photomedicine*, vol. 26, no. 6, pp. 285–289, 2010.
- [69] S. V. Patwardhan, C. Richter, A. Vogt, U. Blume-Peytavi, D. Canfield, and J. Kottner, “Measuring acne using Coproporphyrin III, Protoporphyrin IX, and lesion-specific inflammation: an exploratory study,” *Archives of Dermatological Research*, vol. 309, no. 3, pp. 159–167, 2017.
- [70] L. C. Lucchina, N. Kollias, R. Gillies, S. B. Phillips, J. A. Muccini, M. J. Stiller, R. J. Trancik, and L. A. Drake, “Fluorescence photography in the evaluation of acne,” *Journal of the American Academy of Dermatology*, vol. 35, no. 1, pp. 58–63, 1996.
- [71] G. Peris Fajarnés, M. Moncho Santonja, B. Defez García, and I. Lengua Lengua, “Segmentation methods for acne vulgaris images: Proposal of a new methodology applied to fluorescence images,” *Skin Research and Technology*, vol. 26, no. 5, pp. 734–739, 2020. [Online]. Available: <https://onlinelibrary.wiley.com/doi/10.1111/srt.12865>
- [72] M. Khongsuwan, S. Kiattisin, W. Wongseree, and A. Leelasantitham, “Counting number of points for acne vulgaris using UV fluorescence and image processing,” *BMEiCON-2011 - 4th Biomedical Engineering International Conference*, pp. 142–146, 2011.
- [73] M. A. Suva, A. M. Patel, and N. Sharma, “A Brief Review on Acne Vulgaris : Pathogenesis , Diagnosis and Treatment A Brief Review on Acne Vulgaris : Pathogenesis , Diagnosis and Treatment,” no. January 2015, pp. 0–12, 2016.

- [74] J. R. Balbin, J. C. Dela Cruz, C. O. Camba, A. D. Gozo, S. M. B. Jimenez, and A. C. Tribiana, "Facial fluid synthesis for assessment of acne vulgaris using luminescent visualization system through optical imaging and integration of fluorescent imaging system," *Second International Workshop on Pattern Recognition*, vol. 10443, no. June 2017, p. 1044311, 2017.
- [75] F. S. Abas, B. Kaffenberger, J. Bikowski, and M. N. Gurcan, "Acne image analysis: lesion localization and classification," in *Medical Imaging 2016: Computer-Aided Diagnosis*, vol. 9785. SPIE, 2016, pp. 64 – 72.
- [76] K. J. McGINLEY, G. F. WEBSTER, and J. J. LEYDEN, "Facial follicular porphyrin fluorescence: correlation with age and density of *Propionibacterium acnes*," *British Journal of Dermatology*, vol. 102, no. 4, pp. 437–441, 1980.
- [77] J. J. Leyden, K. J. McGinley, O. H. Mills, and A. M. Kligman, "Age related changes in the resident bacterial flora of the human face," *Journal of Investigative Dermatology*, vol. 65, no. 4, pp. 379–381, oct 1975.
- [78] S. W. Youn, J. H. Kim, J. E. Lee, S. O. Kim, and K. C. Park, "The facial red fluorescence of ultraviolet photography: Is this color due to propionibacterium acnes or the unknown content of secreted sebum?" *Skin Research and Technology*, vol. 15, no. 2, pp. 230–236, 2009.
- [79] D. T. Xu, J. N. Yan, W. Liu, X. X. Hou, Y. Zheng, W. W. Jiang, Q. Ju, C. C. Zouboulis, and X. L. Wang, "Is Human Sebum the Source of Skin Follicular Ultraviolet-Induced Red Fluorescence? A Cellular to Histological Study," *Dermatology*, vol. 234, no. 1-2, pp. 43–50, 2018.
- [80] M. Tanida, M. Katsuyama, and K. Sakatani, "Relation between mental stress-induced prefrontal cortex activity and skin conditions: A near-infrared spectroscopy study," *Brain Research*, vol. 1184, no. 1, pp. 210–216, dec 2007.

- [81] A. Lihachev, A. Derjabo, I. Ferulova, M. Lange, I. Lihacova, and J. Spigulis, “Autofluorescence imaging of basal cell carcinoma by smartphone RGB camera,” *Journal of Biomedical Optics*, vol. 20, no. 12, p. 120502, 2015.
- [82] K. Tsuchida and M. Kobayashi, “Oxidative stress in human facial skin observed by ultraweak photon emission imaging and its correlation with biophysical properties of skin,” *Scientific reports*, vol. 10, no. 1, p. 9626, 2020.
- [83] G. Sauermann, A. Herpens, U. Hoppe, and A. Kligman, “A Novel Fluorimetric Method to Investigate Sebaceous Glands in Humans,” *Noninvasive Methods for the Quantification of Skin Functions*, pp. 252–271, 1993.
- [84] Z. V. Lim, F. Akram, C. P. Ngo, A. A. Winarto, W. Q. Lee, K. Liang, H. H. Oon, S. T. G. Thng, and H. K. Lee, “Automated grading of acne vulgaris by deep learning with convolutional neural networks,” *Skin Research and Technology*, vol. 26, no. 2, pp. 187–192, 2019.
- [85] M. Becker, T. Wild, and C. C. Zouboulis, “Objective assessment of acne,” *Clinics in Dermatology*, vol. 35, no. 2, pp. 147–155, 2017.
- [86] H. Tagami, “Electrical measurement of the hydration state of the skin surface in vivo,” *British Journal of Dermatology*, vol. 171, pp. 29–33, 2014.
- [87] T. Rong, N. Yue-qing, G. Jian-mei, Z. Shao-min, and W. Yan, “The relationship between subjective skin type and skin barrier function,” *Journal of Clinical Dermatology*, pp. 44–47.
- [88] K. Koseki, H. Kawasaki, T. Atsugi, M. Nakanishi, M. Mizuno, E. Naru, T. Ebihara, M. Amagai, and E. Kawakami, “Assessment of skin barrier function using skin images with topological data analysis,” *NPJ Systems Biology and Applications*, vol. 6, no. 1, pp. 1–9, 2020.

- [89] M. Boer, E. Duchnik, R. Maleszka, and M. Marchlewicz, "Structural and biophysical characteristics of human skin in maintaining proper epidermal barrier function," *Postepy Dermatologii i Alergologii*, vol. 33, no. 1, pp. 1–5, 2016.
- [90] S. Luebberding, N. Krueger, and M. Kerscher, "Age-related changes in skin barrier function - Quantitative evaluation of 150 female subjects," *International Journal of Cosmetic Science*, vol. 35, no. 2, pp. 183–190, 2013.
- [91] E. Berardesca, M. Loden, J. Serup, P. Masson, and L. M. Rodrigues, "The revised EEMCO guidance for the in vivo measurement of water in the skin," *Skin Research and Technology*, vol. 24, no. 3, pp. 351–358, 2018.
- [92] T. V. Westermann, V. R. Viana, C. Berto Junior, C. B. Detoni da Silva, E. L. S. Carvalho, and C. G. Pupe, "Measurement of skin hydration with a portable device (SkinUp® Beauty Device) and comparison with the Corneometer®," *Skin Research and Technology*, no. November 2019, pp. 1–6, 2020.
- [93] X. Ou, W. Pan, and P. Xiao, "In vivo skin capacitive imaging analysis by using grey level co-occurrence matrix (GLCM)," *International Journal of Pharmaceutics*, vol. 460, no. 1-2, pp. 28–32, 2014.
- [94] D. Batisse, F. Giron, and J. L. L  v  que, "Capacitance imaging of the skin surface," *Skin Research and Technology*, vol. 12, no. 2, pp. 99–104, may 2006.
- [95] E. Xhaufaire-Uhoda, G. Loussouarn, C. Haubrechts, D. S. L  ger, and G. E. Pi  rard, "Skin capacitance imaging and corneosurfametry. A comparative assessment of the impact of surfactants on stratum corneum," *Contact Dermatitis*, vol. 54, no. 5, pp. 249–253, 2006.
- [96] M. Egawa, M. Yanai, N. Maruyama, Y. Fukaya, and T. Hirao, "Visualization of Water Distribution in the Facial Epidermal Layers of Skin Using High-Sensitivity Near-Infrared (NIR) Imaging." *Applied spectroscopy*, no. 4, pp. 481–487, apr 2015.

- [97] H. Arimoto, M. Yanai, and M. Egawa, “Analysis of absorption and spreading of moisturizer on the microscopic region of the skin surface with near-infrared imaging,” *Skin Research and Technology*, vol. 22, no. 4, pp. 505–512, 2016.
- [98] B. P. Yakimov, D. A. Davydov, V. V. Fadeev, G. S. Budylin, and E. A. Shirshin, “Comparative analysis of the methods for quantitative determination of water content in skin from diffuse reflectance spectroscopy data,” *Quantum Electronics*, vol. 50, no. 1, pp. 41–46, jan 2020.
- [99] T. Y. Masahiko Ooe, Keioko Tanida, “influence of hydration for optical properties of stratum corneum,” *Journal of Society Cosmetic Chemistry Japan*, 2001.
- [100] Z. X. Jiang and J. DeLaCruz, “Appearance benefits of skin moisturization,” *Skin Research and Technology*, vol. 17, no. 1, pp. 51–55, feb 2011.
- [101] S. M. Pizer, E. P. Amburn, J. D. Austin, R. Cromartie, A. Geselowitz, T. Greer, B. ter Haar Romeny, J. B. Zimmerman, and K. Zuiderveld, “ADAPTIVE HISTOGRAM EQUALIZATION AND ITS VARIATIONS.” *Computer vision, graphics, and image processing*, vol. 39, no. 3, pp. 355–368, sep 1987.
- [102] S. Ma, H. Ma, Y. Xu, S. Li, C. Lv, and M. Zhu, “A low-light sensor image enhancement algorithm based on HSI color model,” p. 3583, oct 2018. [Online]. Available: [www.mdpi.com/journal/sensors.\(2021-07-23\)](http://www.mdpi.com/journal/sensors.(2021-07-23))
- [103] S. Liaqat, K. Dashtipour, K. Arshad, and N. Ramzan, “Non invasive skin hydration level detection using machine learning,” *Electronics (Switzerland)*, vol. 9, no. 7, pp. 1–10, 2020.
- [104] W. Y. Liu, B. W. Wang, J. X. Yu, F. Li, S. X. Wang, and W. X. Hong, “Visualization classification method of multi-dimensional data based on radar chart mapping,” in *Proceedings of the 7th International Conference on Machine Learning and Cybernetics, ICMLC*, vol. 2, 2008, pp. 857–862.

- [105] R. Garland, “The Mid-Point on a Rating Scale: Is it Desirable?” *Marketing Bulletin*, vol. 2, pp. 66–70, 1991.
- [106] J. M. Linacre, “Optimizing Rating Scale Category Effectiveness,” *Journal of Applied Measurement*, vol. 3, no. 1, pp. 85–106, 2002.
- [107] D. J. Day, C. M. Littler, R. W. Swift, and S. Gottlieb, “The Wrinkle Severity Rating Scale: A validation study,” *American Journal of Clinical Dermatology*, vol. 5, no. 1, pp. 49–52, aug 2004.
- [108] J. I. Silverberg, “Validity and reliability of a novel numeric rating scale to measure skin-pain in adults with atopic dermatitis,” *Archives of Dermatological Research*, pp. 1–7, feb 2021. [Online]. Available: <https://doi.org/10.1007/s00403-021-02185-3>(2021-07-23)
- [109] E. K. Yeoung, R. Mann, L. H. Engrav, M. Goldberg, V. Cain, B. Costa, M. Moore, D. Nakamura, and J. Lee, “Improved burn scar assessment with use of a new scar-rating scale,” *The Journal of burn care rehabilitation*, vol. 18, no. 4, pp. 353–355, 1997.
- [110] S. Kasolang, W. A. Adlina, N. A. Rahman, and N. R. N. Roseley, “Common skin disorders: A review,” *Jurnal Tribologi*, vol. 25, pp. 59–82, 2020.
- [111] Y. Albo, J. Lanir, P. Bak, and S. Rafaeli, “Off the Radar: Comparative Evaluation of Radial Visualization Solutions for Composite Indicators,” *IEEE Transactions on Visualization and Computer Graphics*, vol. 22, no. 1, pp. 569–578, jan 2016.